National Library of Canada

Acquisitions and Bibliographic Services Branch

395 Wellington Street
Ottawa, Ontario
K1A 0N4

Bibliothèque nationale du Canada

Direction des acquisitions et des services bibliographiques

395, rue Wellington
Ottawa (Ontario)
K1A 0N4

Your file Votre référence

Our file Notre référence

NOTICE

The quality of this microform is heavily dependent upon the quality of the original thesis submitted for microfilming. Every effort has been made to ensure the highest quality of reproduction possible.

If pages are missing, contact the university which granted the degree.

Some pages may have indistinct print especially if the original pages were typed with a poor typewriter ribbon or if the university sent us an inferior photocopy.

AVIS

La qualité de cette microforme dépend grandement de la qualité de la thèse soumise au microfilmage. Nous avons tout fait pour assurer une qualité supérieure de reproduction.

S'il manque des pages, veuillez communiquer avec l'université qui a conféré le grade.

La qualité d'impression de certaines pages peut laisser à désirer, surtout si les pages originales ont été dactylographiées à l'aide d'un ruban usé ou si l'université nous a fait parvenir une photocopie de qualité inférieure.

Canada

LINEAR AND NONLINEAR FINITE STRIP ANALYSIS OF BRIDGES

A thesis submitted to the
School of Graduate Studies and Research
in partial fulfillment of the thesis requirements
for the degree of Doctor of Philosophy
in the Department of Civil Engineering

Ph.D. Candidate: Wenchang Li
Thesis Supervisor: M. S. Cheung

Department of Civil Engineering
Faculty of Engineering
University of Ottawa
Ottawa, Canada

ISBN 0-315-80004-6

UNIVERSITÉ D'OTTAWA
UNIVERSITY OF OTTAWA

ABSTRACT

The analysis of highway bridges such as slab-on-girder bridges, box-girder bridges, cable-stayed bridges etc. is a very complicated undertaking. Analytical methods are applicable only for the simplest structures. Finite element method is the most powerful and versatile tool , which can be applied to analyze any types of bridge and any load cases. However, the efficiency of that method needs to be improved because the finite element solutions usually require too much computer time, too large core storage and too many input data.

If a structure has a uniform cross-section and line end supports (in fact, a high proportion of bridges can be simplified to such a structure), the finite strip method has proven to be the most efficient numerical structural analysis method, which employs a series of functions to simulate the variation of displacements in the longitudinal direction of the structure. Thus, the number of dimensions of analysis is reduced by at least one. Consequently, the computer time, storage and input data are reduced significantly. Since this method was first published in 1968, it has been extensively used for linear and nonlinear, static and dynamic analysis of rectangular, skew and curved slab bridges, slab-on girder bridges box-girder bridges etc.

In the present study, the following efforts are made:

1. Extending the finite strip method to the analysis of continuous haunched slab-on-girder bridges and box-girder bridges.

2. Extending the spline finite strip method to the analysis of continuous haunched slab-on-girder bridges and box-girder bridges.

3. Extending the finite strip method to nonlinear analysis of cable-stayed bridges.

4. Improving the efficiency of geometrically nonlinear finite strip analysis of plates.

5. Improving the accuracy of materially nonlinear finite strip analysis of reinforced concrete slabs.

6. Combining the finite strip method with finite element method and boundary element method for analysis of rectangular plates with some irregularities.

A number of numerical examples will show the accuracy and efficiency of the methods developed in the present study.

ACKNOWLEDGEMENTS

The author wishes to express his sincere appreciation to his research supervisor, Dr. M.S. Cheung, for his constructive suggestions, valuable discussions and continued assistance throughout the course of the study.

Sincere thanks are also expressed to Dr. L.G. Jaeger, Dr. A.G. Razaqpur, Dr. M. Saatcioglu, Dr. S.F. Ng and Dr. Tanaka for their important information, valuable advice and generous assistance in choosing topics, solving difficult questions, reviewing the Thesis Proposal etc.

The financial support from the Natural Sciences and Engineering Research Council of Canada is gratefully acknowledged.

Contents

List of Figures

List of Tables

NOMENCLATURE

$\{a\}$	displacement vector
b	width of strip
$[B]$	strain matrix
D	$= Eh^3/12(1-\nu^2)$
$[D]$	elastic matrix
E	Young's modulus
f'_c	uniaxial compressive strength of concrete
f'_t	uniaxial tensile strength of concrete
$\{F\}$	force vector
$[F]$	flexibility matrix
h	thickness of strip, length of longitudinal section
$[K]$	stiffness matrix
l	length of strip
$L(y)$	Lagrange interpolation expression
m	number of longitudinal sections in a strip
$[N]$	matrix of shape function
$\{P\}$	load vector
q	loading per unit area, weight per unit length
r	number of series terms used in analysis
r_1, r_2	curvature radii of curvilinear coordinate lines
R	curvature radius of bottom flange
$\{R\}$	vector of redundant forces or resistant forces
$[T], [t]$	coordinate transformation matrices for displacements
$[T_\epsilon]$	coordinate transformation matrices for strains
u, v, w	displacements in x,y and z directions
U	strain energy
W	potential energy of external loading

$Y_m(y)$	free vibration eigenfunction of beam
α	amplification factor of flexural stiffness, ratio σ_1/σ_2
$\{\delta\}_m$	vector of displacement parameters
ϵ_{iu}	equivalent uniaxial strain
$\{\epsilon\}$	strain vector
μ_m	free vibration eigenvalue of beam
ν	Poisson's ratio
Φ	total potential energy
Φ_i	B_3 spline function centered at y_i
$\{\sigma\}$	vector of stresses and moments
σ_1, σ_2	principal stresses
$\sigma_{ic}, \epsilon_{ic}$	maximum compressive stress and corresponding strain of concrete
θ	transverse slope $\partial w/\partial x$

Chapter 1

INTRODUCTION

1.1 ANALYSIS OF HIGHWAY BRIDGES

In service, highway bridges such as slab on girder bridges, box girder bridges, cable-stayed bridges etc. undergo not only longitudinal bending but also transverse bending, torsion, distortion and shear deformation. The load distribution among the girders, the support reactions and cable-tensions are highly statically indeterminate and material and geometrical nonlinearities due to concrete cracking, cable sagging and P-Δ effect etc. are often significant. Therefore, the analysis of a bridge is a complex undertaking.

There exist some analytical methods for bridge analysis, such as the load distribution technique for right simply supported slab-type bridges [1,2,3], the stiffness method of analysis for steel orthotropic deck systems [4] and the extended folded-plate theory for box-girder bridges [5]. However, because these analytical methods can only be used to analyze highly simplified structures, their applicability is lim-

ited.

The finite element method is the most powerful and versatile tool for analysis of bridges [6,7]. That method can be applied to deal with any specific configuration of bridge structure and supports. It is suitable for analysis involving all types of statical and dynamical loads and all kinds of elastic and inelastic deformation. Nevertheless, the finite element solution usually requires a significant amount of computer time, large core storage and tedious and lengthy input data files. Therefore, the efficiency of this method needs to be improved.

In fact, the simply supported right deck of uniform section (or a structure which may be realistically analyzed as such) constitutes a high proportion of the large number of bridges being built. For analyzing this type of bridge, the finite strip method has proven to be the most efficient numerical method; it uses a series of orthogonal functions in the longitudinal direction, y, combined with the conventional finite element polynomial shape function in the transverse direction, x, to simulate all the displacement components of the structure. In this way, the number of dimensions of the analysis is reduced by at least one. Consequently, computer time, storage and input data requirements are reduced significantly.

1.2 DEVELOPMENT OF FINITE STRIP METHOD

The finite strip method was first published by Y.K.Cheung [8] for analysis of simply supported bridge deck structures in 1968. The finite strip method for rectangular

slab-type bridge decks was also suggested independently by Powell and Ogden [9] in 1969. Since then, considerable research and development on that method have been carried out in many countries. In the late 1960' and early 1970', the field of research extended to many types of bridge and loading conditions, such as:

- rectangular slabs with end boundary conditions other than simple supports, [10] in 1968,
- simply supported box girder bridges, [11] in 1969,
- curved slab and box girder bridges, [12] in 1969 and [13] in 1971,
- slab-type bridges with intermediate column supports using the flexibility approach, [14] in 1970,
- rectangular slabs with variable cross section in the spanwise direction, [14] in 1970,
- the frequency analysis of some simple and continuous rectangular slabs, [15] in 1971,
- skew slab bridges, [16] in 1972,
- skew box girder bridges, [17] in 1975,
- the initial buckling analysis of box-type structures, [18] in 1973 and [19] in 1974,
- continuous box girder bridges with transverse diaphragms, using the flexibility approach, [20] in 1976,

- slab and box girder bridges continuous over rigid supports, using continuous beam eigenfunctions and a direct stiffness method, [21,22] in 1974 and 1978,
- analysis of general plates, [23] in 1978.

Y.K.Cheung and Y.C.Loo have published their books [24,25] to summarize the basic theory of the finite strip method and its applications in bridge engineering as the results of research work during that period.

Since the middle 1970's, enormous efforts have been devoted to more complicated topics. Among them, the main subjects related to the finite strip analysis in bridge engineering may be listed as follows:

- compound finite strip method for analysis of plates continuous over intermediate flexible beams and columns using a direct stiffness methodology [26,27],since 1983,
- post-buckling behavior and geometrically nonlinear analysis of plate structures, [28-33] since 1978,
- material nonlinear analysis of steel structures,[34-36] since 1986,
- material nonlinear analysis of reinforced concrete slabs,[37] 1988,
- large deflection elasto-plastic analysis of plate structures [38], 1989.

In spite of a number of advantages, the above mentioned semi-analytical finite strip method experienced difficulties in dealing with concentrated forces, multiple spans, discrete supports at strip ends etc. To overcome these difficulties and to retain the advantages of the finite strip method, a mathematical tool called 'B_3 spline function' was used for displacement functions to form the spline finite strips for analysis of rectangular plates by Y.K.Cheung et al [39] in 1982.

The B_3 spline function can ensure continuity up to the second derivative (the so-called C_2 continuity). However, in order to achieve the same continuity condition, the finite element method needs three times as many unknowns at the element nodes. Hence, the use of B_3 splines is computationally much more efficient than the finite element method with C_2 continuity. When using theB_3 spline function, the penalty function approach [6] is readily utilized to impose any type of boundary conditions. Thus, the spline finite strip method is more flexible than the semi-analytical finite strip method. In addition, the second derivative of B_3 splines varies linearly in each longitudinal section, as a result of which it can more easily simulate peak values of bending moment at the loaded section or at an intermediate support.

In later years, the spline finite strip method was extended to box girder bridges [40] in 1983, to skew plates [41,42] in 1984 and 1988, to arbitrary shaped slabs and arbitrary curved slab bridges [43,44] in 1986, to vibration and stability analysis [45,46] in 1987 and to postbuckling analysis [47] in 1989.

Indeed, during the past two decades, a very large number of researchers and engineers have made so many important contributions to the development of the finite strip method and its application in engineering that it is impossible to list all of their accomplishments here.

1.3 SCOPE OF STUDY

The primary objective of this thesis is to extend the finite strip method to more complicated structures and more difficult analysis, thus making the method more accurate and efficient.The main topics and efforts are focussed on the following areas:

A. SEMI-ANALYTICAL FINITE STRIP METHOD:

1. finite strip method for continuous structure
2. finite strip analysis of haunched, continuous bridges
3. finite strip analysis of haunched, continuous box girder bridges

B. SPLINE FINITE STRIP METHOD:

1. spline finite strip analysis of haunched, continuous bridges
2. spline finite strip analysis of haunched, continuous box girder bridges

C. NONLINEAR FINITE STRIP ANALYSIS OF BRIDGES:

1. nonlinear finite strip analysis of cable-stayed bridges
2. geometrical nonlinear analysis of plates
3. material nonlinear analysis of reinforced concrete slab

D. FINITE STRIP METHOD COMBINED WITH OTHER NUMERICAL METHOD:

1. finite strip analysis of plate combined with finite element method
2. finite strip method combined with boundary element method

Each of the above topics has formed a seperate chapter in the thesis.

Chapter 2

FINITE STRIP METHOD

2.1 CONVENTIONAL FINITE STRIP METHOD

The finite strip method was first published by Y.K.Cheung for analysis of simply supported bridge deck structures in 1968 [8]. Since then, this method has been extended to many types of bridge such as rectangular, curved and skew box-girder bridges of single span or multispan, etc. Y.K.Cheung and Y.C.Loo have published their books [24,25] to summarize the basic theory of the finite strip method and its applications in bridge engineering as the results of research work during the late 1960' and early 1970'. In this section, the basic concept of the traditional finite strip method for analysis of rectangular box-girder bridges with single or multispan is reviewed briefly.

The finite strip method can be considered as a special form of finite element procedure using the displacement approach or as the so-called semi-analytical finite element method. If a structure has constant cross-section and its boundary con-

ditions at both ends do not change transversely, then for its stress analysis the structure can be divided into a number of finite strips (Fig.2.1) instead of finite elements. In each strip, the displacement components at any point are expressed in terms of the displacement parameters of nodal lines by means of simple polynomials in the transverse direction and continuously differentiable smooth series in the longitudinal direction, with the stipulation that such series should satisfy a priori the boundary conditions at the ends of strips.

2.1.1 SERIES PART OF DISPLACEMENT FUNCTION

The most commonly used series are the beam eigenfunctions which are derived from the solution of the beam vibration differential equation

$$\frac{d^4Y}{dy^4} = \mu^4 Y \tag{2.1}$$

The general form of the beam eigenfunctions is

$$Y(y) = c_1 \sin(\mu y) + c_2 \cos(\mu y) + c_3 \sinh(\mu y) + c_4 \cosh(\mu y) \tag{2.2}$$

with the coefficients c_i to be determined by the end conditions.

These have been worked out explicitly for the various end conditions and are listed below:

(a) Both ends simply supported ($Y(0) = Y''(0) = 0$, $Y(l) = Y''(l) = 0$).

$$Y_m(y) = \sin(\mu_m y),$$

$$(\mu_m = \frac{m\pi}{l})$$

(b) Both ends clamped ($Y(0) = Y'(0) = 0$, $Y(l) = Y'(l) = 0$).

$$Y_m(y) = \sin(\mu_m y) - \sinh(\mu_m y) - \alpha_m[\cos(\mu_m y) - \cosh(\mu_m y)],$$

$$\alpha_m = \frac{\sin(\mu_m l) - \sinh(\mu_m l)}{\cos(\mu_m l) - \cosh(\mu_m l)}$$

$\mu_m l$ are the solutions of equation $1 - \cos(\mu l)\cosh(\mu l) = 0$, the first twelve values are:

4.730040744862704, 7.853204624095837, 10.99560783800167, 14.13716549125746, 17.27875965739948, 20.42035224562606, 23.56194490204045, 26.70353755550818, 29.84513020910325, 32.98672286269282, 36.12831551628262, 39.26990816987241.

For m greater than 12, $\mu_m = (m + 0.5)\pi/l$ can be taken as a very close approximation.

(c) One end simply supported and the other end clamped

$$(Y(0) = Y''(0) = 0, Y(l) = Y'(l) = 0).$$

$$Y_m(y) = \sin(\mu_m y) - \alpha_m \sinh(\mu_m y),$$

$$\alpha_m = \frac{\sin(\mu_m l)}{\sinh(\mu_m l)}$$

$$(\mu_m l = 3.9266, 7.0685, 10.2102, ..., \frac{4m+1}{4}\pi).$$

(d) Both ends free ($Y''(0) = Y'''(0) = 0$, $Y''(l) = Y'''(l) = 0$).

$$Y_1(y) = 1, \mu_1 = 0,$$

$$Y_2(y) = 1 - \frac{2y}{l}, \mu_2 = 1,$$

$$Y_m(y) = \sin(\mu_m y) + \sinh(\mu_m y) - \alpha_m[\cos(\mu_m y) + \cosh(\mu_m y)],$$

$$\alpha_m = \frac{\sin(\mu_m l) - \sinh(\mu_m l)}{\cos(\mu_m l) - \cosh(\mu_m l)}$$

$$(\mu_m l = 4.7300, 7.8532, 10.9960, ..., \frac{2m-3}{2}\pi, m = 3, 4, ..., \infty).$$

(e) One end clamped and the other end free

$$(Y(0) = Y'(0) = 0, Y''(l) = Y'''(l) = 0).$$

$$Y_m(y) = \sin(\mu_m y) + \sinh(\mu_m y) - \alpha_m[\cos(\mu_m y) - \cosh(\mu_m y)],$$

$$\alpha_m = \frac{\sin(\mu_m l) + \sinh(\mu_m l)}{\cos(\mu_m l) + \cosh(\mu_m l)}$$

$$(\mu_m l = 1.875, 4.694, ..., \frac{2m-1}{2}\pi).$$

(f) One end simply supported and the other end free

$$(Y(0) = Y''(0) = 0, Y''(l) = Y'''(l) = 0).$$

$$Y_1(y) = \frac{y}{l}, \mu_1 = 1,$$

$$Y_m(y) = \sin(\mu_m y) + \alpha_m \sinh(\mu_m y),$$

$$\alpha_m = \frac{\sin(\mu_m l)}{\sinh(\mu_m l)}$$

$$(\mu_m l = 3.9266, 7.0685, 10.2102, 13.3520, ..., \frac{2m-3}{4}\pi,$$

$$m = 2, 3, ..., \infty).$$

The beam eigenfunctions possess the valuable properties of orthogonality, i.e.

$$\int_0^l Y_m Y_n dy = 0 \qquad for \quad m \neq n$$

$$\int_0^l Y_m'' Y_n'' dy = 0 \qquad for \;\; m \neq n$$

Utilization of these properties will result in a significant saving in computation effort for the calculation of stiffness matrices.

2.1.2 DISPLACEMENT FUNCTIONS

In slab on girder bridges and box-girder bridges, each finite strip is subjected to in-plane stresses and out-of-plane bending forces(Fig. 2.2). This type of strip is called a folded plate strip. The nodal displacement parameters and the nodal force vector of the strip corresponding to the m-th series term are:

$$\{\delta\}_m = (u_1 \; v_1 \; w_1 \; \theta_1 \; u_2 \; v_2 \; w_2 \;\; \theta_2)_m^T$$

$$\{F\}_m = (U_1 \; V_1 \; W_1 \; M_1 \; U_2 \; V_2 \; W_2 \; M_2)_m^T$$

The displacement components at any point (x,y) within the strip are expressed in terms of the nodal displacement parameters as follows:

$$u = \sum_{m=1}^{r}((1-X)u_{1m} + Xu_{2m})Y_m(y)$$

$$v = \sum_{m=1}^{r}((1-X)v_{1m} + Xv_{2m})Y_m'(y)/\mu_m$$

$$w = \sum_{m=1}^{r}(C_1 w_{1m} + C_2\theta_{1m} + C_3 w_{2m} + C_4\theta_{2m})Y_m(y) \qquad (2.3)$$

where,

$$C_1 = (1 - 3X^2 + 2X^3)$$

$$C_2 = x(1 - 2X + X^2)$$

$$C_3 = (3X^2 - 2X^3)$$

$$C_4 = x(X^2 - X)$$

$$X = x/b$$

and r is the total number of terms considered in the analysis.

These expressions can be written in the following more compact form:

$$\{f\} = \{u, v, w\}^T = \sum_{m=1}^{r} [N]_m \{\delta\}_m \tag{2.4}$$

2.1.3 STRAINS

Once the displacement functions are known, it is possible to obtain the strains, curvatures and twist, through appropriate differentiations with respect to the coordinates x and y in the well-known manner, yielding the following:

$$\begin{aligned} \epsilon_x &= \frac{\partial u}{\partial x} \\ \epsilon_y &= \frac{\partial v}{\partial y} \\ \gamma_{xy} &= \frac{\partial u}{\partial y} + \frac{\partial v}{\partial x} \\ \chi_x &= -\frac{\partial^2 w}{\partial x^2} \\ \chi_y &= -\frac{\partial^2 w}{\partial y^2} \\ \chi_{xy} &= 2\frac{\partial^2 w}{\partial x \partial y} \end{aligned} \tag{2.5}$$

The matrix form of these equations is as follows:

$$\{\epsilon\} = \{\epsilon_x, \epsilon_y, \gamma_{xy}, \chi_x, \chi_y, \chi_{xy}\}^T = \sum_{m=1}^{r} [B]_m \{\delta\}_m \tag{2.6}$$

2.1.4 STRESSES

The stresses are related to the strains by

$$\{\sigma\} = \{N_x, N_y, N_{xy}, M_x, M_y, M_{xy}\}^T = [D]\{\epsilon\} = \sum_{m=1}^{r} [D][B]_m \{\delta\}_m \tag{2.7}$$

where [D] is the elasticity matrix. For an isotropic folded plate,

$$[D] = \begin{bmatrix} [D]_{pl} & 0 \\ 0 & [D]_b \end{bmatrix} \tag{2.8}$$

in which

$$[D]_{pl} = \frac{Eh}{1-\nu^2} \begin{bmatrix} 1 & \nu & 0 \\ \nu & 1 & 0 \\ 0 & 0 & \frac{1-\nu}{2} \end{bmatrix}$$

$$[D]_b = \frac{Eh^3}{12(1-\nu^2)} \begin{bmatrix} 1 & \nu & 0 \\ \nu & 1 & 0 \\ 0 & 0 & \frac{1-\nu}{2} \end{bmatrix}$$

2.1.5 MINIMIZATION OF TOTAL POTENTIAL ENERGY

The strain energy of a folded plate strip is given by

$$U = \frac{1}{2} \int \{\epsilon\}^T \{\sigma\} dA$$

By virtue of (2.6) and (2.7), the strain energy can be expressed as

$$U = \frac{1}{2}\sum_{m=1}^{r}\sum_{n=1}^{r}\{\delta\}_m^T[K]_{mn}\{\delta\}_n \tag{2.9}$$

where $[K]_{mn}$ is the stiffness submatrix of the strip and is given by the following area integral:

$$[K]_{mn} = \int [B]_m^T[D][B]_n dA \tag{2.10}$$

The potential energy due to the external distributed loads $\{q\} = \{q_x, q_y, q_z\}^T$ can be written simply as

$$W = -\int \{f\}^T\{q\}dA \tag{2.11}$$

Substituting (2.4) into (2.11) gives

$$W = -\sum_{m=1}^{r}\{\delta\}_m^T\{F\}_m \tag{2.12}$$

where $\{F\}_m$ is the equivalent nodal force vector of the external load and is given by the following integral:

$$\{F\}_m = \int [N]_m^T\{q\}dA \tag{2.13}$$

For a point load the above integral is reduced to the simple expression of load multiplied by the corresponding displacement.

The total potential energy of the entire structure,Φ, is the sum of U and W contributions from all the strips. Thus

$$\begin{aligned}\Phi &= \sum_{s=1}^{NS}(U+W) \\ &= \sum_{s=1}^{NS}(\frac{1}{2}\sum_{m=1}^{r}\sum_{n=1}^{r}\{\delta\}_m^T[K]_{mn}\{\delta\}_n - \sum_{m=1}\{\delta\}_m^T\{F\}_m)\end{aligned} \tag{2.14}$$

in which NS is the number of strips.

According to the principle of minimum potential energy, the values of the displacement parameters must be such as to make the total potential energy of the structure assume a minimum value. In mathematical form this requires that

$$\{\frac{\partial \Phi}{\partial \{\delta\}}\} = \{0\} \tag{2.15}$$

Substituting (2.14) into (2.15) and performing the partial differentiation produces a set of linear algebraic equations which can be written in the following matrix form:

$$[K]\{\delta\} = \{F\} \tag{2.16}$$

in which [K],$\{\delta\}$ and $\{F\}$ are the stiffness matrix, the nodal displacement vector and the nodal load vector of the whole structure. They are the assembles of the corresponding matrices or vectors of all the strips in the structure. Solving the set of equations for the unknown displacement parameters and substituting them into (2.4) and (2.7) will give the displacements and stresses at any point of interest.

Because of the orthogonal property of the beam eigenfunctions, for structures with both ends simply supported, the derivation shows that all the terms of the series are uncoupled, namely, $[K]_{mn} = 0$ for $m \neq n$. Thus, the stiffness matrix has a very narrow half-bandwidth, and the required computer storage and time consumption are reduced significantly.

2.1.6 COORDINATE TRANSFORMATION

All of the above derivations are carried out in a local coordinate system , wherein the x and y axes coincide with the mid-surface of a strip. In folded plate structures, any two plates will in general meet at an angle, and in order to assemble the stiffness matrices, the displacement vectors and the load vectors of non-coplanar strips, a common coordinate system is obviously required.

In Fig. 2.3 the individual coordinates of a strip are labelled as x',y',z' and the common coordinates as x,y,z. y and y' are coincident with each another and also with the intersection line of two adjoining strips. The transformation of displacements between the two sets of coordinate systems is given by

$$\{\delta'\}_m = [T]\{\delta\}_m \tag{2.17}$$

in which [T] is the transformation matrix

$$[T] = \begin{bmatrix} [t] & 0 \\ 0 & [t] \end{bmatrix} \tag{2.18}$$

where

$$[t] = \begin{bmatrix} \cos\beta & 0 & \sin\beta & 0 \\ 0 & 1 & 0 & 0 \\ -\sin\beta & 0 & \cos\beta & 0 \\ 0 & 0 & 0 & 1 \end{bmatrix} \tag{2.19}$$

Substituting (2.17) into (2.9) and (2.12) leads to the following results, it being noted that in (2.9) and (2.12) $[K]_{mn}$, $\{F\}_m$, $\{\delta\}_m$ and $\{\delta\}_n$ are in local coordinates and hence are primed:

$$[K]_{mn} = [T]^T[K']_{mn}[T] \tag{2.20}$$

$$\{F\}_m = [T]^T\{F'\}_m \tag{2.21}$$

2.1.7 FLEXIBILITY METHOD

In conjunction with the flexibility method or force method, the finite strip method can also be used to analyze continuous bridge decks.

The bridge deck is first released from all the internal supports and is analyzed by the finite strip method. The deflections at all the internal supports due to external loads can be easily found, and is here denoted by a column vector $\{a\}$. Next,a unit vertical force is applied at internal support j alone and the deflection f_{ij} of each internal support i is obtained. This procedure produces the flexibility matrix $[F] = [f_{ij}]$.

For simplicity, all the internal supports are assumed to be rigid. Thus, the compatibility requirement of displacements yields following equations:

$$[F]\{R\} + \{a\} = 0 \tag{2.22}$$

from which the true reactions $\{R\}$ at the internal supports can be calculated.

Applying external loads and the reactions of the internal supports to the released structure will then give the final displacements and internal forces.

For plates and bridges over continuous line supports, it is also possible to treat each individual span as simply supported, with continuity of slopes over the supports (at the nodal line only) being subsequently restored. In this case the support moments are chosen as the redundant forces [24].

The combination of finite strip analysis with the flexibility method is also appli-

cable to box-girder bridges with intermediate diaphragm [25].

2.2 COMPOUND FINITE STRIP METHOD

Since 1983, a compound finite strip method has been developed for analysis of linear elastic flat plate systems continuous over deflecting supports such as flexible beams and columns [26,27]. This approach incorporates the effects of the support elements in a direct stiffness methodology, which makes the solution more straightforward than with the flexibility method.

The so-called compound strip is a finite plate strip which is composite with the supporting elements such as longitudinal beams, transverse beams and columns. All of these elements deform together, and their displacements can be expressed in terms of the nodal displacement parameters of the strip by means of the displacement functions of the strip (2.3). The strain energy of a compound strip includes not only the strain energy of the plate strip but also the following strain energy of the supporting elements:

(a) The flexural and torsional strain energy of the longitudinal beams

$$U_L = \sum_{i=1}^{NL}(\frac{EI}{2}\int(\frac{\partial^2 w}{\partial y^2})^2 dy + \frac{GJ}{2}\int(\frac{\partial^2 w}{\partial x \partial y})^2 dy)_i \qquad (2.23)$$

in which EI and GJ are the flexural and the torsional rigidity of a beam respectively; NL is the number of longitudinal beams in the strip.

(b) The flexural and torsional strain energy of the transverse beams

$$U_T = \sum_{i=1}^{NT}(\frac{EI}{2}\int(\frac{\partial^2 w}{\partial x^2})^2 dx + \frac{GJ}{2}\int(\frac{\partial^2 w}{\partial x \partial y})^2 dx)_i \tag{2.24}$$

in which NT is the number of the transverse beams in the strip.

(c) The axial strain energy and the flexural strain energy of columns

$$U_C = \sum_{i=1}^{NC}(\frac{1}{2}K_A w_c^2 + \frac{1}{2}K_{cx}(\frac{\partial w_c}{\partial x})^2 + \frac{1}{2}K_{cy}(\frac{\partial w_c}{\partial y})^2)_i \tag{2.25}$$

where K_A is the axial stiffness of column; K_{cx} and K_{cy} are the flexural stiffness of column in the directions x and y respectively; NC is the number of the columns supporting the strip.

Thus, the total strain energy of the compound strip, U_S, is the sum of following items:

$$U_S = U_P + U_L + U_T + U_C \tag{2.26}$$

where U_P is the flexural strain energy in the plate strip.

Substituting the expression of displacements (2.3) into (2.26), the strain energy U_S can be expressed in terms of the nodal displacement parameters of the strip in the form:

$$U_S = \frac{1}{2}\sum_{m=1}^{r}\sum_{n=1}^{r}\{\delta\}_m^T[K]_{mn}\{\delta\}_n \tag{2.27}$$

The stiffness submatrix of the compound strip, $[K]_{mn}$, is readily obtained.

This method has been successfully applied to the analysis of a variety of continuous plate structures.

2.3 EIGENFUNCTIONS OF CONTINUOUS BEAMS

In the analysis of continuous folded plates, the conventional finite strip method combined with flexibility approach and the compound strip method both experience difficulties in evaluation of the maximum negative bending moment at intermediate supports, because both methods employ the smooth beam eigenfunctions relevant to a single span to simulate the sharp peaks of the bending moment. The direct stiffness approach using eigenfunctions of continuous beams can solve this problem. This approach was applied to the dynamic analysis of continuous plates in 1974 [21], and was extended to static analysis of continuous folded plates under distributed loading in 1978 [22].

The eigenfunctions of a continuous beam with both ends simply supported can be obtained as follows [48].

The free vibration differential equation of the continuous beam is

$$\frac{d^4Y}{dy^4} = \mu^4 Y \tag{2.28}$$

Because the entire beam vibrates at the same frequency, μ is the same for all the spans. The general solution of this equation for the i-th span can then be expressed as

$$Y_i(y) = c_{i1}\sin(\mu y) + c_{i2}\cos(\mu y) + c_{i3}\sinh(\mu y) + c_{i4}\cosh(\mu y) \tag{2.29}$$

in which $c_{i1}...c_{i4}$ are constants which should be determined from the end conditions of the span.

If the first span is simply supported at the end $y_1 = 0$ (Fig. 2.4 a), the end conditions are $Y_1(0) = Y_1''(0) = 0$, $Y_1(l_1) = 0$. Equation (2.29) then becomes

$$Y_1(y) = A_1(\sin(\mu y_1) - \alpha_1 \sinh(\mu y_1)) \tag{2.30}$$

and

$$\alpha_1 = \sin(\mu l_1)/\sinh(\mu l_1).$$

For the last span n (Fig.2.4.b), in order to simplify mathematic procedures, it is convenient to use a new coordinate system, $y_n' = l_n - y_n$, to express the general solution for this span. Thus,

$$Y_n(y_n') = A_n(\sin(\mu y_n') - \alpha_n \sinh(\mu y_n')) \tag{2.31}$$

and

$$\alpha_n = \sin(\mu l_n)/\sinh(\mu l_n).$$

Each intermediate span i (Fig.2.5) can be treated as a combination of the above-mentioned two situations, i.e.,

$$Y_i(y) = A_{i1}(\sin(\mu y_i) - \alpha_i \sinh(\mu y_i)) + A_{i2}(\sin(\mu y_i') - \alpha_i \sinh(\mu y_i')) \tag{2.32}$$

where

$$\alpha_i = \sin(\mu l_i)/\sinh(\mu l_i)$$

and

$$y_i' = l_i - y_i.$$

Evidently, the first span and the last span of a continuous beam can be considered as the particular case of an intermediate span, with $A_{12} = 0$ and $A_{n1} = 0$. Therefore, (2.32) can be used to express the solutions for all spans. The slope, dY_i/dy,

and the curvature, d^2Y_i/dy^2 of a continuous beam can then be obtained as

$$\frac{dY_i}{dy} = \mu A_{i1}(\cos(\mu y_i) - \alpha_i \cosh(\mu y_i)) - \mu A_{i2}(\cos(\mu y_i') - \alpha_i \cosh(\mu y_i')) \quad (2.33)$$

$$\frac{d^2Y_i}{dy^2} = -\mu^2 A_{i1}(\sin(\mu y_i) + \alpha_i \sinh(\mu y_i)) - \mu^2 A_{i2}(\sin(\mu y_i') + \alpha_i \sinh(\mu y_i')) \quad (2.34)$$

For simplicity, the following notation is introduced:

$$SL_i = \cos(\mu l_i) - \alpha_i \cosh(\mu l_i) \quad (2.35)$$

The continuity conditions between span (i-1) and span i at support i

(Fig.2.6, $y_{i-1} = l_{i-1}$, $y_{i-1}' = 0$, $y_i = 0$, $y_i' = l_i$) are

1. The slope of adjacent spans must be equal. Therefore, by virtue of (2.33) and (2.35), the following equation can be obtained:

$$A_{i-1,1} SL_{i-1} - A_{i-1,2}(1 - \alpha_{i-1}) = A_{i1}(1 - \alpha_i) - A_{i2} SL_i \quad (2.36)$$

2. The bending moment and, consequently, the curvatures must also be continuous over support i. From equations (2.34) and (2.32) the following equation can similarly be obtained:

$$A_{i-1,1} \sin(\mu l_{i-1}) = A_{i2} \sin(\mu l_i) \quad (2.37)$$

The values of μ and A_{ij} (i=1...n, j=1,2) have to satisfy the continuity conditions (equation (2.36) and (2.37)) at all the intermediate supports. Further, μ must also satisfy the end conditions of the beam :

$$A_{12} = 0 \quad , \quad A_{n1} = 0 \quad (2.38)$$

Equation[2.38] states that $M_y = 0$ at both ends of the beam.

The A_{ij} represent only the mode shape, not its size; hence the following values may be adopted, without loss of generality,

$$A_{11} = 1 \quad , \quad A_{12} = 0 \tag{2.39}$$

For a given μ, A_{i1} and A_{i2} can be evaluated from the known values $A_{i-1,1}$ and $A_{i-1,2}$ by using equations (2.36) and (2.37). Doing this span by span, finally, all the A_{ij} up to A_{n1} and A_{n2}, which are the functions of μ, can be calculated.

If all the A_{ij} are not simultaneously zero, and the value of μ makes

$$A_{n1}(\mu) = 0 \tag{2.40}$$

then μ and A_{ij} have satisfied both the continuity conditions and the end conditions, therefore these values give a valid solution.

In solving equations (2.36) and (2.37), different procedures must be followed, depending on whether or not $\sin(\mu l_i) = 0$ and $\sin(\mu l_{i-1}) = 0$.

1. If $\sin(\mu l_i) \neq 0$, from equations (2.36) and (2.37)

$$A_{i2} = A_{i-1,1} \sin(\mu l_{i-1}) / \sin(\mu l_i) \tag{2.41}$$

$$A_{i1} = (A_{i-1,1} SL_{i-1} - A_{i-1,2}(1 - \alpha_{i-1}) + A_{i,2} SL_i)/(1 - \alpha_i) \tag{2.42}$$

2. If $\sin(\mu l_i) = 0$, $\mu l_i = m\pi$ (m=1,2...). From equation (2.32), it can then be seen that $\alpha_i = 0$ and

$$Y_i = A_{i1} \sin(\mu y_i) + A_{i2} \sin(\mu y')$$

$$= A_{i1} \sin(\mu y_i) + A_{i2} \sin(m\pi - \mu y_i)$$

$$= (A_{i1} - (-1)^m A_{i2}) \sin(\mu y_i)$$

This means that the coefficients A_{i1} and A_{i2} are dependent variables. Hence, and again without loss of generality, $A_{i2} = 0$ can be assumed, so that

$$Y_i = A_{i1} \sin(\mu y_i) \tag{2.43}$$

It is noted, however, that the calculation of A_{i1} still depends on the value of $\sin(\mu l_{i-1})$ associated with the previous span (i-1), and it must be considered separately for the two cases of $\sin(\mu l_{i-1}) = 0$ and $\sin(\mu l_{i-1}) \neq 0$.

a. If $\sin(\mu l_{i-1}) = 0$, then $Y_{i-1} = A_{i-1,1} \sin(\mu y_{i-1})$, $A_{i-1,2} = 0$ and equation (2.37) becomes an "identity". Then, from the slope continuity condition alone (2.36) we can obtain

$$A_{i1} = A_{i-1,1} \cos(\mu l_{i-1}) \tag{2.44}$$

b. If $\sin(\mu l_{i-1}) \neq 0$, $A_{i-1,1}$ must be zero, otherwise it does not satisfy equation(2.37). Then from the slope continuity condition alone (2.36), we can obtain

$$A_{i1} = -A_{i-1,2}(1 - \alpha_{i-1}) \tag{2.45}$$

However, in the case of the first interior support (between spans 1 and 2), if $\sin(\mu l_1)$ is not equal to zero but $sin(\mu l_2) = 0$, it can result in $A_{i,j} = 0$ $(i = 2...n, j = 1,2)$ from equations (2.39) (2.43) (2.44) etc. In this case, although $A_{n1} = 0$, μ is still not a solution of equation (2.28), because it violates the curvature continuity condition (equation (2.37)) at the first interior supports.

In the case of the last span, if $\sin(\mu l_n) = 0$, the curvature at the last end of beam is automatically equal to zero. Therefore, in this case, even though equation (2.40) is not satisfied, μ may still be a solution of the equation (2.28).

The first-order Reguli-Falsi iteration can be employed to solve the μ and A_{ij},(Fig.2.7).

Starting with the point μ_0, μ is increased by a small increment $\delta\mu$ in every step. At every trial point μ, $A_{n1}(\mu)$ is determined from $A_{11} = 1$ and $A_{12} = 0$ by using equations (2.41),(2.42), etc. However in some cases, if A_{n1} changes its sign between two trial points $\mu^{(0)} = \mu - \delta\mu$ (the previous trial point) and $\mu^{(1)} = \mu$ (the present trial point), the straight line is drawn between the points $(\mu^{(0)}, A_{n1}(\mu^{(0)}))$ and $(\mu^{(1)}, A_{n1}(\mu^{(1)}))$ as shown in Fig. 2.7. The intersection of the straight line with the μ axis is at $\mu^{(2)}$ which is closer to the solution $\bar{\mu}$ than $\mu^{(1)}$.

From $\mu^{(2)}$ the point $(\mu^{(2)}, A_{n1}(\mu^2))$ is located and the straight-line is connected to $(\mu^{(0)}, A_{n1}(\mu^{(0)}))$ or $(\mu^{(1)}, A_{n1}(\mu^{(1)}))$ depending on at which point A_{n1} has different sign from $A_{n1}(\mu^{(2)}))$. This locates $\mu^{(3)}$ on the μ axis,which is closer to the desired result than $\mu^{(2)}$.The process is repeated until

$$| A_{n1}(\mu) | < \epsilon_1 \tag{2.46}$$

The iteration formula is

$$\mu^{(r+1)} = \mu^{(r)} - A_{n1}(\mu^{(r)})(\mu^{(r)} - \mu^{(0)})/(A_{n1}(\mu^{(r)}) - A_{n1}(\mu^{(0)})) \tag{2.47}$$

Continuing to increase μ by $\delta\mu$ for every step, eventually, the necessary eigenvalues, μ_m, and modes, $A_{ij}^{(m)}$ are identified, these being as many as required by the finite strip analysis.

When the equation (2.41) was applied to determine A_{i2} from [illegible], both sides of equation (2.37) were divided by $\sin(\mu l_i)$, which might result in missing the solution of $\sin(\mu l_i) = 0$. Therefore, if during a particular increment of μ, $\sin(\mu l_i)$ changes

its sign, then $\mu = m\pi/l_i$ must be used as the trial point to calculate A_{ij} and see if this is one of the eigenvalues. However, in any other case, it must not take any trial value of μ equal to $m\pi/l_i$ so as to avoid situations such as $\sin(\mu l_2) = 0$ while $\sin(\mu l_1) \neq 0$, which will result in an erroneous value of $A_{n1}(\mu)$.

In the computer program, the following values were used:

$$\delta\mu = \pi/30l_{imax}$$

$$\mu_0 = 29.5\delta\mu$$

$$\epsilon_1 = 10^{-10}$$

and it is assumed that $\sin(\mu l_i) = 0$ if $\mid \sin(\mu l_i) \mid < 10^{-10}$.

If the lengths of all the spans are not exactly the same, but slightly different from each other, then,$\mu = m\pi/l_i$ is not a solution, and the sign of $A_{n1}(\mu)$ changes drastically near $\mu = m\pi/l_i$. In this case, smaller increments of $\delta\mu$ must be used in order to prevent the possibility of missing modes. For example, if all of the spans have magnitude either l_{max} or l_{min}, and if $0 < (l_{max} - l_{min})/l_{max} < 0.05$, it requires great care not to miss the solution near $m\pi/l_{max}$. The recommended remedial measure is that if there has been $m\pi/l_{max} - \mu < \delta\mu$, the increment is reduced to $\delta\mu' = m\pi(1/l_{min} - 1/l_{max})/4$ and the next trial value of μ is changed into $\mu = m\pi/l_{max} + \delta\mu'/2$. After the eigenvalue near $m\pi/l_{max}$ has been found, the original increment $\delta\mu = m\pi/30l_{imax}$ is resumed.

2.4 ANALYSIS OF CONTINUOUS HAUNCHED BRIDGES

In the present study, the finite strip method was extended to the analysis of haunched, continuous slab-on-girder bridges ([49], 1988) and haunched continuous box-girder bridges ([50], 1989).

In such an analysis, three types of strip are used, these being the top flange plate strip (Fig.2.2), the vertical web strip (Fig.2.8) and the bottom flange shell strip (Fig.2.9).

2.4.1 STRAIN-DISPLACEMENT RELATIONSHIP

For the top flange plate strip, the Cartesian coordinate system is used and the strain-displacement relationships (2.5) are applicable.

For the web strip of variable depth, the curvilinear orthogonal coordinate system $(\xi - \eta)$ is more convenient, in which η has units of length. The web can be divided into a number of equal or unequal width strips. The width of each strip is taken as $b = c \times b_w$, where b_w is the depth of web, with $0 < c \leq 1$. In the web, the most important deformation is in-plane bending, and the most significant strain components are the longitudinal normal strain ϵ_η and the longitudinal shear strain $\gamma_{\xi\eta}$. According to the actual proportion of ordinary haunched box-girder bridges,

the relationship between displacements and strains can be written as:

$$\begin{aligned}
\epsilon_\xi &= \frac{1}{b}\frac{\partial u}{\partial \xi} \\
\epsilon_\eta &= -\frac{u}{r_2} + \frac{\partial v}{\partial \eta} \\
\gamma_{\xi\eta} &= \frac{\partial u}{\partial \eta} + \frac{1}{b}\frac{\partial v}{\partial \xi} - \frac{u}{r_1} \\
\chi_\xi &= -\frac{1}{b^2}\frac{\partial^2 w}{\partial \xi^2} \\
\chi_\eta &= -\frac{\partial^2 w}{\partial \eta^2} \\
\chi_{\xi\eta} &= \frac{2}{b}\frac{\partial^2 w}{\partial \xi \partial \eta}
\end{aligned} \tag{2.48}$$

where r_1 and r_2 are the radii of curvature of coordinate lines (Fig.2.8), and the following approximate geometrical relationship can be taken with reasonable accuracy:

$$\frac{1}{r_2} = \frac{x'}{b_w}\frac{d^2 b_w}{d\eta^2} \tag{2.49}$$

$$r_1 = \frac{b_w}{\frac{db_w}{d\eta}}. \tag{2.50}$$

For the bottom flange shell strip, cylindrical surface coordinates are used, and the relationships between displacements and strains [59] are

$$\begin{aligned}
\epsilon_x &= \frac{\partial u}{\partial x} \\
\epsilon_y &= \frac{\partial v}{\partial y} - \frac{w}{R} \\
\gamma_{xy} &= \frac{\partial u}{\partial y} + \frac{\partial v}{\partial x} \\
\chi_x &= -\frac{\partial^2 w}{\partial x^2} \\
\chi_y &= -\frac{\partial^2 w}{\partial y^2} - \frac{w}{R^2}
\end{aligned} \tag{2.51}$$

$$\chi_{xy} = 2\frac{\partial^2 w}{\partial x \partial y} + \frac{2}{R}\frac{\partial v}{\partial x}$$

where R is the radius of curvature of the middle surface in the longitudinal direction, this is usually a function of y. In ordinary haunched box-girder bridges it can be assumed that

$$\frac{1}{R} = \frac{d^2 b_w}{d\eta^2} \tag{2.52}$$

2.4.2 DISPLACEMENT FUNCTIONS

The choice of suitable displacement functions is the most crucial and difficult part of the analysis. The right choice should lead to satisfactory results for maximum deflection and maximum longitudinal stress using only a very few terms of series if the analyzed bridge is subjected to uniform load (according to our experience, the required number of terms in series should be less than 5 times the number of spans).

After comprehensive research and experiments, the following formulations are worked out.

The strip displacement parameters for the m-th term are taken as:

$$\{\delta\}_m = (u_1\ v_1\ \bar{v}_1\ w_1\ \theta_1\ u_2\ v_2\ \bar{v}_2\ w_2\ \theta_2)_m^T$$

where v_1 and v_2 mainly represent the longitudinal movements due to in-plane bending and $\bar{v}_1$ and $\bar{v}_2$ mainly represent displacements in the y direction caused

by the longitudinal elongation or compression of the strip. The displacements within a plate strip are as follows:

$$u = \sum_{m=1}^{r}((1-X)u_1^m + Xu_2^m)Y_m(y)$$

$$v = \sum_{m=1}^{r}((1-X)v_1^m + Xv_2^m)Y_m^*(y) + \sum_{m=1}^{r}((1-X)\bar{v}_1^m + X\bar{v}_2^m)\bar{Y}_m(y) \tag{2.53}$$

$$w = \sum_{m=1}^{r}((1-3X^2+2X^3)w_1^m + x(1-2X+X^2)\theta_1^m + (3X^2-2X^3)w_2^m + x(X^2-X)\theta_2^m)Y_m(y)$$

where Y_m is the eigenfunction of a continuous beam which has the span lengths of the actual bridge, and

$$Y_m^*(y) = (b_w\frac{dY_m}{dy} - \frac{db_w}{dy}Y_m) \tag{2.54}$$

$$\bar{Y}_m(y) = \int_y (Y_m(y)/R)\,dy \tag{2.55}$$

$$X = x/b.$$

In (2.55) the interval of integration is from the origin of the first span to the current coordinate y. If the bottom line of web in each span is a parabolic curve, R can be assumed to be a constant(2.52), and the integration can be implemented analytically.

For the web strip, similar equations can be obtained by replacing X by ξ, x by bξ and y by η in the above equations.

These equations can also represent the displacements in the bottom flange shell strip without any change. However, in this case, x, y and z are cylindrical surface

coordinates, and u, v and w are the corresponding displacement components in this coordinate system (Fig.2.9) .

The expressions of u and w meet the boundary conditions at the end and intermediate supports which are assumed to be diaphragms that are infinitely stiff in their own planes, so that u=0 and w=0 there.

Substituting the displacement functions (2.53) for the web strip into the expression for $\gamma_{\xi\eta}$ in (2.48) and taking into consideration (2.50) and (2.54), $\gamma_{\xi\eta}$ can be expressed in terms of displacement parameters as follows:

$$\begin{aligned}
\gamma_{\xi\eta} &= \frac{\partial u}{\partial \eta} + \frac{1}{b}\frac{\partial v}{\partial \xi} - \frac{u}{r_1} \\
&= \sum_{m=1}^{r}((1-\xi)u_1^m + \xi u_2^m)\frac{dY_m}{d\eta} + \sum_{m=1}^{r}\{(-v_1^m + v_2^m)Y_m^*/b + (-\bar{v}_1^m + \bar{v}_2^m)\bar{Y}_m/b\} \\
&\quad - \sum_{m=1}^{r}((1-\xi)u_1^m + \xi u_2^m)Y_m/\frac{b_w}{\frac{db_w}{d\eta}} \\
&= \sum_{m=1}^{r}((1-\xi)u_1^m + \xi u_2^m)(\frac{dY_m}{d\eta} - \frac{db_w}{d\eta}Y_m/b_w) \\
&\quad + \sum_{m=1}^{r}\{(-v_1^m + v_2^m)Y_m^*/cb_w + (-\bar{v}_1^m + \bar{v}_2^m)\bar{Y}_m/b\} \\
&= \sum_{m=1}^{r}((1-\xi)u_1^m + \xi u_2^m)Y_m^*/b_w \\
&\quad + \sum_{m=1}^{r}\{(-v_1^m + v_2^m)Y_m^*/cb_w + (-\bar{v}_1^m + \bar{v}_2^m)\bar{Y}_m/b)
\end{aligned}$$

From the above expression, it can be seen that $\gamma_{\xi\eta} = 0$ if $u_1^m = u_2^m$, $u_1^m = (v_1^m - v_2^m)/c$ and $\bar{v}_1^m = \bar{v}_2^m$. This means that the displacement functions (2.53) can simulate the pure in-plane bending of webs at the term level.

Substituting the displacement functions (2.53) for the shell strip into the expression

for ϵ_y in (2.51), ϵ_y can be expressed in the following form:

$$\begin{aligned}\epsilon_y &= \frac{\partial v}{\partial y} - \frac{w}{R} \\ &= \sum_{m=1}^{r}((1-X)v_1^m + Xv_2^m)\frac{\partial Y_m^*}{\partial y} + \sum_{m=1}^{r}((1-X)\bar{v}_1^m + X\bar{v}_2^m)\frac{\partial \bar{Y}_m(y)}{\partial y} \\ &\quad - \sum_{m=1}^{r}((1-3X^2+2X^3)w_1^m + x(1-2X+X^2)\theta_1^m \\ &\quad +(3X^2-2X^3)w_2^m + x(X^2-X)\theta_2^m)Y_m(y)/R \end{aligned} \tag{2.56}$$

Using (2.55), we have

$$\frac{d\bar{Y}_m(y)}{dy} = \frac{d}{dy}\int_y (Y_m(y)/R)\,dy = Y_m(y)/R.$$

Substituting this expression into (2.56) gives the following result

$$\begin{aligned}\epsilon_y &= \sum_{m=1}^{r}((1-X)v_1^m + Xv_2^m)\frac{\partial Y_m^*}{\partial y} + \sum_{m=1}^{r}((1-X)\bar{v}_1^m + X\bar{v}_2^m)Y_m(y)/R \\ &\quad - \sum_{m=1}^{r}((1-3X^2+2X^3)w_1^m + x(1-2X+X^2)\theta_1^m \\ &\quad +(3X^2-2X^3)w_2^m + x(X^2-X)\theta_2^m)Y_m(y)/R \end{aligned}$$

From this expression, it is not difficult to find that all the terms of $Y_m(y)/R$ can be cancelled out if $\theta_1^m = 0$, $\theta_2^m = 0$, and $w_1^m = w_2^m = v_1^m = v_2^m$. Similar derivations can also prove that the longitudinal normal strains on any given curve $\xi = constant$ in the web strip and the entire top flange strip due to the arching effect w/R may be released under proper combinations of displacement parameters. This means that the displacement shape functions (2.53) are capable of reflecting that the arching effect can affect the distribution of longitudinal stress on the cross-section but may not cause any longitudinal stress at the neutral axis of the cross-section, because in any continuous bridge only the supports at one cross-section are fixed in the longitudinal direction.

If the displacement functions can not simulate the pure in-plane bending of the web ($\gamma_{\xi\eta} = 0$) or the stress-free longitudinal expansion of the bridge, the structure will seem much stiffer than it really is, and the correct answer may never be obtained.

2.4.3 SOLUTION PROCEDURES

Substituting the displacement functions (2.53) into (2.5),(2.48) and (2.51) respectively, the strains for each type of strip can be expressed in terms of displacement parameters in the following matrix form:

$$\{\epsilon\} = \sum_{m=1}^{r} [B]_m \{\delta\}_m$$

The stiffness matrix of the strip corresponding to the m-th and n-th series terms can then be expressed as (2.10):

$$[K]_{mn} = \int_L \int_b [B]_m^T [D][B]_n \, dx \, dy$$

In the x direction , the integration can be implemented numerically or analytically. However, in the y direction the Gaussian integration method has to be used, because of the complexity of the integration in the stiffness matrix. Since $\int_L Y'_m Y'_n \, dy$ and $\int_L Y''_m Y_n dy$ are not equal to zero when m and n are different, the terms of the series are coupled. In evaluating the stiffness matrix, we should choose the proper number of Gaussian integration points to achieve the desired accuracy and efficiency. When necessary, every span can be divided into several segments. In each segment, 8 to 10 integration points should be used. The selection of segment size and Gaussian integration points depends mainly on the number of highest-order harmonics in a given span, $n_\mu = \mu_{max} l_i / \pi$. Based on our experience the selection

	b_w is constant		b_w is variable	
N_μ	N_{seg}	N_G	N_{seg}	N_G
1,2	1	S	1	S
3,4	1	10	1	10
5,6	2	S	2	S
7,8	2	10	2	10
9	2	10	3	10
10,11	3	S	3	10
12-14	3	10	3	10
15-17	4	10	4	10
18	4	10	5	10
19-24	5	10	5	10
25-30	6	10	6	10
$N_\mu = \mu_{max} l_i/\pi$ N_{seg}: Number of Segments in Span i N_G: Number of Gauss Points in Each Segment				

Table 2.1: The Proper Number of Segments and Gauss Points

which will best achieve a reasonable balance between accuracy and efficiency of the solution is given in Table (2.1).

Following the procedures described in section 2.1, it is not difficult to obtain the final solutions required, including the distribution of displacements and stresses within the whole structure.

2.4.4 NUMERICAL EXAMPLES

1. Two span haunched continuous concrete box-girder bridge.

A multi cell box-girder bridge that is continuous over two equal spans is shown in Fig.2.10. It is haunched over the interior supports, with c=2.40m. The bridge span l is chosen equal to 40m, spacing between webs $b_2 = 0.075l = 3.00m$; thickness of

top slab, $h_1 = 0.005l = 0.20m$; thickness of bottom slab, $h_2 = 0.004l = 0.16m$; thickness of web, $b1 = 0.01125l = 0.45m$; length of haunched portion is considered to cover a distance of 12.00m. In this portion, the generating line of the bottom flange is a parabola. Total depth of the box girder(excluding the haunch), h=1.20m.

Due to symmetry, only half a cell needed to be analyzed; this half was divided into 3 strips, i.e. top flange strip AB, web strip BC and bottom Flange strip CD, as shown in the lower part of Fig. 2.10. The applied load is self-weight, corresponding to a specific weight of material of $24KN/m^3$. The material properties are E=25 GPa,$\nu = 0.2$.

Because the geometry of the bridge and applied loads are symmetrical with respect to the intermediate support, the deflection must also be symmetrical. Therefore we take only the symmetrical modes as the displacement functions in the longitudinal direction. The longitudinal stresses in a number of cross-sections are given in Table 2.2. These results were obtained by using 10 symmetrical terms in the series.

For comparison, the finite element program ADINA was also used to analyze the same structure. In this case, each flange is divided into 1 row of 16-node shell elements; the web is divided into 2 rows. Each row includes 8 elements (Fig.2.11). The results from this method are also given in Table 2.2. It can be seen that the results obtained from the finite strip analysis are in close agreement with the results obtained from the ADINA finite element analysis.

y_2 (m)	Method	σ_y (MPa) along nodal line			
		A	B	C	D
0	ADINA	4.226	4.292	-3.268	-4.287
	FSM	3.792	3.732	-4.075	-4.108
3	ADINA	4.373	4.378	-4.662	-4.343
	FSM	4.335	4.323	-4.869	-4.606
6	ADINA	4.389	4.610	-5.262	-4.729
	FSM	4.596	4.620	-5.353	-4.964
12	ADINA	1.566	1.403	-1.649	-1.814
	FSM	1.733	1.745	-2.061	-2.049
20	ADINA	-3.264	-3.535	4.115	3.803
	FSM	-3.142	-3.177	3.703	3.668
30	ADINA	-4.383	-4.637	5.398	5.109
	FSM	-4.344	-4.367	5.095	5.074

Table 2.2: Longitudinal Stresses in Two Span Box-Girder Bridge

2. Five span composite box-girder bridge

The bridge is a two-lane steel-concrete composite box-girder structure and is continuous over five spans. There are two steel boxes with a cast-in-place reinforced concrete deck. Figure 2.12 shows the elevation of the bridge, the depth of the webs and its typical cross sections. The loads are two five-axle trucks. Their wheel weights and positions are shown in Figure 2.13. For steel, the material properties are $E = 210GPa$, $\nu = 0.3$; for reinforced concrete ,$E = 25GPa$, $\nu = 0.2$.

The structure is divided into 22 strips with 21 nodal lines (Fig.2.14). 10 terms of the eigenfunction series are used in the analysis. The distribution of the longitudinal stress along cross-section x-x is depicted in Fig.2.15. The experimental values [60] of the same stress are also shown in this figure for comparison purpose. The maximum longitudinal stress of web is at the bottom corner of web No.1,its numerical value is 26.25 MPa while the experimental value is 24.47 MPa. The

maximum longitudinal stress of the flange appears in the bottom flange adjacent to web No.1,its numerical value is 25.67 MPa while the experimental value is 29.64 MPa.

It may be concluded that the numerical results are in good agreement with the experimental results for all high stress regions. Stress comparisons for other regions seem to be less favorable. However, this may be attributed to the accuracy of the experimental measurements themselves. Several irregularities of the experimental results, as shown in Fig.2.15, clearly indicate this possibility.

2.4.5 CONCLUSION

Having chosen the appropriate shape functions,the finite strip method can be effectively employed for analyzing continuous, haunched box-girder bridges. The method is simple, accurate and easy for engineers to use. In addition, because this method directly uses the eigenfunctions of a continuous beam as its shape functions in the longitudinal direction, it converges very quickly, especially for distributed loads. Therefore, it is more effective than both the finite element method and the conventional finite strip method.

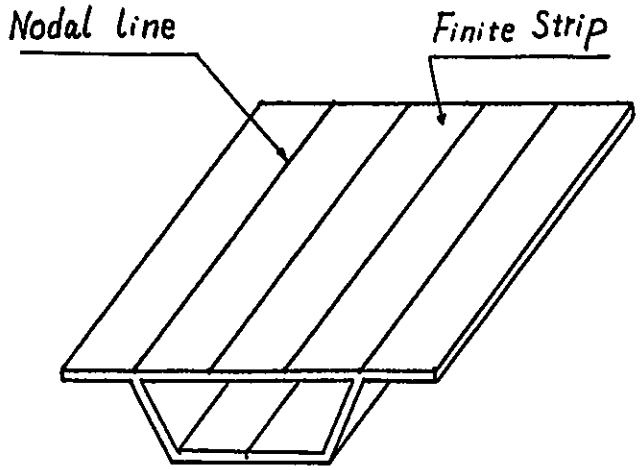

Figure 2.1: Structure Analyzed by F.S.M.

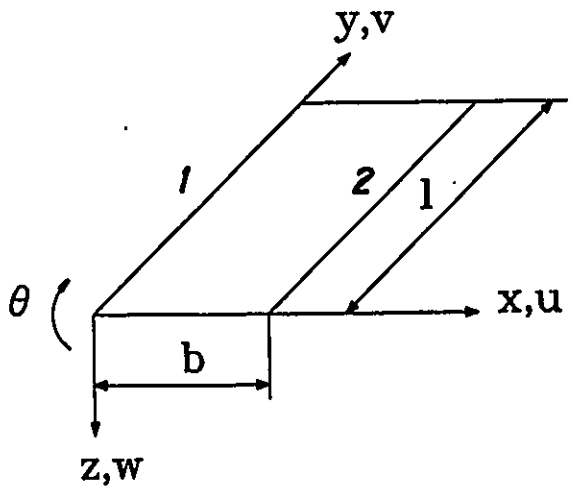

Figure 2.2: Folded Plate Strip

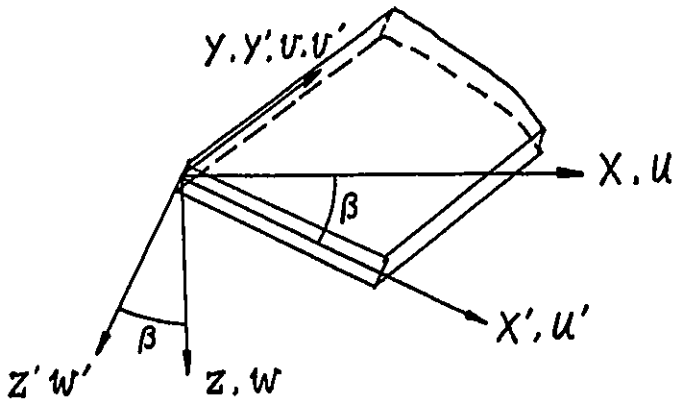

Figure 2.3: Individual and Common Coordinate System

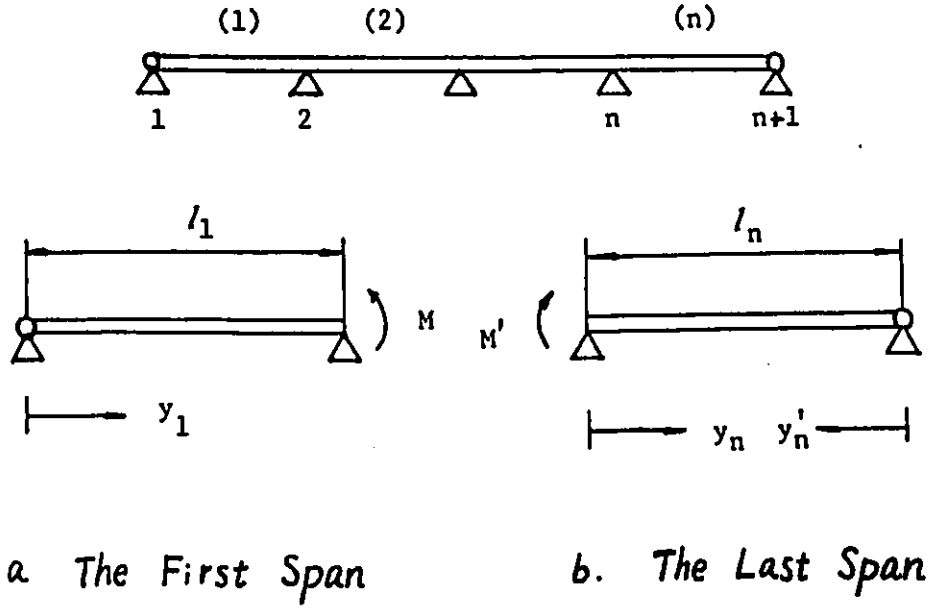

Figure 2.4: Continuous Beam

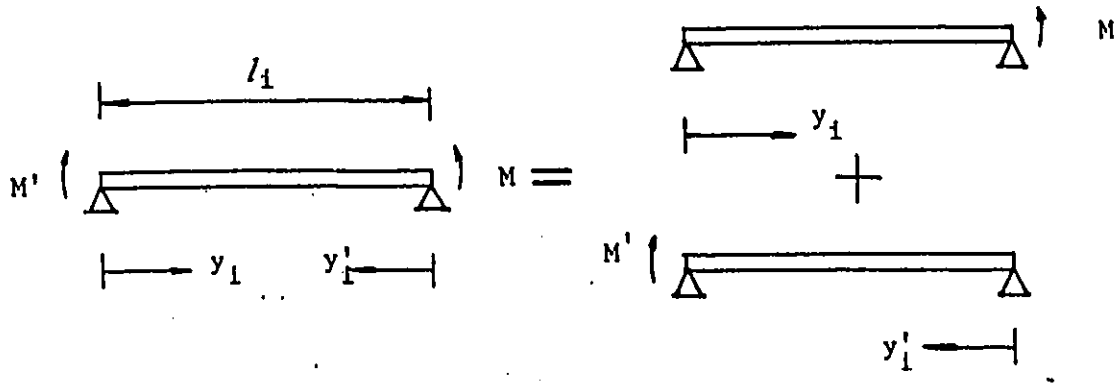

Figure 2.5: Span i

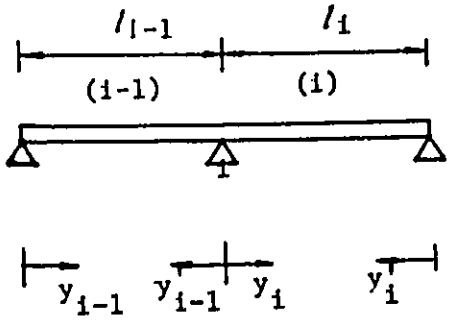

Figure 2.6: Support i

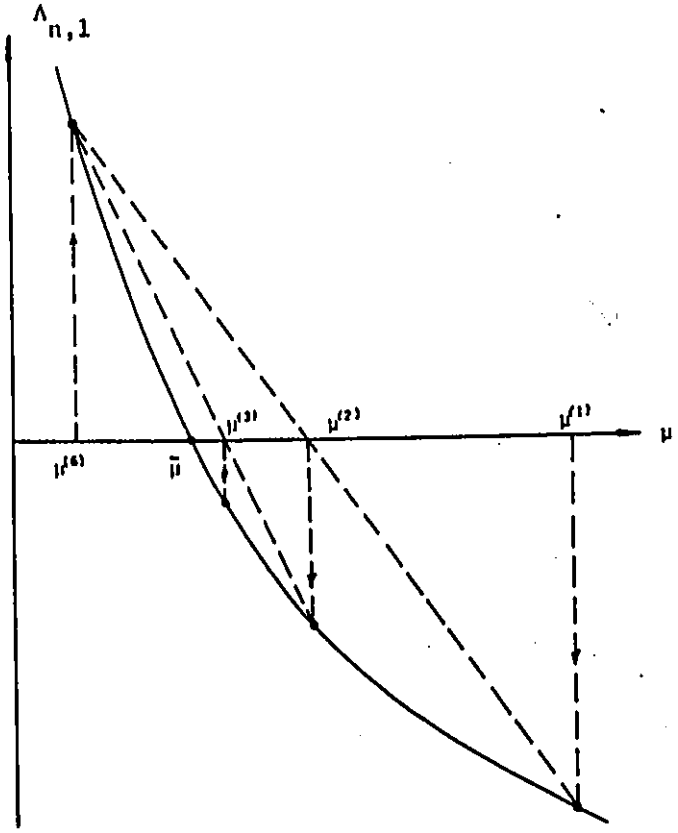

Figure 2.7: Reguli-Falsi Iteration

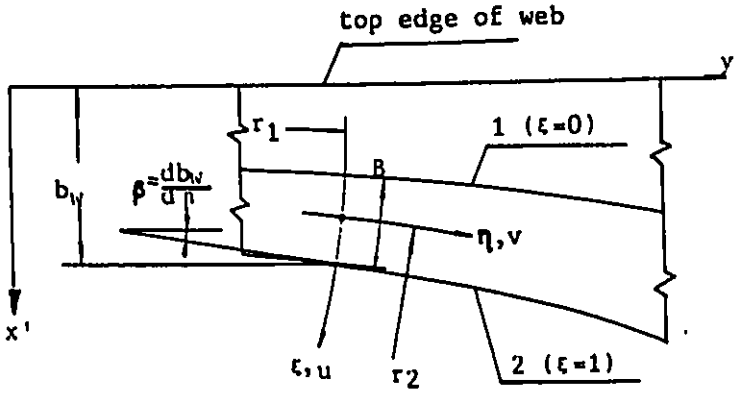

Figure 2.8: Web Strip

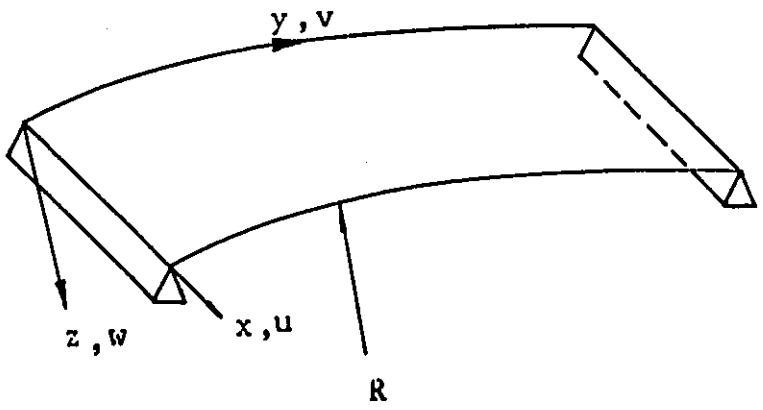

Figure 2.9: Shell Strip

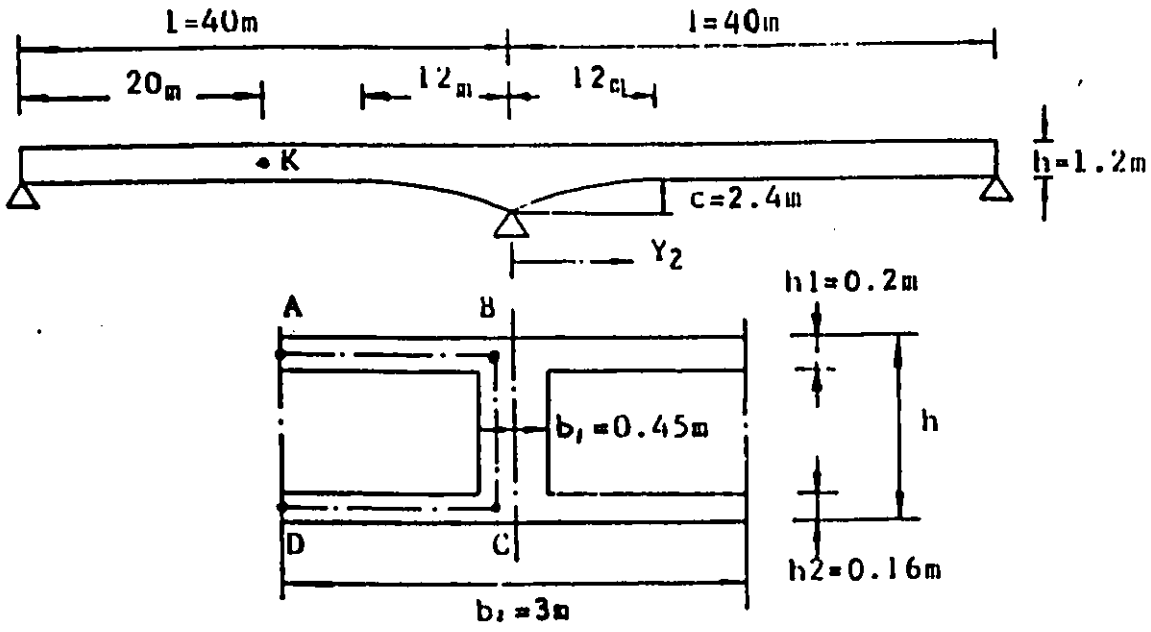

Figure 2.10: Continuous Box-Girder Bridge

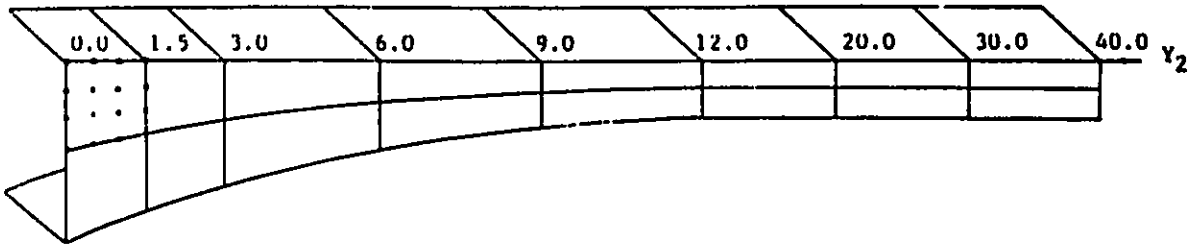

Figure 2.11: The Mesh of Shell Elements

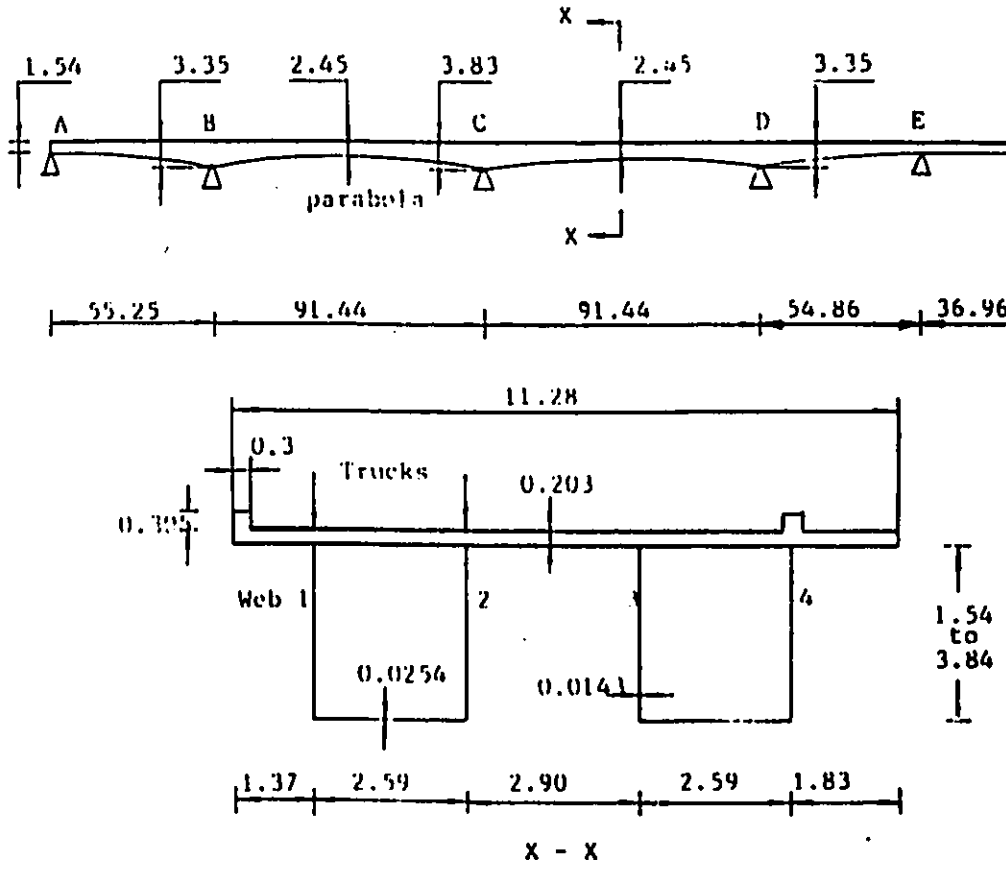

Figure 2.12: Five Span Composite Box-Girder Bridge (in M)

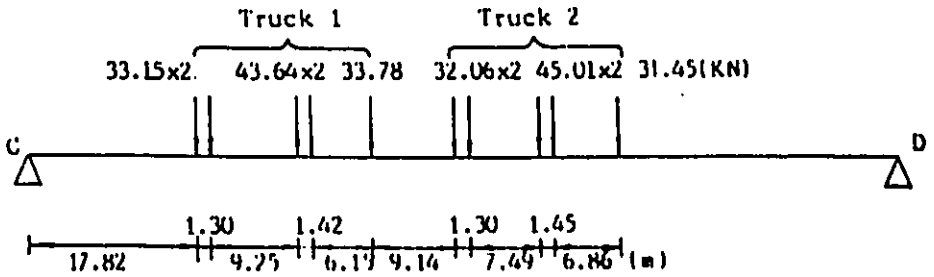

Figure 2.13: Wheel Weight of Two Trucks

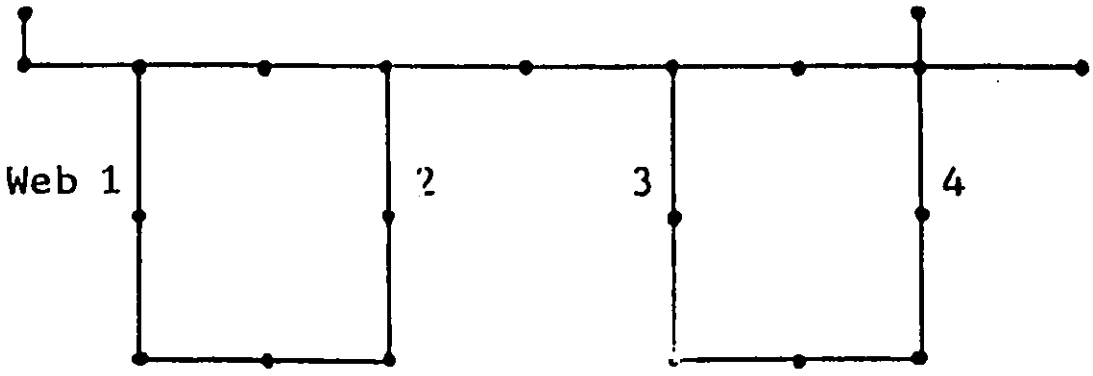

Figure 2.14: Division of Strips

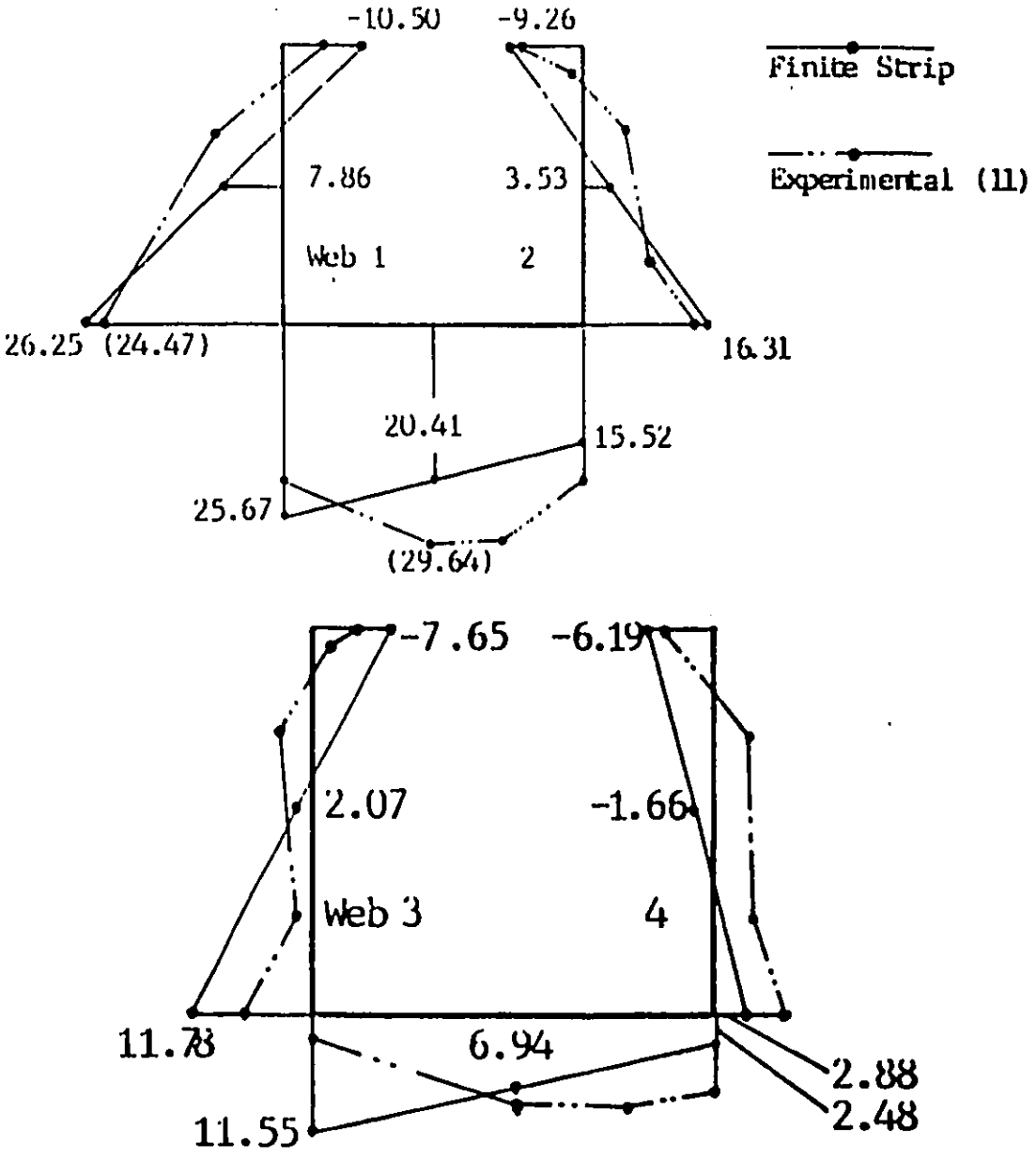

Figure 2.15: Longitudinal Stresses in Steel Girder at Section X-X (in Mpa)

Chapter 3

SPLINE FINITE STRIP METHOD

3.1 INTRODUCTION

The semi-analytical finite strip method is very efficient for analysis of prismatic structures under distributed loading. Nevertheless, the use of this method can sometimes lead to difficulties. For instance, because the beam functions are continuously differentiable, it is difficult to use such functions to simulate the abrupt changes of bending moment at internal supports or at loaded cross-sections of point forces. In addition, the beam functions must satisfy the end conditions of a strip a priori; hence, these functions can not deal with discrete supports at strip ends.

In order to overcome these difficulties, the mathematical tool called 'B_3 spline' was used as the longitudinal displacement functions to form the spline finite strips for analysis of rectangular plates by Y.K.Cheung et al [39] in 1982.

In this method, each nodal line is divided into a number of sections by evenly spaced knots, and every knot is taken as the center of a local B_3 spline, which is symmetrical to the center and has non-zero values over four consecutive sections (Fig.3.1). All the B_3 splines on a nodal line form a series which is utilized to simulate the longitudinal variation of displacements.

The B_3 spline functions can ensure continuity up to the second derivative (the so-called C_2 continuity). By comparison, in order to achieve the same continuity condition, the finite element method needs three times as many unknowns at the element nodes. Hence, when C_2 continuity is required, the use of B_3 splines is computationally much more efficient than the finite element method.

The second derivative of B_3 splines varies linearly in each longitudinal section, as a result of which it can more easily simulate peak values of bending moment at the loaded cross-section or at an intermediate support.

Furthermore, similarly to the finite element method, a spline finite strip can easily take up any prescribed external and internal boundary conditions e.g. by a penalty function approach. Thus, the spline strip method is more flexible than the semi-analytical finite strip method in imposing boundary conditions.

At a later stage in its development, the spline finite strip method was applied to the analysis of skew and arbitrary shaped plates, arbitrary curved slab bridges, rectangular box-girder bridges and to vibration, stability and postbuckling analysis [40 through 47].

In the present study, the spline finite strip method is extended to the analysis of continuous haunched slab on girder bridges [51] and box-girder bridges [52].

3.2 SPLINE FUNCTION INTERPOLATION

"Spline" was originally the name of a small flexible wooden strip employed by draughtsmen as a tool for drawing a continuous smooth curve segment by segment. Actually, the spline function can be derived with any required continuity (discontinuity) conditions. In the present study, the B_3 spline of equal section length [61] is chosen to represent the displacement. This function is a piecewise cubic polynomial with continuity up to the second derivative.

In order to use spline functions to interpolate an arbitrary function f(y) on the interval $a \leq y \leq b$, the interval is divided into a number of sections by evenly spaced knots y_i ($0 \leq i \leq m$, $y_0 = a$, $y_m = b$, $y_i = y_0 + i(b-a)/m$). The spline function $\Phi_i(y)$ with $y = y_i$ as the center is defined by

$$\Phi_i(y) = \frac{1}{h^3} \begin{cases} (y - y_{i-2})^3 & y_{i-2} \leq y \leq y_{i-1} \\ h^3 + 3h^2(y - y_{i-1}) + 3h(y - y_{i-1})^2 - 3(y - y_{i-1})^3 & y_{i-1} \leq y \leq y_i \\ h^3 + 3h^2(y_{i+1} - y) + 3h(y_{i+1} - y)^2 - 3(y_{i+1} - y)^3 & y_i \leq y \leq y_{i+1} \\ (y_{i+2} - y)^3 & y_{i+1} \leq y \leq y_{i+2} \\ 0 & \text{otherwise} \end{cases} \tag{3.1}$$

$\Phi_i(y)$ and its first and second derivatives are shown graphically in Fig.3.1, and their values at knots are given in Table 3.1. It can be seen that the function $\Phi_i(y)$ is twice continuously differentiable on the entire interval, and its second derivative is a linear function of y.

	y_{i-2}	y_{i-1}	y_i	y_{i+1}	y_{i+2}
$\Phi_i(y)$	0	1	4	1	0
$\Phi_i'(y)$	0	3/h	0	-3/h	0
$\Phi_i''(y)$	0	$6/h^2$	$-12/h^2$	$6/h^2$	0

Table 3.1: Values of Spline Function at Knots

The spline functions centered at all the knots comprise a series s(y) which is used to interpolate f(y). In each section the value of s(y) is related to four splines which are centered at the two ends of this section and the two knots next to those ends respectively. Therefore, two additional knots y_{-1} and y_{m+1} are needed to interpolate f(x) in the first and the last sections. Thus the series of the spline functions can be expressed as follows:

$$s(y) = \sum_{i=-1}^{m+1} c_i \Phi_i(y) \tag{3.2}$$

in which the c_i are coefficients to be determined by interpolation requirements such as:

$$\begin{aligned} s'(y_0) &= f'(y_0) \\ s(y_i) &= f(y_i) \quad 0 \le i \le m \\ s'(y_m) &= f'(y_m) \end{aligned} \tag{3.3}$$

Substituting (3.2) into (3.3) and using the values in Table 3.1 yield a set of linear equations with c_i as unknowns:

$$\begin{aligned} \frac{3}{h}(-c_{-1} + c_1) &= f'(y_0) \\ c_{i-1} + 4c_i + c_{i+1} &= f(y_i) \quad 0 \le i \le m \\ \frac{3}{h}(-c_{m-1} + c_{m+1}) &= f'(y_m) \end{aligned}$$

Solving these equations for c_i gives the required series of spline functions for interpolation:

$$s(y) = \sum_{i=-1}^{m+1} c_i \Phi_i(y) = f(y)$$

3.3 ANALYSIS OF CONTINUOUS HAUNCHED BRIDGES

A spline finite strip method for analysis of continuous haunched slab-on-girder bridges and box-girder bridges is developed in the present study. In this analysis, three types of strips are used, these being the top flange plate strip (Fig.3.2), the vertical web strip (Fig.3.3) and bottom flange shell strip (Fig.3.4).

3.3.1 STRAIN-DISPLACEMENT RELATIONSHIP

For the top flange plate strip, the strain-displacement relationships (2.5) are applicable.

For the vertical web strip, Eq.(2.5) are also valid. However, in this case, the x,y and z are referred to the axes of an individual local Cartesian coordinate system (see section 2.1.6), and u,v,w are the displacement components in the directions x,y and z respectively.

For the bottom flange shell strip, the strain-displacement relationships (2.51) can be used. It will be noted that Eq.(2.51) are given in the cylindrical surface coordinate system; in order to facilitate the assembling procedure of structure matrices,

the following coordinate transformations are required:

$$u' = u$$

$$v' = v\cos\beta + w\sin\beta$$

$$w' = -v\sin\beta + w\cos\beta$$

$$\frac{\partial}{\partial x'}f(x,y) = \frac{\partial}{\partial x}f(x,y)$$

$$\frac{\partial}{\partial y'}f(x,y) = \cos\beta\frac{\partial}{\partial y}f(x,y)$$

where x,y,z are the common Cartesian coordinates, and u,v,w are the corresponding displacements, whilst the primed ones are referred to the cylindrical surface coordinate system; f(x,y) represents an arbitrary function of x and y; and

$$\beta = arctan(\frac{db_w}{dy})$$

Performing the above coordinate transformations and doing some simplifications according to the theory of shallow shells, the relationships between strains in the bottom flange shell strip and its displacement components expressed in the common Cartesian coordinate system can be obtained in the following form:

$$\begin{aligned}
\epsilon'_x &= \frac{\partial u}{\partial x} \\
\epsilon'_y &= \frac{\partial v'}{\partial y'} - \frac{w'}{R} \\
&= \cos\beta\frac{\partial}{\partial y}(v\cos\beta + w\sin\beta) - \frac{w'}{R} \\
&= \cos\beta\{\frac{\partial v}{\partial y}\cos\beta + \frac{\partial w}{\partial y}\sin\beta) + (-v\sin\beta + w\cos\beta)\frac{\partial\beta}{\partial y}\} - \frac{w'}{R} \\
&= \cos\beta(\frac{\partial v}{\partial y}\cos\beta + \frac{\partial w}{\partial y}\sin\beta) + w'\frac{\partial\beta}{\partial y'} - \frac{w'}{R} \\
&= \frac{\partial v}{\partial y}\cos^2\beta + \frac{\partial w}{\partial y}\cos\beta\sin\beta
\end{aligned}$$

$$\begin{aligned}
\gamma'_{xy} &= \frac{\partial u'}{\partial y'} + \frac{\partial v'}{\partial x'} \\
&= \frac{\partial u}{\partial y}\cos\beta + \frac{\partial v}{\partial x}\cos\beta + \frac{\partial w}{\partial x}\sin\beta \\
\chi'_x &= -\frac{\partial^2 w}{\partial x^2} \\
\chi'_y &= -\frac{\partial^2 w}{\partial y^2} \\
\chi'_{xy} &= 2\frac{\partial^2 w}{\partial x \partial y}
\end{aligned} \tag{3.4}$$

where $1/R = \partial\beta/\partial y'$ is the curvature of the shell strip and can be calculated by means of (2.52).

3.3.2 DISPLACEMENT FUNCTIONS

In analysis, each nodal line is divided into an even number of sections by knots, and these sections are grouped pair by pair (Fig.3.2). The B_3 spline expressions are employed as the longitudinal displacement functions for displacement components u and w, and quadratic interpolation in each pair of sections is used as the longitudinal displacement function for v.

The displacement parameters of the strip corresponding to the i th section knot are

$$\{\delta\}_i = (u_1\ v_1\ w_1\ \theta_1\ u_2\ v_2\ w_2\ \theta_2)_i^T$$

The displacement field within a top flange plate strip or a bottom flange shell strip is:

$$u = \sum_{i=-1}^{m+1}((1-X)u_{1i} + Xu_{2i})\Phi_i(y)$$

$$v = \sum_{j=1}^{3}((1-X)v_{1j} + Xv_{2j})L_j(y) \tag{3.5}$$

$$w = \sum_{i=-1}^{m+1}((1-3X^2+2X^3)w_{1i} + x(1-2X+X^2)\theta_{1i} + (3X^2-2X^3)w_{2i} + x(X^2-X)\theta_{2i})\Phi_i(y)$$

where $X = x/b$, m is the number of sections, Φ_i is the B_3 spline expression with $y = y_i$ as the center, j is the local number of knot i in the corresponding pair of sections, and L_j are quadratic interpolations in the following form:

$$L_1(y) = (1-Y)(1-0.5Y)$$

$$L_2(y) = Y(2-Y)$$

$$L_3(y) = 0.5Y(Y-1)$$

in which, $Y = y'/h$ (see Fig.3.2).

Eq. (3.5) are also applicable for the vertical web strip. However, in this case, the x,y,z are local Cartesian coordinates, and u,v,w are corresponding displacement components. In addition, X is not only a function of coordinate x, but also of the coordinate y in the form:

$$X = \frac{x-x_1}{b} = \frac{x}{cb_w(y)} - \frac{c_1}{c}$$

where $b_w(y)$ is the variable depth of the web, $b = cb_w$ is the width of the strip and $x_1 = c_1 b_w$ is the coordinate of nodal line 1, with c and c_1 being constant (Fig. 3.3).

Substituting the displacement functions of the web strip into the expression for ϵ_y in (2.5) yields the following relationship:

$$\epsilon_y = \frac{\partial v}{\partial y}$$

$$= \sum_{j=1}^{3}\{\frac{\partial}{\partial y}((1-X)v_{1j}+Xv_{2j})L_j(y)+((1-X)v_{1j}+Xv_{2j})\frac{dL_j}{dy}(y)\}$$

$$= \sum_{j=1}^{3}\{(v_{1j}-v_{2j})\frac{x}{cb_w^2}\frac{db_w}{dy}L_j(y)+((1-X)v_{1j}+Xv_{2j})\frac{dL_j}{dy}(y)\} \qquad (3.6)$$

It can be seen that ϵ_y depends not only on the first derivative of the longitudinal displacement function $\frac{dL_j}{dy}$, but also on the slope of bottom line of the web, $\frac{db_w}{dy}$. In the actual structure, the slope of the bottom line of web may have abrupt changes, especially at intermediate supports. This may cause discontinuities of the resulting strain ϵ_y and significant error in the results of the most important stress component σ_y if the B_3 spline functions (with undesired continuity of their first derivatives) are used as the longitudinal displacement function for v. The use of quadratic interpolations as the longitudinal displacement functions of v can solve this problem as long as the abrupt changes of the slope are located at the ends of the pairs, because the first derivatives of $L_j(y)$ can be discontinuous across these locations. An alternative method of treating this problem is to use the spline function with only C_0 continuity as the longitudinal displacement functions of v; however, this will produce constant longitudinal strain and, consequently, poor convergence.

Once the displacement functions for the strips have been chosen, the strip characteristics, including stiffness, load etc., can be obtained in line with the standard finite strip formulation (see Section 2.1).

3.3.3 PENALTY FUNCTION APPROACH

A number of methods for imposing boundary conditions have been proposed by Cheung et al [39-44]. In the present study, the penalty function approach is chosen to treat end and intermediate support conditions of the strips.

As an example, it is assumed that the displacement component w at point (x, y) is prescribed to be zero, that is:

$$w = \sum_i N_i(x, y) w_i = 0$$

where $N_i(x, y)$ and w_i are associated displacement function and displacement parameter respectively.

In order to impose this constraint in analysis, a fictitious spring with large stiffness α might be introduced in the corresponding direction at the point (x,y). Its strain energy or penalty function is:

$$U = \frac{1}{2}\alpha w^2 = \frac{1}{2}\alpha \sum_i \sum_j N_i(x, y) N_j(x, y) w_i w_j$$

From this expression it can be seen that the stiffness matrix of this imaginary spring is:

$$[k_{ij}] = [\alpha N_i(x, y) N_j(x, y)]$$

If the first derivative of deflection, say $\frac{\partial w}{\partial y}$, at point (x, y) is prescribed to be zero, then

$$\frac{\partial w}{\partial y} = \sum_i \frac{\partial N_i(x, y)}{\partial y} w_i = 0$$

Following the same procedure, the required stiffness matrix for this constraint can be obtained as:

$$[k_{ij}] = [\alpha \frac{\partial N_i(x,y)}{\partial y} \frac{\partial N_j(x,y)}{\partial y}]$$

Assembling the stiffness matrices of all point constraints with the structural stiffness matrix will accomplish the treatment of boundary conditions.

An elastic support can also be included by the same method, as long as the α is the actual stiffness of this support.

3.3.4 NUMERICAL EXAMPLES

1. Continuous Beam with Variable Depth under Point Load

The beam is continuous over two equal spans $l_1 = l_2 = 10$ m (Fig.3.5). The depth of beam is 1.0 m at both ends, 2.0 m over the intermediate support, and varies linearly in-between. The width of the beam is 1.0 m. The properties of material are E=10000 MPa and $\nu = 0$. A vertical point force $P = 2.0MN$ is acting at the center of the second span. The beam is analyzed by using only one web strip. The deflection at the loaded cross section and the longitudinal stresses at several points along the bottom nodal line are listed in Table 3.2, in which the values from beam theory (shear deformation included) are also given for comparison. It can be seen that this method is accurate and that it converges very rapidly.

2. 2-Span Haunched Continuous Concrete Slab-on-Girder Bridge

The bridge with span $l_1 = 12m$ and $l_2 = 16m$ is shown in Fig.3.6. The end of shorter span is simply supported, and the other end is fixed. The thickness of the

Number of sections	w (m) y=15 m	σ_y (MPa) y=5 m	y=10 m	y=15 m
8	0.011279	-3.520	-4.111	9.998
16	0.011480	-3.370	-3.826	9.995
24	0.011524	-3.347	-3.777	10.002
beam theory	0.011265	-3.339	-3.756	9.994

Table 3.2: Deflection and Longitudinal Stresses in Continuous Beam

slab is 0.2 m and the thickness of all webs is 0.4 m. The spacing of webs is 2.8 m. The bottom line of the web is parabola in each span. The depth of web (from its bottom to the middle plane of slab) is 0.5 m at the simply supported end, 1.1 m over the intermediate support, 0.5 m at the center of longer span, and 0.8 m at the fixed end. The material properties are E=27000 MPa, $\nu = 0.15$. In loading case 1, a unit vertical point load P=1.0 MN acts on the top of the exterior girder at the center of the longer span; in case 2, the same load moves to the top of the central girder on the same cross section. In analysis, the structure is divided into 12 slab strips, 7 web strips and 28 longitudinal sections. The resulting longitudinal stresses on the top and bottom of webs at a number of cross sections are listed in Table 3.3.

If the load is put on the second or third girder, the maximum longitudinal stress occurs at the bottom of the loaded girder at the loaded cross section and its value is little different from the one in loading case 2.

3. Two span haunched continuous steel box-girder bridge.

A multi cell box-girder bridge is continuous over two equal spans as shown in Fig.3.7. It is haunched over the interior supports, with c=2.40 m. The bridge

Loading Case	Cross Section	σ_y (MPa) on the top and bottom of			
		Girder 1	Girder 2	Girder 3	Girder 4
1	A	5.24	1.22	0.01	-
		-10.75	-2.76	0.06	-
	B	-15.64	-2.41	-0.37	-
		45.51	10.75	1.67	-
	C	11.66	3.51	0.55	-
		-29.36	-10.06	-1.15	-
2	A	-	0.14	1.03	1.86
		-	-0.21	-2.87	-6.20
	B	-	-0.42	-1.59	-6.42
		-	1.84	8.62	30.19
	C	-	0.62	2.49	3.95
		-	-1.71	-8.83	-16.10

Table 3.3: Longitudinal Stresses in Two Span Slab-on-Girder Bridge

span 1 is chosen as 40 m, the spacing between webs $b_2 = 2.80$ m; the thickness of the flanges and the webs is 4.0 cm; the haunched portion covers a distance of 12 m. In this portion, the generating line of the bottom flange is a parabola. The depth of the box girder(excluding the haunch) is 1.04 m. The load is self-weight, corresponding to a specific weight of material of $76.4 KN/m^3$. The material properties are E=200,000 MPa, $\nu = 0.3$.

Due to symmetry, only half a cell and one span needed to be analyzed.

For comparison, this structure was first analyzed by the finite element package ADINA. Each flange was divided into 1 row of 16-node shell elements; the web was divided into 2 rows, with each row including 8 elements. Using the Mainframe AMDAHL-5860, a CPU time of 33.6 sec. was required for this analysis.

Next, the semi-analytical finite strip method (see Section 2.4) was employed to an-

alyze the same structure. The top flange, web and bottom flange were divided into one strip each; 10 symmetrical terms were taken in the longitudinal displacement function series. The CPU time needed was 19.3 sec.

Finally, the spline finite strip method was used. The flanges and web were divided into 1 strip with 20 longitudinal sections each. The CPU time needed was reduced to 11.7 sec.

The resulting longitudinal stresses of the middle surface at a number of cross sections are listed in Table 3.4, in which FSM denotes the semi-analytical finite strip method (Section 2.4) and SFSM represents the spline finite strip method.

In the analysis of this structure, the time spent on formation of stiffness matrices is the largest component of total CPU time consumed. The spline function is relatively simpler than the beam eigenfunction, and it is this feature that results in its higher efficiency.

4. Five Span Composite Box-Girder Bridge

The five span continuous haunched box-girder bridge, described in Subsection 2.4.4 Example 2, is analyzed by the spline finite strip method .

In analysis, the structure is divided into 20 strips with 36 longitudinal sections (Fig.3.8). The resulting longitudinal stress distribution at the cross-section X-X (see Fig.2.12) is depicted in Fig.3.9. It can be seen that the maximum longitudinal stress appears at the exterior bottom corner of the box girder under the trucks, where its value is 23.02 MPa. The experimental value of the stress at the same

y_2 (m)	Method	σ_y (MPa) along nodal line	
		B	C
0	ADINA	13.37	-11.75
	FSM	11.72	-11.16
	SFSM	12.46	-11.95
3	ADINA	13.70	-15.11
	FSM	13.58	-16.69
	SFSM	13.88	-14.44
6	ADINA	13.92	-16.85
	FSM	13.95	-18.04
	SFSM	14.03	-16.01
12	ADINA	3.53	-3.69
	FSM	4.36	-4.46
	SFSM	5.02	-4.00
20	ADINA	-10.71	11.19
	FSM	-10.23	10.38
	SFSM	-10.65	10.65
30	ADINA	-14.26	14.26
	FSM	-13.80	13.72
	SFSM	-13.57	13.57

Table 3.4: Longitudinal Stresses in Two Span Box-Girder Bridge

point is 24.47 MPa [60].

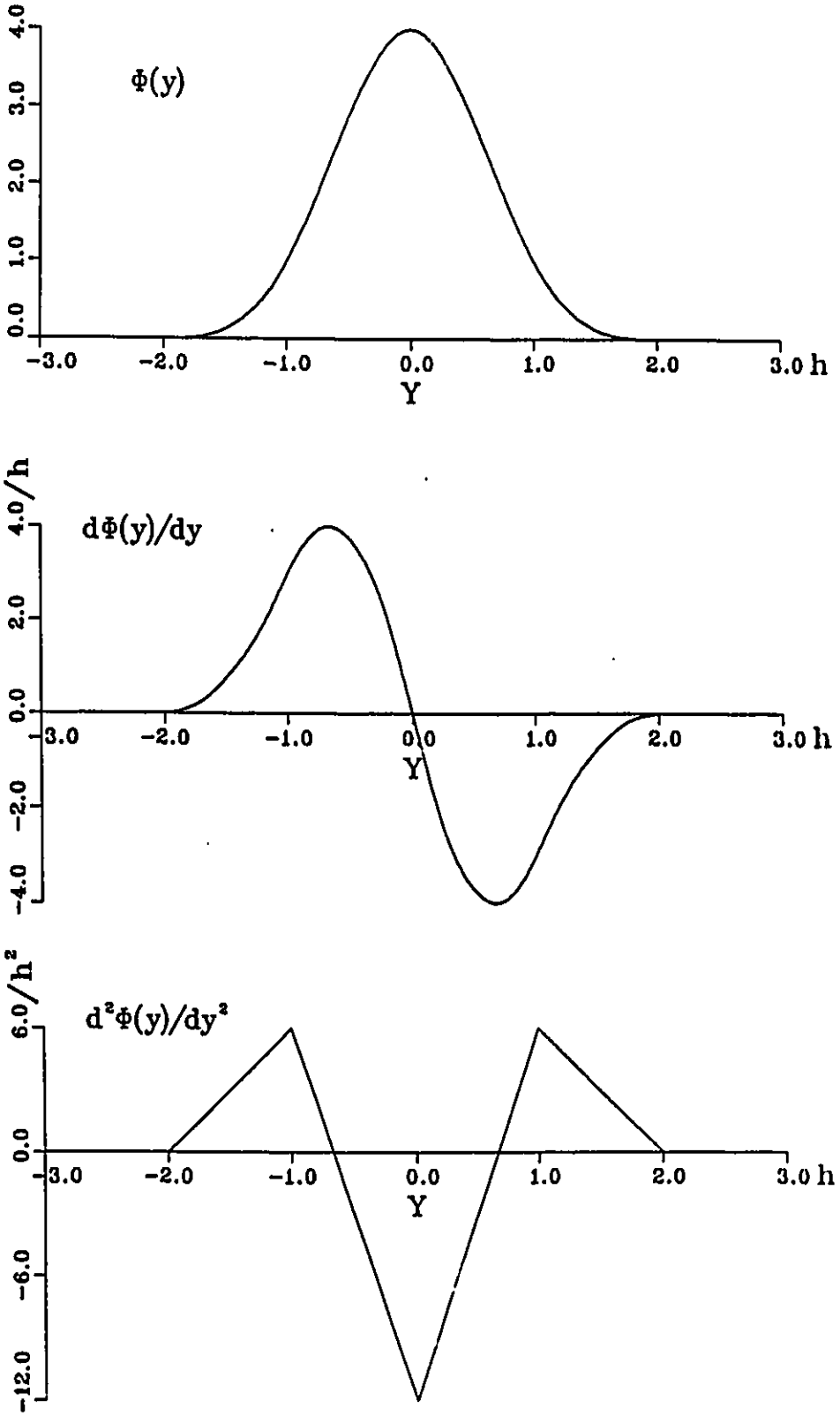

Figure 3.1: Spline Function and Its Derivatives

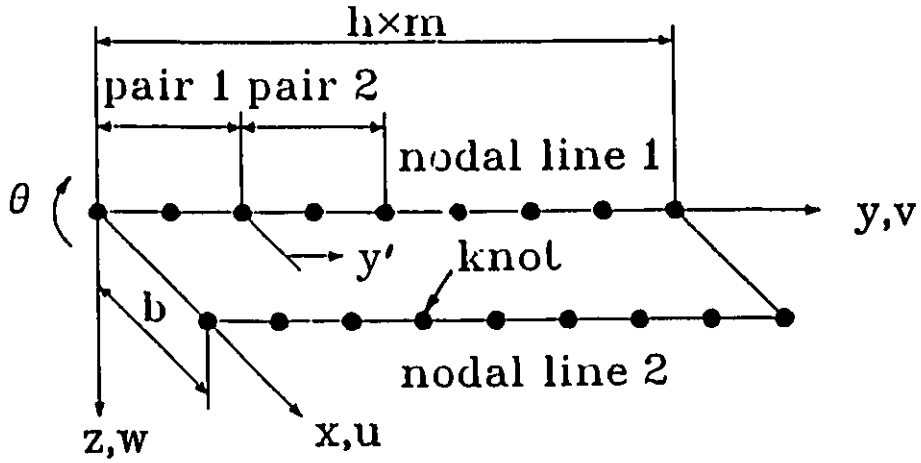

Figure 3.2: Plate Strip

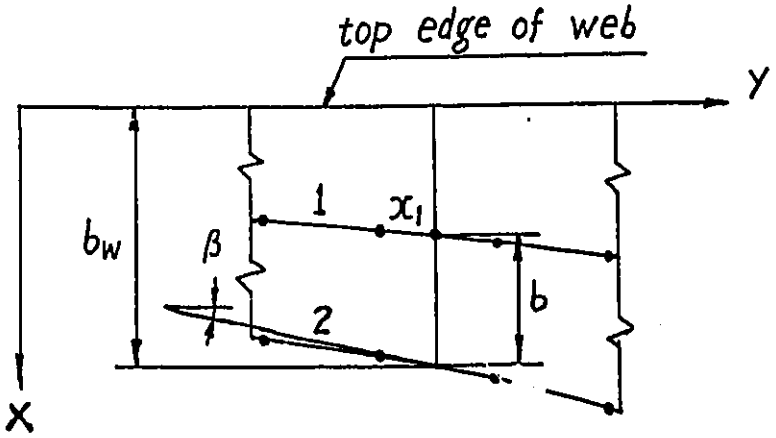

Figure 3.3: Web Strip in Individual System

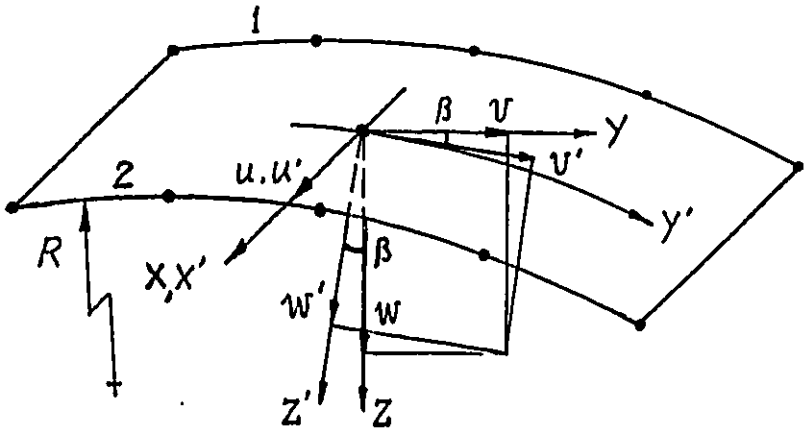

Figure 3.4: Shell Strip

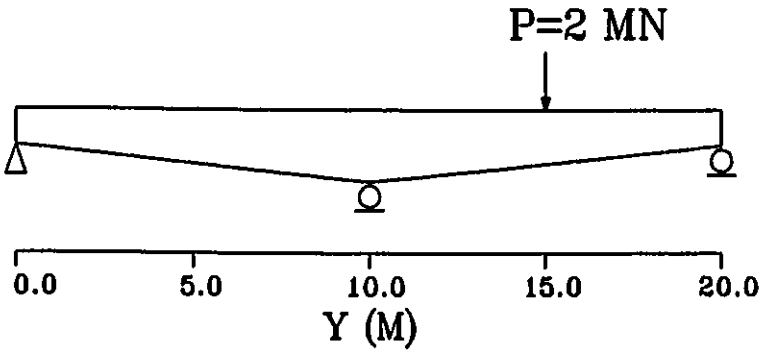

Figure 3.5: Continuous Beam

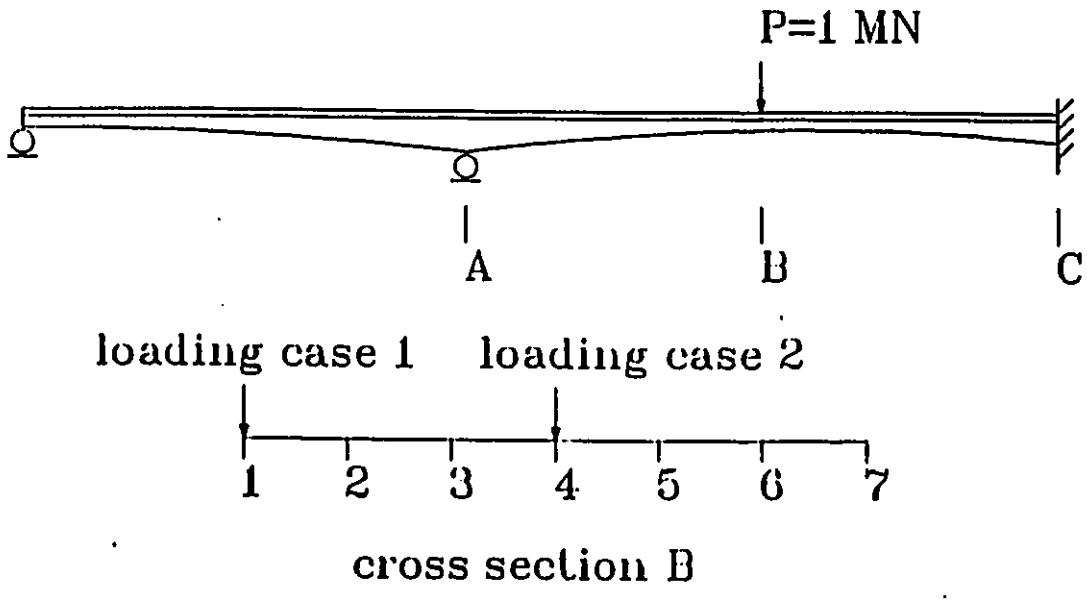

Figure 3.6: Haunched Continuous Bridge

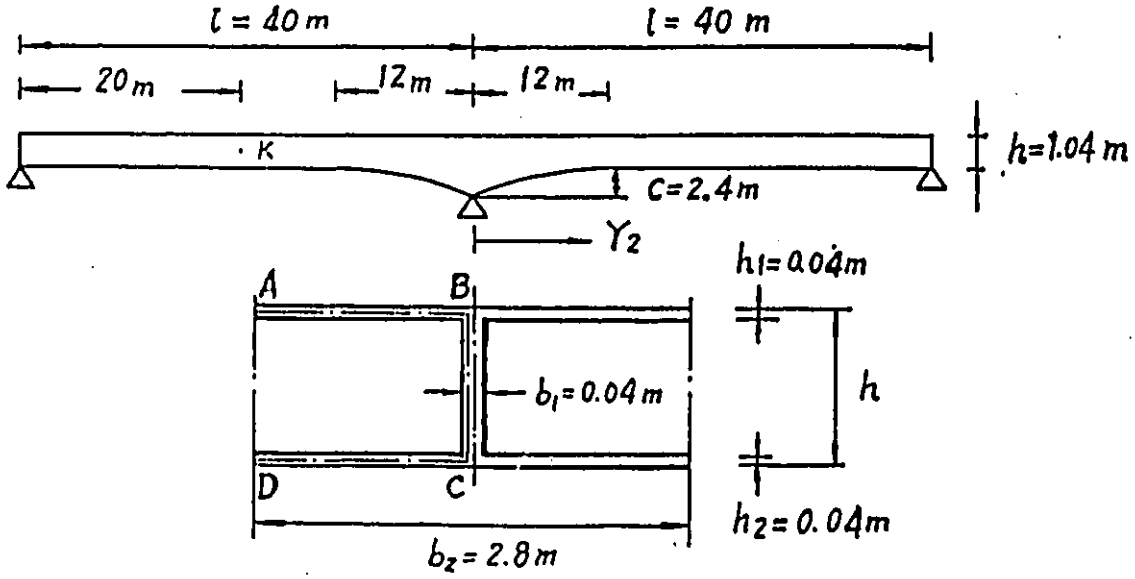

Figure 3.7: Haunched Continuous Box-Girder Bridge

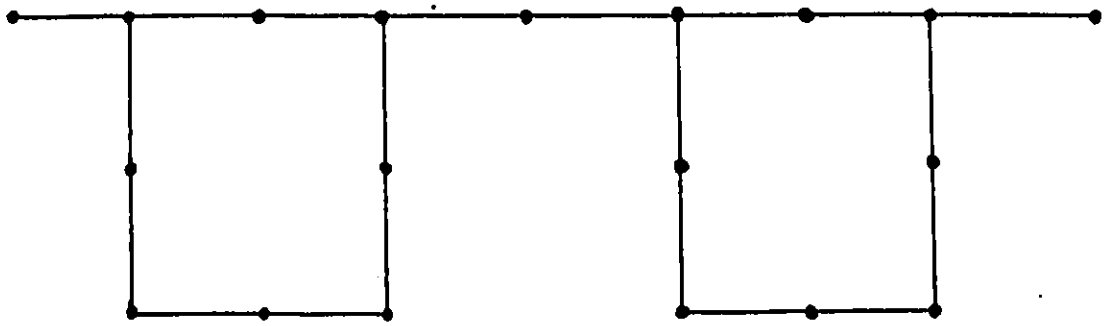

Figure 3.8: Division of Strips

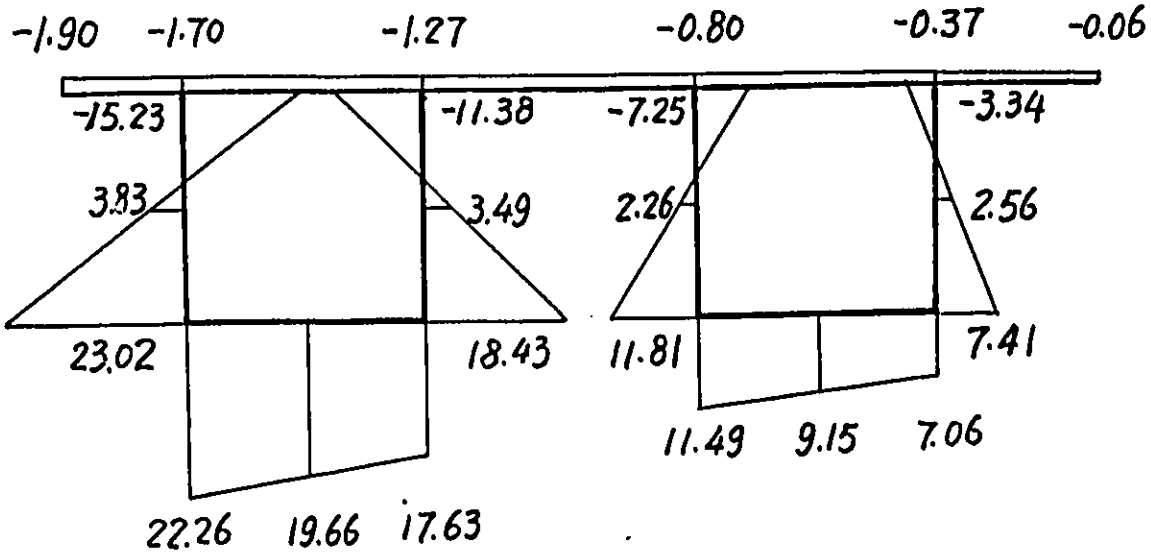

Figure 3.9: Longitudinal Stresses at Cross-Section X-X (in Mpa)

Chapter 4

NONLINEAR ANALYSIS

The finite strip methods have been extended to nonlinear structural analysis such as post-buckling behavior and geometrical nonlinear analysis of plate structures [28-33] since 1978, to material nonlinear analysis of steel structures and reinforced concrete slabs [34-37] since 1986, to large deflection elasto-plastic analysis of plate structures [38] since 1989,etc. All of these developments have confirmed that the advantages of the finite strip methods over finite element methods, which are higher efficiency, less requirement for computer storage, CPU time and input data, hold in respect of nonlinear structural analysis, just as they were known to do in linear analysis.

In the present study, a finite strip method for the nonlinear analysis of cable-stayed bridges [53,54] is developed. Furthermore, A more efficient finite strip method for geometrically nonlinear analysis of plates [55] and a more accurate finite strip method for materially nonlinear analysis of reinforced slabs [56] are also developed.

4.1 NONLINEAR ANALYSIS OF CABLE-STAYED BRIDGES

In the present section, the finite strip method using the eigenfunctions of a continuous beam having the same span lengths as the actual bridge is employed for 3-D analysis of the girder of the cable-stayed bridge.

In order to improve the accuracy of bending moments at the cable attachment points, the eigenfunctions of a fictitious continuous beam with additional supports at all the cable attachment points are added to the series of longitudinal displacement functions.

Using the flexibility approach, the entire girder structure is transformed into a substructure having deflections at the cable attachment points as the only degrees of freedom, so that a matrix of only small size is involved in the nonlinear solution.

The theory of the catenary is utilized in calculating the cable tension from the positions of the cable ends. In this way, the nonlinearity due to sag and angle change of cables is taken into consideration.

The initial-stiffness method is taken in the nonlinear iterations. Hence, the stiffness matrix of the bridge is formed and inverted only once. Because of the high tensions of the cables, the nonlinearity is not very marked, and the convergence can be achieved within very few iterations.

In accordance with the ASCE Task Committee recommendation [62] the nonlin-

cavities of the girder and pylons generally are not taken into account. The effect of axial displacements of girder and pylons on cable tensions is also neglected. It is further assumed that all cables are fixed to the pylons, and that the girder is simply supported on piers as it passes through the pylon legs, which are fixed to the piers.

4.1.1 FINITE STRIP ANALYSIS OF GIRDER

In most publications the girder of a cable-stayed bridge is treated as a beam [63,64]. However, to be more accurate, the girder should be considered as a three dimensional structure, and analyzed by finite element method [65]. Because of the nonlinear behavior of the cables, iterative methods are normally required for the analysis, and if the entire girder has to be analyzed in every iteration the computer time requirement is likely to become unacceptably large.

In most cable-stayed bridges, the girders are continuous over two or three spans. For the three dimensional analysis of such a girder, the finite strip method using the eigenfunctions of a continuous beam which has span lengths equal to those of the actual bridge (Chapter 2), is preferable to finite element analysis, because of its higher efficiency.

Because the second order derivatives of every beam function have smooth variation within each span, it is difficult to simulate the peak value of longitudinal bending moment at any cable attachment point. Actually, the deflection of a girder at any cable attachment point is much smaller than the deflection of the same girder

without cables under the same load. Hence, if an additional support is added under every cable attachment point, the bending moment of the girder will not change very much, which means that the bending moment of a cable-stayed bridge is very similar to that of the continuous beam with additional supports. The bending moment of such a continuous beam is readily represented by its eigenfunctions. Therefore, in analysis, the eigenfunctions of such a continuous beam are added into the series of longitudinal displacement functions. In this way, the accuracy of the bending moments of girder at cable attachment points is improved significantly.

Another measure to improve the efficiency of the iterative process is to use the substructuring technique, transforming the whole girder by means of the flexibility approach into a substructure with only very few nodes at the points of cable attachments. Hence, only the substructure with very few degrees of freedom is involved in every iteration and the solution time is reduced significantly.

The girder, released from all stays, is first analyzed by the above-mentioned finite strip method under external loads. The deflections at all the nodes due to the external loads can be easily found and expressed in terms of a column vector $\{a\}$. Then a unit vertical force is applied at node j alone, with j being 1,2,...n, where n is the number of cable attachment points, and the deflection f_{ij} of every node i (i=1...n) is obtained. This procedure gives the flexibility matrix $[F_g]$ of the substructure:

$$[F_g] = [F_{ij}]$$

The inverse matrix of $[F_g]$ is the stiffness matrix $[K_g]$ of the substructure,

$$[K_g] = [F_g]^{-1}$$

In order to avoid possible singularities in $[F_g]$ and consequent failure to invert it, the number of series terms used in the analysis of the girder must not be less than the number of nodes on any nodal line.

Multiplying the stiffness matrix $[K_g]$ by the displacement vector $\{a\}$ due to external loads gives the equivalent nodal forces $\{P\}$

$$\{P\} = [K_g]\{a\}$$

4.1.2 FORMULAS FOR CABLE

1. INITIAL STIFFNESS MATRIX OF THE CABLE

The displacement vector of a cable is $[w, v]^T$ (Fig.4.1 a). Its linear elastic stiffness matrix can be written as

$$[K_c] = \frac{EA}{S_0}\begin{bmatrix} \sin^2\alpha & \cos\alpha\sin\alpha \\ \cos\alpha\sin\alpha & \cos^2\alpha \end{bmatrix}$$

where E is the modulus of elasticity; A is the area of cross-section; S_0 is the free length of the cable; and α is the angle of inclination of the cable.

2. BASIC THEORY OF THE CATENARY

The shape of a cable under self-weight and end tensions is a catenary. The formulas used in the present analysis are derived as follows.

If q is the self-weight per unit lengths, and T is the cable tension with horizontal component H and vertical component V, the equilibrium conditions of an infinitesimal cable element (Fig.4.1 b) are

$$\sum X = 0, \qquad H_2 - H_1 = 0 \tag{4.1}$$

$$\sum Y = 0, \qquad V_2 - V_1 - qds = 0 \tag{4.2}$$

From (4.1) it can be concluded that $H_2 = H_1 = H$, which means that H is constant along the entire cable.

Taking into consideration that

$$V_2 - V_1 = H\tan\alpha_2 - H\tan\alpha_1 = H(\frac{dy}{dx})_2 - H(\frac{dy}{dx})_1 = H\frac{d^2y}{dx^2}dx$$

and

$$ds = \sqrt{dx^2 + dy^2} = \sqrt{1 + (\frac{dy}{dx})^2}dx$$

(4.2) can be rewritten in the form:

$$H\frac{d^2y}{dx^2} = q\sqrt{1 + (\frac{dy}{dx})^2} \tag{4.3}$$

(4.3) is the differential equation of catenary, whose general solution is

$$y = a\cosh\frac{x - x_0}{a} + c \tag{4.4}$$

where x_0 and c are constants which are determined from the end conditions and

$$a = H/q$$

For a cable with horizontal projection l and vertical projection h (Fig.4.1 c), the end conditions can be assumed as:

$$y(0) = 0 \tag{4.5}$$

$$y(l) = h \tag{4.6}$$

Substituting (4.4) into (4.5) gives

$$a\cosh\frac{-x_0}{a} + c = 0$$

from which the following expressions can be obtained:

$$c = -a\cosh\frac{x_0}{a}$$

and

$$y = a(\cosh\frac{x - x_0}{a} - \cosh\frac{x_0}{a}) \tag{4.7}$$

Substitution of (4.7) into (4.6) yields:

$$a(\cosh\frac{l - x_0}{a} - \cosh\frac{x_0}{a}) = h$$

which can then be rewritten in the form:

$$2a\sinh\frac{l}{2a}\sinh\frac{l - 2x_0}{2a} = h$$

whence

$$\sinh\frac{l - 2x_0}{2a} = \frac{h}{2a\sinh\frac{l}{2a}} \tag{4.8}$$

This equation can be used to find x_0, giving

$$x_0 = \frac{l}{2} - a\sinh^{-1}\frac{h}{2a\sinh\frac{l}{2a}}$$

Because $\sinh^{-1}(t) = \ln(t + \sqrt{1 + t^2})$, the above equation can also be written in the following form:

$$x_0 = \frac{l}{2} - a\ln(t + \sqrt{t^2 + 1}) \tag{4.9}$$

in which

$$t = \frac{h}{2a \sinh \frac{l}{2a}}$$

Once x_0 is defined, (4.7) can be utilized to find any values needed in the analysis, such as the cable tension T and its vertical component V, the curve length S of the cable and its elongation $S - S_0$ due to cable tension T as follows:

(a) Cable Tension T and Its Vertical Component V:

$$V = H\frac{dy}{dx} = H \sinh \frac{x - x_0}{a} \tag{4.10}$$

$$T = \sqrt{H^2 + V^2} = H \cosh \frac{x - x_0}{a} \tag{4.11}$$

(b) Curved Length of the Cable:

$$\begin{aligned} S &= \int_0^l \sqrt{1 + (\frac{dy}{dx})^2} dx \\ &= \int_0^l \sqrt{1 + \sinh^2 \frac{x - x_0}{a}}\, dx \\ &= \int_0^l \cosh \frac{x - x_0}{a}\, dx \\ &= a \sinh \frac{l - x_0}{a} - a \sin \frac{-x_0}{a} \\ &= 2a \sinh \frac{l}{2a} \cosh \frac{l - 2x_0}{2a} \\ &= 2a \sinh \frac{l}{2a} \sqrt{\sinh^2 \frac{l - 2x_0}{2a} + 1} \end{aligned}$$

Substituting (4.8) into the above equation eventually gives the curved length S of the cable as:

$$S = \sqrt{h^2 + 4a^2 \sinh^2 \frac{l}{2a}} \tag{4.12}$$

(c) Elongation of The Cable due to Tension:

$$S - S_0 = \int_0^l \frac{T ds}{EA}$$

$$
\begin{aligned}
&= \frac{1}{EA}\int_0^l T\sqrt{1+(\frac{dy}{dx})^2}\,dx \\
&= \frac{1}{EA}\int_0^l H\cosh\frac{x-x_0}{a}\sqrt{1+\sinh^2\frac{x-x_0}{a}}dx \\
&= \frac{H}{EA}\int_0^l \cosh^2\frac{x-x_0}{a}\,dx \\
&= \frac{H}{2EA}(l+\frac{a}{2}(\sinh\frac{2(l-x_0)}{a}+\sinh\frac{2x_0}{a})) \\
&= \frac{H}{2EA}(l+a\sinh\frac{l}{a}\cosh\frac{l-2x_0}{a}) \\
&= \frac{H}{2EA}(1+a\sinh\frac{l}{a}(2\sinh^2\frac{l-2x_0}{2a}+1))
\end{aligned}
$$

Using (4.8) again and taking into account $sinh\frac{l}{a} = 2\sinh\frac{l}{2a}\cosh\frac{l}{2a}$ and $\coth\frac{l}{2a} = \cosh\frac{l}{2a}/\sinh\frac{l}{2a}$, the above equation can be rewritten in the form:

$$S - S_0 = \frac{H}{2EA}(l+\frac{h^2}{a}\coth\frac{l}{2a}+a\sinh\frac{l}{a}) \tag{4.13}$$

3. SOLUTION PROCEDURE FOR CABLE TENSION

Substituting (4.12) into (4.13) gives following equation:

$$\sqrt{h^2+4(\frac{H}{q})^2\sinh^2\frac{lq}{2H}} - S_0 = \frac{H}{2EA}(l+\frac{qh^2}{H}\coth\frac{ql}{2H}+\frac{H}{q}\sinh\frac{ql}{H}) \tag{4.14}$$

Using (4.9) and (4.10), the vertical force V_1 applied by the cable on the girder and the horizontal force H applied by the cable on the pylon can be related to each other as follows:

$$
\begin{aligned}
t &= \frac{qh}{2H}/\sinh\frac{ql}{2H} \\
x_0 &= \frac{l}{2}-\frac{H}{q}\ln(t+\sqrt{t^2+1}) \\
V_1 &= H\sinh\frac{qx_0}{H}
\end{aligned} \tag{4.15}
$$

Initially, q, l and h are known; thence from the given initial value of V_1, equations (4.15) can be solved numerically for the unknown H, for example by using the

first order Reguli-Falsi iteration (see Section 2.3). In this iteration, for any trial value of H, t can be obtained by means of the first of equations (4.15). Then, substituting t into the second equation gives x_0. Thereafter, V_1 can be computed using the third equation. Substituting the solution for H into equation (4.14) then gives the free length S_0 of the cable.

At any deformed position, after w and v are found, it is easy to obtain h and l. Using a numerical approach again, H can be obtained from equation (4.14). Then V_1 is readily evaluated by substituting H into equation (4.15). Both V_1 and H reflect the nonlinear resistance of the cable to deformation.

4.1.3 STIFFNESS MATRIX OF THE PYLON

In the present analysis, the pylon is treated as a cantilever beam, and only its deflection, not its rotation, is taken into account. For this reason, it is convenient to form its flexibility matrix first, and then let the computer invert it automatically to obtain its stiffness matrix.

The flexibility coefficient f_{ij} of the pylon (Fig.4.2) is defined by

$$f_{ij} = \frac{1}{2EI_p} h_j^2 (h_i - \frac{1}{3} h_j) \qquad (4.16)$$

in which EI_p is the bending stiffness of the pylon; and $h_i \geq h_j$. Hence, by assembling the f_{ij}, the flexibility matrix is obtained as:

$$[F_p] = [f_{ij}] \qquad (4.17)$$

The inverse matrix of $[F_p]$ is the stiffness matrix $[K_p]$ of pylon,

$$[K_p] = [F_p]^{-1} \tag{4.18}$$

4.1.4 INITIAL-STIFFNESS ITERATION

Assembling the linear stiffness matrices of the girder substructure, cables and pylons together produces the initial linear stiffness matrix $[K_0]$ of the whole structure. K_0 is formed and inverted only once and then is used in every iteration for the nonlinear solution [6] without any change. Because of the relatively high cable tension in ordinary cable-stayed bridges, the nonlinearity is usually not very significant, and hence convergence can be achieved within very few iterations.

It is assumed that the structure is divided into a linear part (the girder and pylons) and a nonlinear part(cables).

After k iterations, the resistance of the linear part to displacement $\{a\}^k$ is:

$$\{R_l\}^k = [K_l]\{a\}^k \tag{4.19}$$

where $[K_l]$ is the linear stiffness matrix of this part.

The resistance $\{R_{nl}\}$ of the nonlinear part to the displacement $\{a\}^k$ is the cable tension and can be found from $\{a\}^k$ by following the procedure described in Subsection 4.2.2.

The resistance of the entire structure to this deformation is the combination of

the resistances of both parts.

$$\{R\}^k = \{R_l\}^k + \{R_{nl}\}^k = [K_l]\{a\}^k + \{R_{nl}\}^k \tag{4.20}$$

If the external load $\{P\}$ is not equal to the resistance $\{R\}^k$, the structure will deform further under the action of the so-called "unbalanced force" $\{F\}^k$ (the difference between the load and the resistance) to the next position $\{a\}^{k+1}$, with the initial linear stiffness matrix $[K_0]$ assumed to be unchanged (Fig.4.3). Hence

$$[K_0](\{a\}^{k+1} - \{a\}^k) = \{F\}^k = \{P\} - \{R\}^k \tag{4.21}$$

If the second term in the bracket on the left side of above equation is shifted to the right side, this equation can be rewritten as:

$$\begin{aligned} [K_0]\{a\}^{k+1} &= [K_0]\{a\}^k + \{P\} - \{R\}^k \\ &= ([K_l] + [K_{nl}])\{a\}^k + \{P\} - ([K_l]\{a\}^k + \{R_{nl}\}^k) \\ &= \{P\} + [K_{nl}]\{a\}^k - \{R_{nl}\}^k \end{aligned} \tag{4.22}$$

where $[K_{nl}]$ is the initial linear stiffness matrix of the nonlinear part (cables), and $[K_0] = [K_l] + [K_{nl}]$.

Thus the equation (4.22) can be used to find an improved approximation $\{a\}^{k+1}$ from $\{a\}^k$. This procedure is repeated until convergence is obtained. Convergence may be assumed to occur if the difference in the value of every displacement parameter of every cable, determined from two successive iterations, does not exceed a chosen small percentage(say 0.1 percent).

4.1.5 NUMERICAL EXAMPLES

1. Three Span Cable-Stayed Bridge under Dead Load and Live load.

A single plane cable stayed bridge over three spans is shown in Fig.4.4. In order to compare the results of analysis with beam theory more conveniently, it is assumed that the girder has a narrow width in comparison with its height. The details of the bridge are as follows:

For the girder, $E = 2.0 \times 10^5 MPa$, Poisson's ratio $\nu = 0.3$, and bending moment of inertia $I_g = 1.0m^4$.

For the pylons, $EI_p = 1.0 \times 10^6 m^2 MN$. For the cables, $E_c = 1.52 \times 10^5 MPa$, the specific weight $\gamma_c = 0.0764 MN/m^3$, The areas of cross sections $A_1 = A_4 = 0.10m^2$, $A_2 = A_3 = 0.05m^2$.

In load case 1, the girder is subjected to dead load $q_d = 0.1MN/m$ over all spans, and the deflections at all the cable attachment points are assumed to be zero. The vertical forces V_i in MN (i=1,4) applied to the girder by cable i are listed in Table 4.1.The longitudinal bending moments in MN.m at a number of cross sections are given in Table 4.2. In both tables, n_1 is the number of eigenfunctions associated with the continuous beam over three spans; n_2 is the number of eigenfunctions related to the continuous beam with additional supports at all of the cable attachment points; hence the total number of eigenfunctions employed in the analysis is $n_1 + n_2$.

	n_1+n_2	w_B	w_F	w_H	V_1	V_2	V_3	V_4
Load	6+0	0.0	0.0	0.0	7.377	9.375	8.325	7.901
case	15+0	0.0	0.0	0.0	7.480	9.080	8.074	7.982
1	25+0	0.0	0.0	0.0	7.480	9.060	8.060	7.986
	6+9	0.0	0.0	0.0	7.480	9.041	8.043	7.990
	16+9	0.0	0.0	0.0	7.480	9.046	8.049	7.990
	Theory	0.0	0.0	0.0	-	9.072	8.075	7.985
load	6+0	-0.1499	0.2761	0.5117	5.473	0.068	4.415	3.802
case	15+0	-0.1498	0.2736	0.5110	5.481	0.049	4.341	3.836
2	23+0	-0.1498	0.2735	0.5111	5.481	0.049	4.338	3.837
	6+9	-0.1500	0.2733	0.5112	5.482	0.045	4.332	3.838
	15+8	-0.1500	0.2733	0.5112	5.482	0.045	4.332	3.838
	Theory	-0.1498	0.2735	0.5111	-	0.056	4.343	3.837

Table 4.1: Deflections (in meters) of Girder at Cable Attachment Points and Vertical Forces (in MN) of Cables

	n_1+n_2	M_A	M_B	M_C	M_D	M_E	M_F	M_G	M_H	M_I
load	6+0	0.018	0.021	0.011	0.001	0.005	0.016	0.021	0.020	0.019
case	15+0	45.10	-34.95	20.52	-47.60	27.19	-23.68	20.93	-20.73	20.87
1	25+0	51.95	-43.17	25.30	-44.20	30.76	-32.99	33.39	-32.23	31.49
	45+0	44.70	-53.05	18.82	-46.54	26.10	-41.53	24.07	-40.20	24.34
	6+9	48.27	-61.35	22.17	-44.97	29.07	-48.90	28.23	-48.24	28.69
	16+9	46.49	-70.06	21.43	-46.30	28.58	-55.55	26.71	-50.91	28.68
	36+9	46.08	-67.74	20.74	-48.45	27.36	-54.55	26.30	-53.46	26.71
	Theory	46.19	-67.62	21.43	-49.51	28.08	-54.34	26.26	-53.13	26.87
load	6+0	-7.986	-11.30	-8.720	-2.618	-1.290	0.8137	4.299	8.052	9.711
case	15+0	-4.858	-10.18	-12.66	-15.96	16.39	-13.42	13.49	-1.265	19.89
2	23+0	-4.744	-10.01	-13.32	-14.43	19.07	-18.53	19.69	-7.063	25.37
	45+0	-4.930	-10.04	-13.12	-15.04	16.09	-23.10	15.17	-10.90	21.86
	6+9	-4.935	-9.726	-13.22	-14.97	17.76	-27.12	17.29	-14.59	23.78
	15+8	-5.055	-10.57	-13.28	-14.23	17.64	-29.20	17.02	-15.80	23.60
	36+9	-4.970	-10.10	-13.06	-15.51	16.79	-30.20	16.41	-17.24	22.83
	Theory	-5.054	-10.11	-12.93	-15.74	17.07	-30.11	16.41	-17.07	22.93

Table 4.2: Bending Moment (in MN.m) of Girder

In load case 2, the live load $q_l = 0.05\ MN/m$ is imposed on the entire second span only. The vertical components of the prestressing forces of the cables are $V_{01} = 7.480\ MN$, $V_{02} = 9.071\ MN$, $V_{03} = 8.064\ MN$ and $V_{04} = 7.984\ MN$, consistent with the girder having zero deflection at every cable attachment point in load case 1. The results in load case 2 are also shown in Table 4.1 and Table 4.2. However, in this case, every quantity listed in the tables is its increment due to live load alone.

In fact, even if only the eigenfunctions of a continuous beam with 3 spans are used, the results for the deflection (in m) of the girder at cable attachment points are still satisfactory; their errors are less than 1.0 percent with only 6 series terms used. In this case, the results of the vertical components of the cable tensions are also acceptable, with errors of less than 3.5 percent. However,the accuracy of the bending moments is disappointing,the errors of maximum bending moment being still more than 22 percent in both load cases, despite using 45 series terms. From Table 4.2 it can be seen that the improvement brought about by the additional eigenfunctions associated with the continuous beam with extra fictitious supports at all the cable attachment points is significant. The error of maximum bending moment is less than 5 percent by using $n_1 + n_2 = 16 + 9 = 25$ series terms for load case 1, and by using $n_1 + n_2 = 15 + 8 = 23$ series terms for load case 2. As a comparison, the error of maximum bending moment is 36 percent with $n_1+n_2 = 25+0 = 25$ terms for load case 1, and 38 percent with $n_1+n_2 = 23+0 = 23$ terms for load case 2, when the additional eigenfunctions are not included.

In both tables, the theoretical results are obtained by means of beam theory,

with the beam deflections at the corresponding cable attachment points under the external applied loads being assumed to be the same as the actual girder.

2. Double-Plane Cable-Stayed Concrete Box-Girder Bridge.

A double-plane cable-stayed concrete box-girder bridge is shown in Fig.4.5. The loads are the self-weight of the girder and a live load, distributed uniformly on the whole deck between towers, of intensity $4.488KN/m^2$. The details of the bridge are as follows:

For the girder, $E_g = 25 \times 10^6 KN/m^2$, Poisson's ratio $\nu = 0.2$, specific weight $\gamma_g = 24KN/m^3$; for the pylons, $EI_p = 2.5 \times 10^8 m^2 KN$; for the cables, $E_c = 1.7 \times 10^8 KN/m^2$, $\gamma_c = 78KN/m^3$, the areas $A_1 = A_4 = 0.04m^2$, $A_2 = A_3 = 0.024m^2$; the vertical components of cable prestressing forces under the dead load are $V_{01} = 7849.6KN$, $V_{02} = 9066.5KN$, $V_{03} = 8121.2KN$, $V_{04} = 8322.7KN$, which make the deflections of the girder at the cable attachment points under the dead load equal to zero.

Because of symmetry, only half of the bridge, which is divided into 6 strips by 5 nodal lines, needs to be analyzed. In the finite strip analysis of the girder, the number of terms used in the eigenfunction series is $n_1 + n_2 = 21 + 9$. Convergence is obtained within 8 iterations.

The deflection of the girder along the nodal line 5 is depicted in Fig. 4.6. The vertical forces V, applied to the girder by the cables, and the horizontal components H of cable tension are given in Table 4.3. The maximum negative bending moment

Cable	V	H
1	10.730	25.985
2	9.831	11.841
3	11.315	13.419
4	10.521	25.103

Table 4.3: Vertical Forces of Cables on Girder and Horizontal Forces of Cables on Pylon (in MN)

of the girder is at cross section B , and the maximum positive bending moment is at the central symmetrical cross section F. The distributions of the longitudinal bending stresses on these two cross sections are shown in Fig.4.7 and Fig.4.8.

4.2 GEOMETRICAL NONLINEAR ANALYSIS OF PLATES

If the deflection of a plate is large in comparison with the plate thickness, the deflection may produce supplementary strains and stresses in the middle plane of the plate. These in-plane stresses contribute to resistance to deflection of the plate. As a result, the deflections of the plate are much less than those estimated by linear elastic plate theory. Because of the interaction between deflection and in-plane deformation, the governing differential equations of plates become nonlinear, and the solution of the problem becomes much more complicated [59]. Exact solutions can be obtained only for a few of the simplest cases. Some numerical methods, such as the energy method, perturbation method etc. have been developed, but these are very difficult to apply, because different displacement functions have to be assumed for different loads and plate geometry. The finite element method is

a versatile tool, being applicable for geometrical nonlinear analysis of any type of plate; however its efficiency needs to be improved because of its requirement of too many degrees of freedom and extremely large quantity of input data.

The finite strip method has been effectively used for linear elastic analysis of many types of plates. For the plate with two opposite edges simply supported, the displacements corresponding to different eigenfunctions are uncoupled, that is, the loads corresponding to a given eigenfunction produce only displacements corresponding to the same eigenfunction. Hence, the stiffness matrix of this type of plate has a very narrow half-bandwidth. And consequently, the efficiency of the finite strip analysis is much higher than that of the finite element method.

Since 1978, the finite strip method has been extended to geometrical non-linear analysis of plate structures and has demonstrated that its efficiency is higher than that of the finite element method [28-33]. Nevertheless, hitherto in all existing references the Newton-Raphson method has been used, so that at each new iteration the tangential stiffness matrix of structure has to be reformed and inverted once again. Furthermore, because of the non-linearity of the analysis, the different series terms are coupled in the tangential stiffness matrix even for simply supported plates, with the result that the orthogonal property between different eigenfunctions can not any longer be utilized to reduce the half-bandwidth, and hence that the enhancement of efficiency of non-linear analysis by finite strip method is not as significant as expected.

An effective remedial measure to this problem is to employ Initial Stiffness It-

eration [6]. First, the in-plane and bending displacement functions of ordinary finite plate strips are applied to formulate the linear elastic stiffness matrix and the equivalent nodal forces. Thereafter, it is easy to find the linear elastic displacements, From which, the in-plane and bending strains and stresses can be calculated, with the effects of large deflection on the in-plane strains being taken into consideration. Next, the resistances to the deformation of the plate are obtained from these stresses by means of the principle of virtual work.

Because of the non-linearity of the problem, the above displacements are not the solution of the problem, and the corresponding resistances can not be equal to the external loads. The so-called "unbalanced forces", i.e.the difference between the loads and the non-linear resistances, make the plate deform further. As a result, new displacements, corresponding resistances and "unbalanced forces" are obtained. This procedure is repeated until the non-linear resistances counterbalance the external loads. During all the iterations, the initial stiffness matrix of the plate is assumed to be unchanged. Consequently, the uncoupled problem in linear-elastic analysis will remain uncoupled in the nonlinear analysis, the half-bandwidth of the stiffness matrix also remaining unchanged. Thus, the advantage of finite strip method will not be lost in nonlinear analysis. Also, the stiffness matrix needs not be reformed and inverted in each new iteration. Although the number of iterations will be increased, an overall economy can be achieved in most cases.

In practice, the transverse stiffness of a plate under large deflection is much greater than its corresponding linear elastic stiffness. This may result in divergence of

iteration if the initial bending stiffness matrix remains unchanged during the whole iteration process (Fig.4.9).The simplest method of modifying the bending stiffness matrix is to multiply all the items of this matrix by an amplification factor which is a function of the ratio of current maximum deflection to the thickness of the plate. In our case, a more efficient equivalent method is used, which is that of dividing the "unbalanced nodal force" corresponding to every flexural degree of freedom by the same factor. It has been shown that this method can ensure effective convergence if the value of the amplification factor is reasonably chosen.

Some detailed descriptions follow.

4.2.1 DISPLACEMENT FUNCTIONS AND INITIAL STIFFNESS MATRIX

Under large deflection, each plate strip is subjected to in-plane stresses and out-of-plane bending forces. The nodal displacements and forces of the strip corresponding to the m-th term of the eigenfunction series are (Fig.2.2):

$$\{\delta\}_m = (u_1\ v_1\ w_1\ \theta_1\ u_2\ v_2\ w_2\ \theta_2)_m^T$$

$$\{F\}_m = (U_1\ V_1\ W_1\ M_1\ U_2\ V_2\ W_2\ M_2)_m^T$$

The displacement field within a plate strip [24] is

$$u = \sum_{m=1}^{r}((1-X)u_{1m} + Xu_{2m})Y_m^u(y)$$

$$v = \sum_{m=1}^{r}((1-X)v_{1m} + Xv_{2m})Y_m^v(y)$$

$$w = \sum_{m=1}^{r}(N_{1m}w_{1m} + N_{2m}\theta_{1m} + N_{3m}w_{2m} + N_{4m}\theta_{2m}) \tag{4.23}$$

where $X = x/b$, r is the total number of series terms used in analysis, and

$$Y_m^u(y) = \sin\frac{m\pi y}{l}$$

If both ends of the strip are free to move in the longitudinal direction ($u = 0$, $\sigma_y = 0$ at $y = 0$ and $y = l$), then

$$Y_m^v(y) = \cos\frac{m\pi y}{l}$$

If both ends are immovable ($u = 0$, $v = 0$ at $y = 0$ and $y = l$), then

$$Y_m^v(y) = \sin\frac{(m+1)\pi y}{l}$$

In the expression for w ,

$$N_{1m} = (1 - 3X^2 + 2X^3)Y_m^w(y)$$

$$N_{2m} = x(1 - 2X + X^2)Y_m^w(y)$$

$$N_{3m} = (3X^2 - 2X^3)Y_m^w(y)$$

$$N_{4m} = x(X^2 - X)Y_m^w(y)$$

If both ends are simply supported in bending ($w = 0$, $M_y = 0$ at $y = 0$ and $y = l$), then

$$Y_m^w(y) = \sin\frac{m\pi y}{l}$$

If both ends are clamped ($w = 0$, $\frac{\partial w}{\partial y} = 0$ at $y = 0$ and $y = l$),then

$$Y_m^w(y) = \sin\frac{\mu_m y}{l} - \sinh\frac{\mu_m y}{l} - \alpha_m[\cos\frac{\mu_m y}{l} - \cosh\frac{\mu_m y}{l}]$$

where

$$\alpha_m = \frac{\sin\mu_m - \sinh\mu_m}{\cos\mu_m - \cosh\mu_m}$$

μ_m is the m-th solution of equation $1 - \cos\mu\cosh\mu = 0$; its values are listed in Subsection 2.1.1.

Substituting equations (4.23) into the linear strain-displacement relationships (2.5) yields the linear strain matrix $[B]_m$ in (2.6). Then, the linear stiffness matrix $[K]$ and the equivalent nodal force vector $\{F\}$ of external load can be obtained by using equations (2.10) and (2.13). By following the standard procedure in Section 2.1, it is not difficult to obtain the linear elastic solution for all of the displacement parameters of the plate.

4.2.2 GEOMETRICAL NONLINEAR SOLUTION

After the displacements are obtained, the strains and stresses of the plate under large deflection can be evaluated as follows [59]:

$$\begin{aligned}
\epsilon_x &= \frac{\partial u}{\partial x} + \frac{1}{2}(\frac{\partial w}{\partial x})^2 \\
\epsilon_y &= \frac{\partial v}{\partial y} + \frac{1}{2}(\frac{\partial w}{\partial y})^2 \\
\gamma_{xy} &= \frac{\partial u}{\partial y} + \frac{\partial v}{\partial x} + \frac{\partial w}{\partial x}\frac{\partial w}{\partial y} \\
\chi_x &= -\frac{\partial^2 w}{\partial x^2} \\
\chi_y &= -\frac{\partial^2 w}{\partial y^2} \\
\chi_{xy} &= 2\frac{\partial^2 w}{\partial x \partial y}
\end{aligned} \tag{4.24}$$

$$N_x = \frac{Eh}{1-\nu^2}(\epsilon_x + \nu\epsilon_y)$$

$$N_y = \frac{Eh}{1-\nu^2}(\epsilon_y + \nu\epsilon_x)$$

$$N_{xy} = Gh\gamma_{xy}$$

$$M_x = \frac{Eh^3}{12(1-\nu^2)}(\chi_x + \nu\chi_y)$$

$$M_y = \frac{Eh^3}{12(1-\nu^2)}(\chi_y + \nu\chi_y)$$

$$M_{xy} = \frac{Gh^3}{12}\chi_{xy} \tag{4.25}$$

In the above expressions, E, ν and G are the elastic constants while h is the thickness of the plate.

By substituting equations (4.23) into equations (4.24) and differentiating the resulting expressions, the following equation can be obtained:

$$d\{\epsilon\} = d(\epsilon_x, \epsilon_y, \gamma_{xy}, \chi_x, \chi_y, \chi_{xy})^T = \sum_{m=1}^{r} [\bar{B}]_m d\{\delta\}_m \tag{4.26}$$

and

$$[\bar{B}]_m = [B]_m + [B^{nl}(\delta)]_m \tag{4.27}$$

in which $d\{\epsilon\}$ and $d\{\delta\}_m$ are the infinitesimal increments of strain and displacement vectors of the strip, respectively; $[B]_m$ is the linear strain matrix obtained previously; $[B^{nl}]_m$ is a function of $\{\delta\}$ which reflects the nonlinear effect of large

deflection, and is as follows:

$$[B^{nl}]_m = \begin{pmatrix} 0 & 0 & w_{,x}N_{1m,x} & w_{,x}N_{2m,x} & 0 & 0 & w_{,x}N_{3m,x} & w_{,x}N_{4m,x} \\ 0 & 0 & w_{,y}N_{1m,y} & w_{,y}N_{2m,y} & 0 & 0 & w_{,y}N_{3m,y} & w_{,y}N_{4m,y} \\ & & w_{,x}N_{1m,y}+ & w_{,x}N_{2m,y}+ & & & w_{,x}N_{3m,y}+ & w_{,x}N_{4m,y}+ \\ 0 & 0 & w_{,y}N_{1m,x} & w_{,y}N_{2m,x} & 0 & 0 & w_{,y}N_{3m,x} & w_{,y}N_{4m,x} \\ 0 & 0 & 0 & 0 & 0 & 0 & 0 & 0 \\ 0 & 0 & 0 & 0 & 0 & 0 & 0 & 0 \\ 0 & 0 & 0 & 0 & 0 & 0 & 0 & 0 \end{pmatrix} \tag{4.28}$$

where the subscripts "$,x$" and "$,y$" denote $\frac{\partial}{\partial x}$ and $\frac{\partial}{\partial y}$, respectively; and

$$w_{,x} = \sum_{m=1}^{r}(N_{1m,x}w_{1m} + N_{2m,x}\theta_{1m} + N_{3m,x}w_{2m} + N_{4m,x}\theta_{2m})$$

$$w_{,y} = \sum_{m=1}^{r}(N_{1m,y}w_{1m} + N_{2m,y}\theta_{1m} + N_{3m,y}w_{2m} + N_{4m,y}\theta_{2m})$$

The resistances $\{R\}$ to the large deflections of the plate can then be calculated by means of the principle of virtual work [66]. The so-called resistances $\{R\}$ are referred to the external forces required to maintain a given deformation. If any virtual displacement $d\{\delta\}_m$ occurs from the current equilibrium position of a strip, the work done by the external forces during the virtual displacement is

$$dW_{ex} = d\{\delta\}_m^T\{R\}_m$$

and the work performed by the internal forces is

$$dW_{in} = \int_l\int_b d\{\epsilon\}^T\{\sigma\}dxdy = \int_l\int_b([\bar{B}]_m d\{\delta\}_m)^T\{\sigma\}dxdy = d\{\delta\}_m^T\int_l\int_b[\bar{B}]_m^T\{\sigma\}dxdy$$

According to the principle of virtual work, dW_{ex} must be equal to dW_{in} for any possible $d\{\delta\}_m$; this requires that

$$\{R\}_m = \int_l\int_b[\bar{B}]_m^T\{\sigma\}\,dx\,dy \tag{4.29}$$

where $\{R\}_m$ is the resistance vector of a strip corresponding to m-th term of eigenfunctions,and $\{\sigma\}$ is the stress vector in the strip , $\{\sigma\} = (N_x, N_y, N_{xy}, M_x, M_y, M_{xy})^T$.

The integration in (4.29) can be implemented by the Gaussian integration method.

If the current resistances are not equal to the external loads, the plate deforms further under the "unbalanced forces", i.e. the difference between the external loads $\{F\}$ and the resistances $\{R\}$, with the original linear elastic matrix $[K]$ being assumed to be unchanged:

$$[K]\Delta\{\delta\}^{k+1} = \{F\} - \{R\}^k \tag{4.30}$$

Thence the new displacements are reached:

$$\{\delta\}^{k+1} = \{\delta\}^k + \Delta\{\delta\}^{k+1} \tag{4.31}$$

This procedure is repeated until convergence is achieved, i.e. until

$$\frac{\sqrt{\sum(\Delta\delta_i^{k+1})^2}}{\sqrt{\sum(\delta_i^{k+1})^2}} \leq e \tag{4.32}$$

where e is a prescribed tolerance. In the present study, $e = 0.0002$. In the last three equations, the superscript "k" or "k+1" indicates the number of current iteration. In order to ensure convergence, in each iteration, the "unbalanced forces" corresponding to the bending degrees of freedom on the right side of the equation (4.30) are divided by a "flexural stiffness amplification factor", α. After a number of trials, an appropriate value of α has been found as follows:

$\alpha = 1 + 5.5(\frac{\delta_{max}}{h})^2$ for plates with two opposite clamped edges

$\alpha = 1 + 10.0(\frac{\delta_{max}}{h})^2$ for plates with two opposite simply supported edges

In these expressions, δ_{max} is the maximum displacement parameter found in the current iteration.

4.2.3 NUMERICAL EXAMPLES

1. Cylindrical bending of a uniformly loaded rectangular plate with simply supported immovable edges

The plate is very long in the x direction, so that, the deflected surface of a portion of such a plate at a considerable distance from the ends can be assumed cylindrical. Therefore, the analysis needs only one strip with boundary condition: $u_1 = u_2 = 0$, $\theta_1 = \theta_2 = 0$ along two nodal lines. The length of the strip is $l = 50in$. The thickness is $h = 0.5in$.. The elastic constants of the material are $E = 30000000psi$, $\nu = 0.3$. The intensity of the uniformly distributed load is $q = 20psi$. The maximum linear elastic deflection is $w_0 = 4.740$,$w_0/h = 9.48$. Because of symmetry of deformation, only the eigenfunctions symmetrical to the midspan are used, i.e. $m = 1, 3, 5, ...$ The numerical results of the deflection, w_{max} (in inches), the longitudinal stress of the middle plane, σ_y in psi, and the longitudinal bending moment, M_y in lb-in, at midspan are listed in Table 4.4 .For comparison, the theoretical answers [59] are also given in this table, in which m_{max} is the highest order of eigenfunctions used in these analysis, N_{iter} is the number of iterations up to convergence.

2. Large deflections of a uniformly loaded square plate with clamped edges

A square plate of side 2a and thickness h, clamped along all the immovable edges,

m_{max}	w_{max}	σ_y	M_y	N_{iter}
1	0.6972	1582O.	945.20	17
3	0.6827	15770.	778.70	47
5	0.6841	1584O.	825.60	48
Theory	0.688	15830.	830.14	-

Table 4.4: Deflection and Stresses in Cylindrical Plate Bending

qa^4/Dh	w_0/h	w_{max}/h	$\sigma_n a^2(1-\nu^2)/Eh^2$	N_{iter}	w_{max}/h [59]
50	1.008	0.767	4.22	7	0.76
100	2.016	1.158	7.09	13	1.15
150	3.024	1.418	9.37	17	1.41
200	4.032	1.618	11.33	21	1.60
250	5.040	1.782	13.05	25	1.78

Table 4.5: Deflection and Stresses in Clamped Square Plate

is subjected to a uniformly distributed load q. Using symmetry, only half the plate is analyzed; it is divided into five equal width strips and analyzed by means of five eigenfunctions symmetrical to the midspan ($m_{max} = 9$). The numerical results are listed in Table 4.5, in which D is the flexural rigidity of the plate, $D = Eh^3/12(1-\nu^2)$; w_0 is the linear elastic deflection at the center of plate; w_{max} is the result obtained from nonlinear analysis; σ_n is the maximum normal bending stress at the center of each edge. For comparison, the answers obtained by an energy method with 11 parameters ([59],pp421-433) are also given in the same table. In every case, the whole load is imposed within one step. The number of iterations up to convergence, N_{iter}, is 7 to 25, depending on the ratio of w_0/h. In ordinary structures, this ratio will not be too large; it is concluded that the analysis does not need too many iterations.

4.3 NONLINEAR ANALYSIS OF REINFORCED CONCRETE SLABS

The material nonlinear analysis of reinforced concrete slabs is an important subject for investigating the behavior of many civil engineering structures such as floors, roofs and bridge decks. During the past two decades, finite element methods based on a number of different material models have been used successfully to simulate the material nonlinear response of RC structures. However, the finite strip method has the advantage of considerably reducing the computation, storage requirement and input data preparation. Recently, Guo et al.[37] have developed a layered finite strip method for the nonlinear elasto-plastic analysis of static and dynamic response of concrete slabs using the Von Mises yield criterion. Their results have shown that their method needs much less storage capacity, and spends much less computer time than the finite element method does. However, because they used a relatively simple material model, the discrepancy between their solution and experimental results for concrete slab seems larger than might have been expected.

In this thesis, the model based on orthotropic nonlinear elasticity is used to represent the property of plain concrete under biaxial stresses. This model was proposed by Darwin et al.[67], modified by Kabir [68] and is in close agreement with experimental results [69]. For reinforcement , the bilinear elasto-plastic uniaxial stress strain relationship is employed.

The finite strip is divided into imaginary concrete layers. In addition, each layer of reinforcement is replaced by a smeared steel layer with unchanged original

reinforcement area having stiffness only in the direction of reinforcement.

In every Newton-Raphson iteration, using finite strip interpolation functions and thin plate theory [24,59], the strain state in each layer can be found, After which its stress state can be easily obtained by means of the above-mentioned models. Next, one can calculate the tangential stiffness matrix, unbalanced forces and corresponding displacement increments [70].This procedure is repeated until convergence occurs.

In order to prevent possible oscillations, and to ensure convergence of nonlinear solution, the relaxation technique is applied, that is, in every iteration, the displacement increments are multiplied by a relaxation factor less than unity before being added to the accumulated displacements.

Further details are given below.

4.3.1 MATERIAL MODEL OF CONCRETE

Concrete is treated as an incrementally orthotropic linear elastic material [67-69].

$$\begin{pmatrix} d\sigma_1 \\ d\sigma_2 \\ d\tau_{12} \end{pmatrix} = [D_c] \begin{pmatrix} d\epsilon_1 \\ d\epsilon_2 \\ d\gamma_{12} \end{pmatrix} \tag{4.33}$$

where

$$[D_c] = \frac{1}{1-\nu^2} \begin{pmatrix} E_1 & \nu\sqrt{E_1 E_2} & 0 \\ & E_2 & 0 \\ sym & & \frac{1}{4}\beta(E_1 + E_2 - 2\nu\sqrt{E_1 E_2}) \end{pmatrix} \tag{4.34}$$

in which E_1, E_2 and $\nu = \sqrt{\nu_1 \nu_2}$ are stress-dependent material properties, $\beta = 1.0$ prior to cracking and $0 < \beta \leq 1.0$ after cracking. Material axes 1 and 2 coincide

with the current principal stress axes.

The concept of "equivalent uniaxial strain" is introduced in order to transform the actual biaxial stress state to two "independent uniaxial stress states". It is defined as :

$$\epsilon_{iu} = \sum_{all\ load\ increments} \frac{\Delta\sigma_i}{E_i} \tag{4.35}$$

with $\Delta\sigma_i$ = incremental change in principal stress; and E_i = varying tangent stiffness for load increment corresponding to $\Delta\sigma_i$.

The relationship between the principal stress σ_i and the equivalent uniaxial strain ϵ_{iu} is shown in Fig.4.10.

For compressive loading prior to the maximum stress, the compressive principal stress and elastic modulus can be calculated as follows:

$$\sigma_i = \frac{\epsilon_{iu} E_0}{1 + (\frac{E_0}{E_c} - 2)q + q^2} \tag{4.36}$$

$$E_i = \frac{\partial\sigma_i}{\partial\epsilon_{iu}} = \frac{E_0(1 - q^2)}{1 + (\frac{E_0}{E_c} - 2)q + q^2} \tag{4.37}$$

$$q = \epsilon_{iu}/\epsilon_{ic}$$

where E_0 = the tangent modulus of elasticity at zero stress; $E_c = \sigma_{ic}/\epsilon_{ic}$ = the secant modulus at the point of maximum compressive stress σ_{ic}, and ϵ_{ic} = the equivalent uniaxial strain at the maximum compressive stress.

σ_{ic} and ϵ_{ic} depend on the principal stress ratio $\alpha = \sigma_1/\sigma_2$. The analytical maximum strength envelope may be employed to determine the dependence of σ_{ic} on α (Fig.4.11).

For tensile stress prior to cracking, the linear elastic σ_i- ϵ_{iu} relationship is applied:

$$\sigma_i = E_0 \epsilon_{iu} \tag{4.38}$$

The four regions of the strength envelope with the accompanying equations for the maximum stresses σ_{ic} and corresponding equivalent strains ϵ_{ic} are summarized as follows [71]:

1. For σ_1 = compression, σ_2 = compression. $0 \leq \alpha \leq 1$

$$\sigma_{2c} = \frac{1 + 3.65\alpha}{(1+\alpha)^2} f'_c$$

$$\sigma_{1c} = \alpha \sigma_{2c}$$

$$\epsilon_{2c} = \epsilon_c(3p_2 - 2)$$

$$\epsilon_{1c} = \epsilon_c(-1.6p_1^3 + 2.25p_1^2 + 0.35p_1)$$

where $p_1 = \sigma_{1c}/f'_c$, $p_2 = \sigma_{2c}/f'_c$ and f'_c = the uniaxial compressive strength.

2. For σ_1 = tension, σ_2 = compression. $-0.17 \leq \alpha \leq 0$

$$\sigma_{2c} = \frac{1 + 3.28\alpha}{(1+\alpha)^2} f'_c$$

$$\sigma_{1t} = \alpha \sigma_{2c}$$

$$\epsilon_{2c} = \epsilon_c(4.42 - 8.38p_2 + 7.54p_2^2 - 2.58p_2^3)$$

where

$$p_2 = \sigma_{2c}/f'_c$$

$$\epsilon_{1t} = \sigma_{1t}/E_0$$

3. For σ_1 = tension,σ_2 = compression. $-\infty \leq \alpha \leq -0.17$

$$\sigma_{2c} = 0.65 f_c'$$

$$\sigma_{1t} = f_t'$$

$$\epsilon_{2c} = \epsilon_c(4.42 - 8.38p_2 + 7.54p_2^2 - 2.58p_2^3)$$

$$p_2 = \sigma_{2c}/f_c' \leq 0.65$$

$$\epsilon_{1t} = \sigma_{1t}/E_0$$

4. For σ_1 = tension, σ_2 = tension. $1 \leq \alpha \leq \infty$

$$\sigma_{1t} = \sigma_{2t} = f_t'$$

$$\epsilon_{1t} = \epsilon_{2t} = f_t'/E_0$$

in which f_t' is uniaxial tensile strength.

Cracks are assumed to open perpendicular to the highest principal tensile stress direction when the failure envelope in Fig.4.11 has been reached, and σ_1 and E_1 are assumed to become zero as soon as the cracking occurs.

4.3.2 MATERIAL MODEL OF REINFORCEMENT

For the stress-strain relationship of reinforcement, the uniaxial bilinear elasto-plastic model (Fig.4.12) is employed and the following notations are used: E_s = Young's Modulus, E_{sh} = strain hardening modulus, σ_y = yield stress and ϵ_{su} = ultimate strain.

In concrete, when σ_1 reaches σ_{1t} at some point, primary cracks form at finite spacing in the surrounding region. The total tensile force is transferred across

ϵ_s/ϵ_t	1.0-1.5	1.5-3.0	3.0-5.0	5.0-8.0	8.0-11.0	11.0-14.0	other
K	4.0	2.7	2.0	1.6	1.15	1.05	1.0

Table 4.6: Coefficient K for Stress of Steel after Concrete Cracking

each crack by the tensile steel, but between the cracks the tensile concrete carries stress locally, mainly in the direction of the steel bars, due to the bond between the concrete and the reinforcement. This is called the tension stiffening effect. As the load increases, secondary cracks form around the reinforcement and between the primary cracks so that the load carried by the concrete and the average stress in the concrete decrease progressively. In order to incorporate this effect, after the surrounding concrete has cracked, the stress of steel, σ_s is magnified as follows [72]:

$$\sigma_s = K\sigma_s' \tag{4.39}$$

where σ_s' is the stress of reinforcement found by the bilinear model in Fig.4.12 and K is a coefficient shown in Table 4.6, in which ϵ_s is the strain of steel and ϵ_t is the uniaxial strain at concrete cracking, $\epsilon_t = f_t'/E_0$. The concrete is assumed to carry no stress normal to a crack but an additional stress will be carried at the steel level. This additional stress represents the total internal tensile force in fact carried by the concrete between the cracks, conveniently lumped at the level of the tensile reinforcement and oriented in the direction of the bar.

E_s and E_{sh} are also multiplied by the same coefficient K in formulation of the strip stiffness matrices after cracking of the surrounding concrete.

4.3.3 FINITE PLATE STRIP

Each plate strip is subjected to in-plane stresses and to out-of-plane bending forces. The nodal displacements and forces of the strip corresponding to the m-th term of eigenfunctions are (Fig.2.2):

$$\{\delta\}_m = (u_1\ v_1\ w_1\ \theta_1\ u_2\ v_2\ w_2\ \theta_2)_m^T$$

$$\{F\}_m = (U_1\ V_1\ W_1\ M_1\ U_2\ V_2\ W_2\ M_2)_m^T$$

If both ends are simply supported ($u = 0$, $w = 0$, $\sigma_y = 0$, $M_y = 0$ at $y = 0$ and $y = l$), then the displacement components in the middle plane of the strip are:

$$u = \sum_{m=1}^{r}((1-X)u_{1m} + Xu_{2m})Y_m(y)$$

$$v = \sum_{m=1}^{r}((1-X)v_{1m} + Xv_{2m})\frac{l}{m\pi}\frac{dY_m(y)}{dy}$$

$$w = \sum_{m=1}^{r}((1-3X^2+2X^3)w_{1m} + x(1-2X+X^2)\theta_{1m} + (3X^2-2X^3)w_{2m} + x(X^2-X)\theta_{2m})Y_m(y) \qquad (4.40)$$

where $X = x/b$, r is the total number of series terms used in analysis, and

$$Y_m(y) = \sin\frac{m\pi y}{l}$$

In the vertical direction,z, the finite strip is divided into several concrete layers; each reinforcement layer is replaced by a smeared steel layer with unchanged original reinforcement area and having stiffness only in the direction of the reinforcement (Fig.4.13).

According to the theory of thin plates and shells [59], the strain at any point of each layer can be expressed in terms of nodal displacement parameters as follows:

$$\{\epsilon\} = \begin{pmatrix} \epsilon_x \\ \epsilon_y \\ \gamma_{xy} \end{pmatrix} = \begin{pmatrix} \frac{\partial u}{\partial x} - z\frac{\partial^2 w}{\partial x^2} \\ \frac{\partial v}{\partial y} - z\frac{\partial^2 w}{\partial y^2} \\ \frac{\partial v}{\partial x} + \frac{\partial u}{\partial y} + 2z\frac{\partial^2 w}{\partial x \partial y} \end{pmatrix} = \sum_{m=1}^{r} [B]_m \{\delta\}_m \qquad (4.41)$$

where

$$[B]_m = \begin{bmatrix} -\frac{1}{b}Y_m & 0 & (6\frac{z}{b^2} - \frac{12xz}{b^3})Y_m & (\frac{4z}{b} - \frac{6xz}{b^2})Y_m \\ 0 & (1-\frac{x}{b})\frac{l}{m\pi}Y_m'' & -z(1-3\frac{x^2}{b^2}+2\frac{x^3}{b^3})Y_m'' & -z(x-2\frac{x^2}{b}+\frac{x^3}{b^2})Y_m'' \\ (1-\frac{x}{b})Y_m' & -\frac{1}{b}\frac{l}{m\pi}Y_m' & 12z(\frac{x}{b^2}-\frac{x^2}{b^3})Y_m' & -2z(1-4\frac{x}{b}+3\frac{x^2}{b^2})Y_m' \\ \frac{1}{b}Y_m & 0 & (\frac{-6z}{b^2}+\frac{12xz}{b^3})Y_m & (-\frac{6xz}{b^2}+\frac{2z}{b})Y_m \\ 0 & \frac{x}{b}\frac{l}{m\pi}Y_m'' & -z(3\frac{x^2}{b^2}-2\frac{x^3}{b^3})Y_m'' & -z(\frac{x^3}{b^2}-\frac{x^2}{b})Y_m'' \\ \frac{x}{b}Y_m' & \frac{1}{b}\frac{l}{m\pi}Y_m' & -12z(\frac{x}{b^2}-\frac{x^2}{b^3})Y_m' & -2z(3\frac{x^2}{b^2}-2\frac{x}{b})Y_m' \end{bmatrix} \qquad (4.42)$$

in which $Y_m' = \frac{dY_m}{dy}$ and $Y_m'' = \frac{d^2Y_m}{dy^2}$.

4.3.4 NONLINEAR SOLUTION

The loads are applied in a number of steps. In each loading step, the Newton-Raphson iteration method [6] is utilized for nonlinear solution. For each iteration an incremental linear stress-strain relationship is assumed, the displacement increment calculated, the strain and stress state determined and the material matrix updated. The following steps [71] are used to determine the states of strain and stress at any point in a concrete layer of a strip for the k-th iteration:

1. From the displacement increment vector $\Delta\{\delta\}^k$ obtained from the previous iteration, the strain increment vector is computed as:

$$\Delta\{\epsilon\}^k = (\Delta\epsilon_x^k, \Delta\epsilon_y^k, \Delta\gamma_{xy}^k)^T = \sum_{m=1}^{r} [B]_m \Delta\{\delta\}_m^k \tag{4.43}$$

where $[B]_m$ is strain matrix in Equation (4.42).

2. Using Equation (4.33) and performing coordinate transformation [66], the approximate stress increments can be calculated as:

$$\Delta\{\sigma\}^k = (\Delta\sigma_x^k, \Delta\sigma_y^k, \Delta\tau_{xy}^k)^T = [T_\epsilon^{k-1}]^T [D_c^{k-1}][T_\epsilon^{k-1}]\Delta\{\epsilon\}^k \tag{4.44}$$

where $[T_\epsilon]$ is the strain coordinate transformation matrix from x-y axes to the principal axes, as given below:

$$[T_\epsilon] = \begin{bmatrix} \cos^2\theta & \sin^2\theta & \sin\theta\cos\theta \\ \sin^2\theta & \cos^2\theta & -\cos\theta\sin\theta \\ -2\sin\theta\cos\theta & 2\sin\theta\cos\theta & \cos^2\theta - \sin^2\theta \end{bmatrix} \tag{4.45}$$

in which θ is the angle between σ_1 and x, obtained from the previous iteration.

The stress increments are only approximate because of the linearized material matrix. The current total approximate stresses are then obtained as:

$$\{\sigma\}^k = \{\sigma\}^{k-1} + \Delta\{\sigma\}^k \tag{4.46}$$

3. From the total approximate stresses the approximate principal stresses σ_i^k (i=1,2) and θ^k are calculated.

4. The equivalent uniaxial strains are then evaluated from (4.35):

$$\epsilon_{iu}^k = \epsilon_{iu}^{k-1} + (\sigma_i^k - \sigma_i^{k-1})/E_i^{k-1} \tag{4.47}$$

5. The biaxial stress ratio is determined from

$$\alpha^k = \sigma_1^k / \sigma_2^k \tag{4.48}$$

Then, σ_{ic}^k and ϵ_{ic}^k or σ_{it} are obtained from the biaxial strength envelope in Subsection 4.3.1.

6. The principal stresses σ_i^k and elastic moduli E_i^k corresponding to ϵ_i^k can then be computed from (4.36-4.38) and Fig.4.10. The current total stress vector $\{\sigma\}^k$ is obtained by transforming the principal stresses to the x-y axes. The material matrix $[D_c^k]$ is also updated to reflect the new tangent moduli.

The contribution of concrete layers to the tangential stiffness matrix of the strip in the k-th iteration, corresponding to the m-th and n-th terms of eigenfunctions, is

$$[K^k]_{mn} = \int [B]_m^T [T_c^k]^T [D_c^k][T_c^k][B]_n \, dv \tag{4.49}$$

Similarly, the stress state of reinforcement and its contribution to the tangential stiffness matrix of the strip can also be computed using the corresponding material model.

According to the principle of virtual work, in each plate strip, the resistance vector corresponding to the m-th term of eigenfunctions is:

$$\{R\}_m^k = \int [B]_m^T \{\sigma\}^k \, dv \tag{4.50}$$

For the two integrations given above, the Gaussian integration method is employed in both x and y directions. In each strip, 4 Gauss points are used in the x direction, whilst in the y direction the strip is divided into a

number of segments, and 4 Gauss points are used in each segments. The number of segments used must be sufficient to ensure satisfactory accuracy of integration for the highest order series term.

Next, the incremental displacements are evaluated as follows:

$$[K^k]\Delta\{\delta\}^{k+1} = \lambda(\{F\} - \{R\}^k) \tag{4.51}$$

and the new displacements are reached:

$$\{\delta\}^{k+1} = \{\delta\}^k + \Delta\{\delta\}^{k+1} \tag{4.52}$$

where $\{F\}$ is the vector of equivalent nodal forces of external loads, and λ is the relaxation coefficient. In order to prevent possible oscillation and divergence in iterations, the value of λ must be less than unity, $\lambda < 1.0$ ($\lambda = 0.8$ in the present study). This procedure is repeated until the convergence is achieved:

$$\frac{\sqrt{\sum(\Delta\delta_i^{k+1})^2}}{\sqrt{\sum(\delta_i^{k+1})^2}} \leq e$$

in which e is a prescribed allowable error (e=0.002 in the present study).

4.3.5 NUMERICAL EXAMPLE

A simply supported two-way square reinforced concrete slab is subjected to uniform load. This slab, with a thickness of 2 in. and a span of 72 in., is reinforced in both directions with uniform spacing.

Due to symmetry, only a quarter of the slab needs to be analyzed. Therefore, half of slab is modeled by 4 strips, and the integration in calculating the

tangential stiffness matrix and resistance to deformation is carried out over only half the span. 4 symmetrical series terms are used in this analysis.

The cross section is divided into 10 concrete layers and 2 orthogonal reinforcing steel layers of 3/16 in.diameter bars with the spacing shown in Fig.4.14. The following material properties are used for the analysis:

Concrete: $E_0 = 4700$ ksi, $f_c' = 5940$ psi, $f_t' = 550$ psi, $\epsilon_c = 0.0025$, $\nu = 0.18$.

Reinforcing Steel: $E_s = 30000$ ksi, $E_{sh} = 2000$ ksi, $f_y = 54.5$ ksi, $\epsilon_{su} = 0.1$.

The Newton-Raphson method is used. The deflections at the center of the slab under increasing uniform load are shown in Fig.4.15. For comparison, the results obtained from experiment [73], finite element analysis [71] and finite strip analysis [37] are also shown in the same figure. It can be seen that the present research improved the accuracy of nonlinear finite strip analysis of the RC slab significantly.

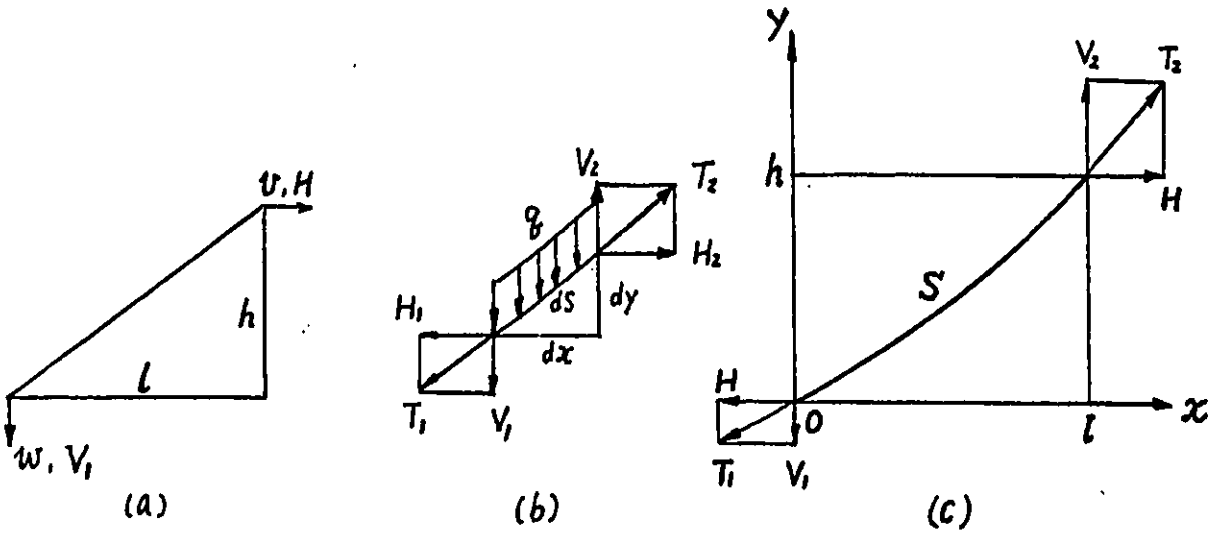

Figure 4.1: Cable

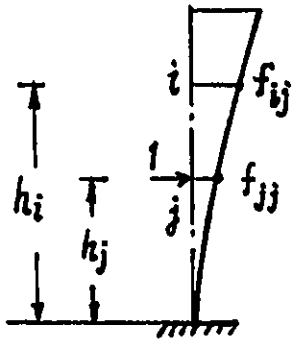

Figure 4.2: Pylon

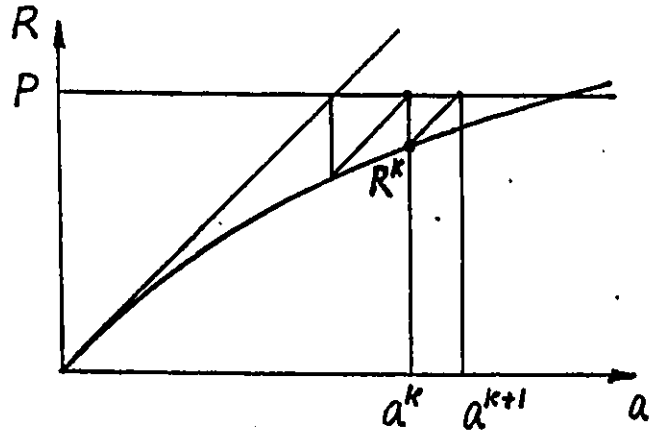

Figure 4.3: Initial Stiffness Method

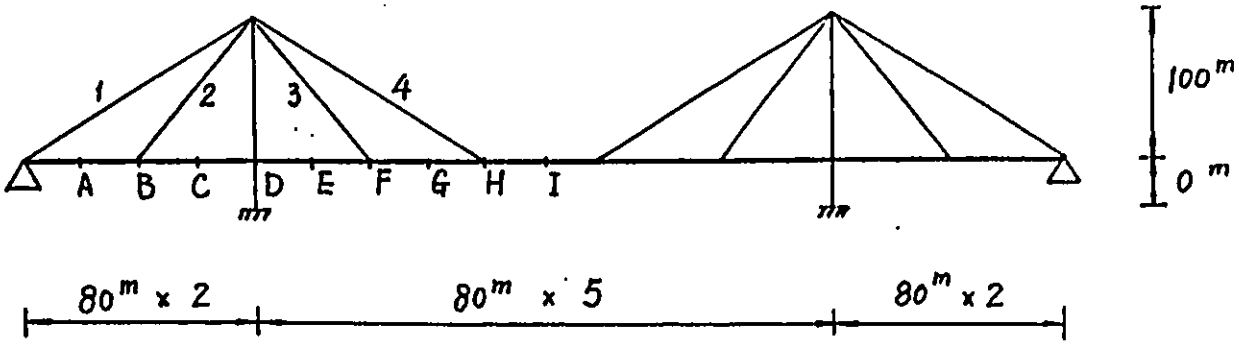

Figure 4.4: Single Plane Cable-Stayed Bridge

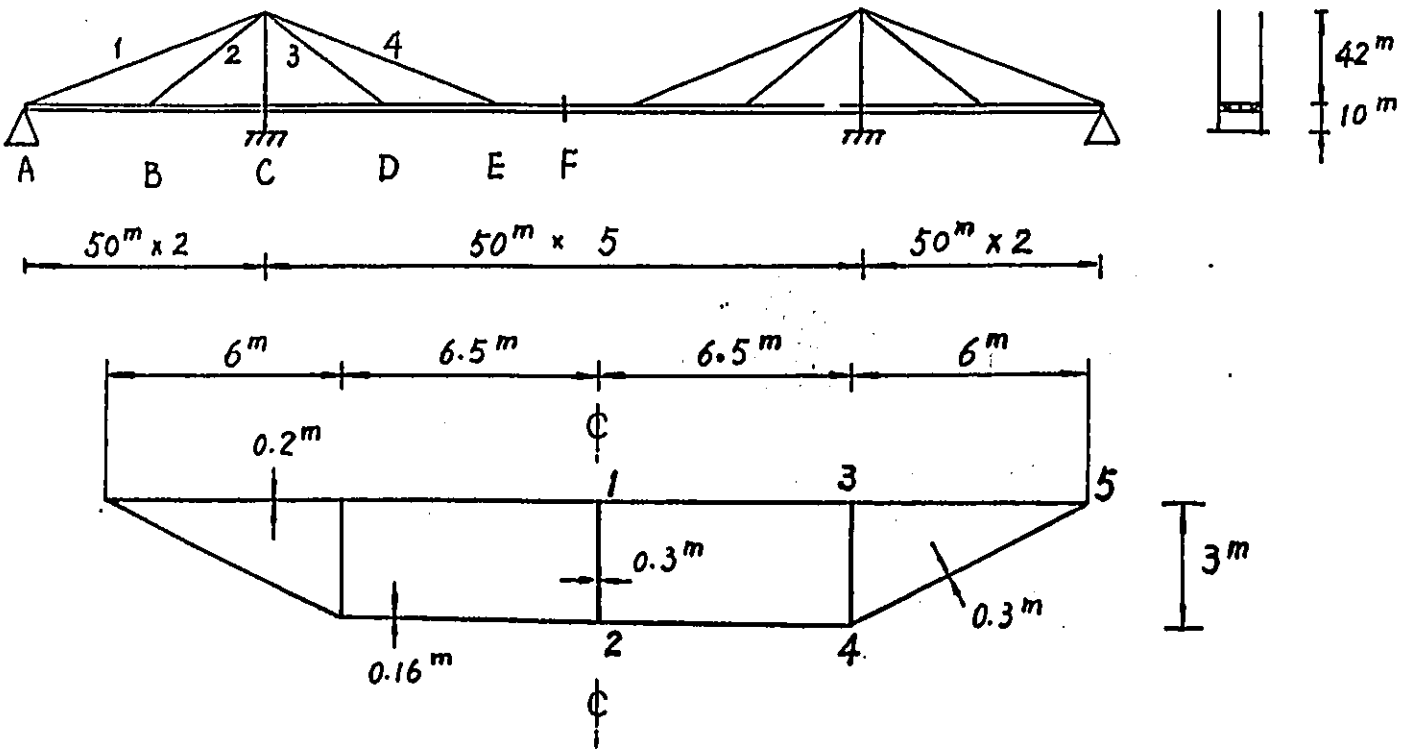

Figure 4.5: Double Plane Cable-Stayed Bridge

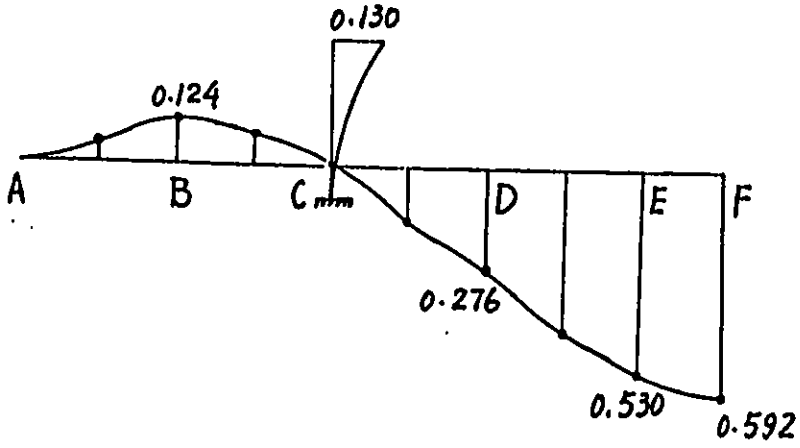

Figure 4.6: Deflection of Girder and Pylon

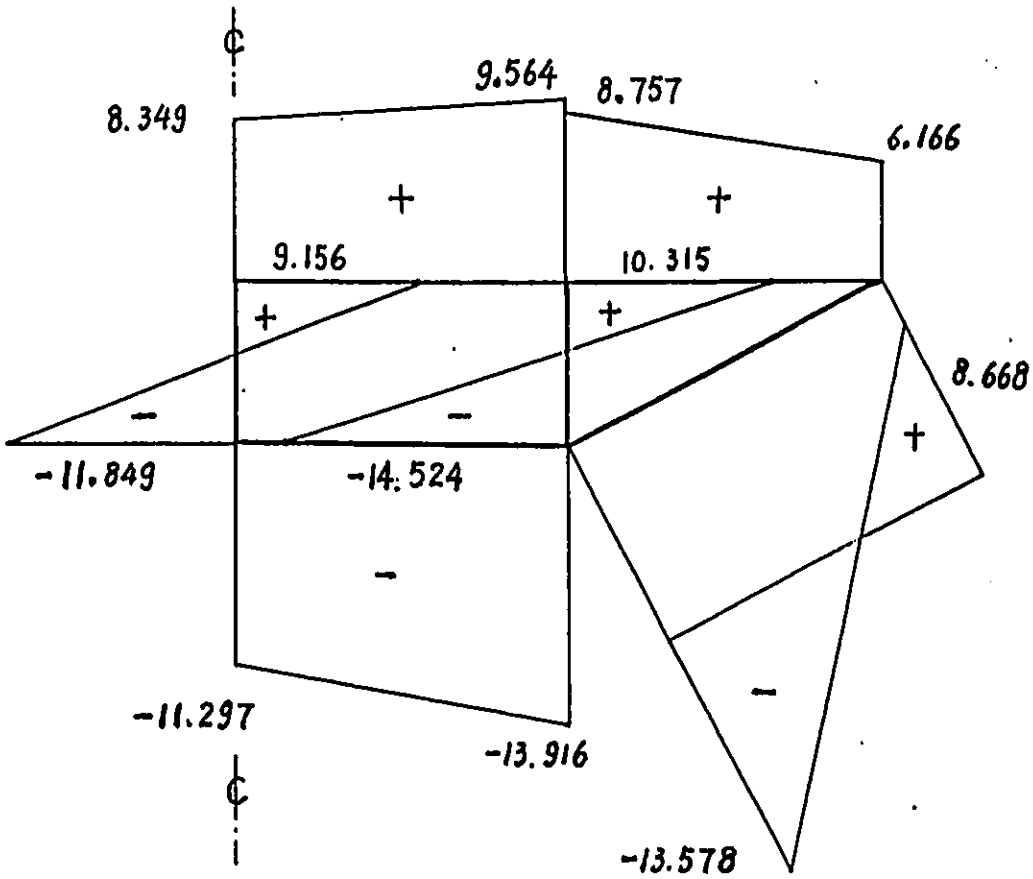

Figure 4.7: Longitudinal Stresses at Cross-Section B (in Mpa)

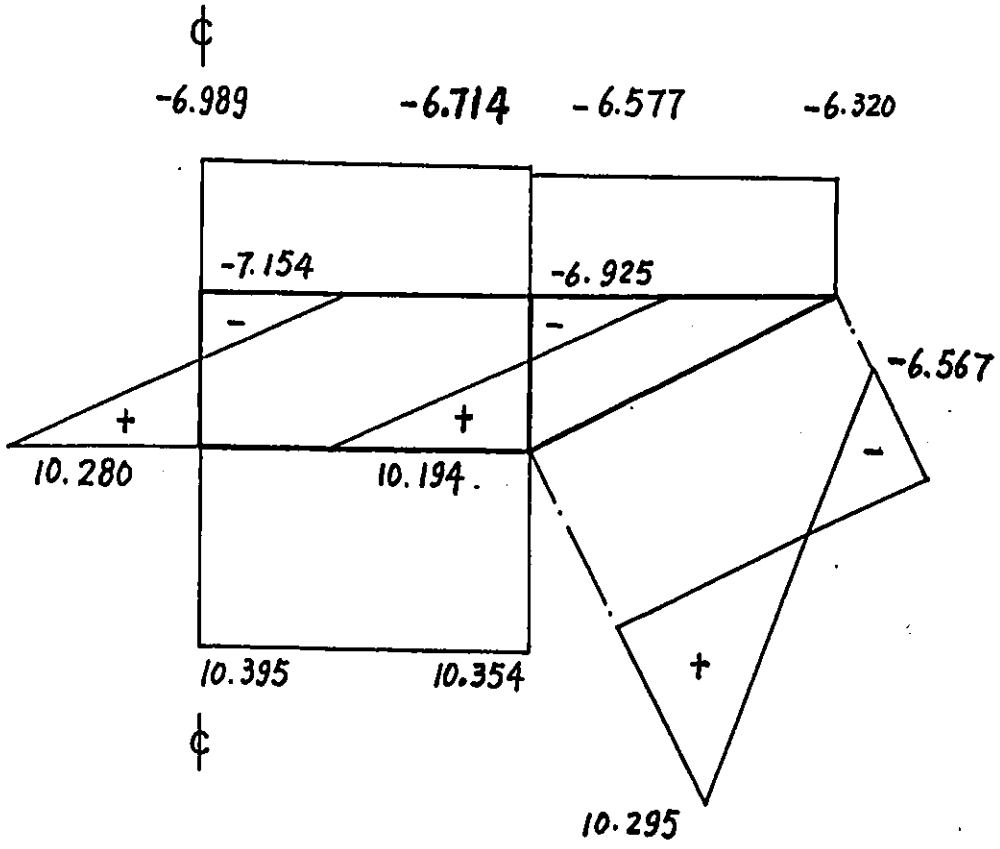

Figure 4.8: Longitudinal Stresses at Cross-Section F (in Mpa)

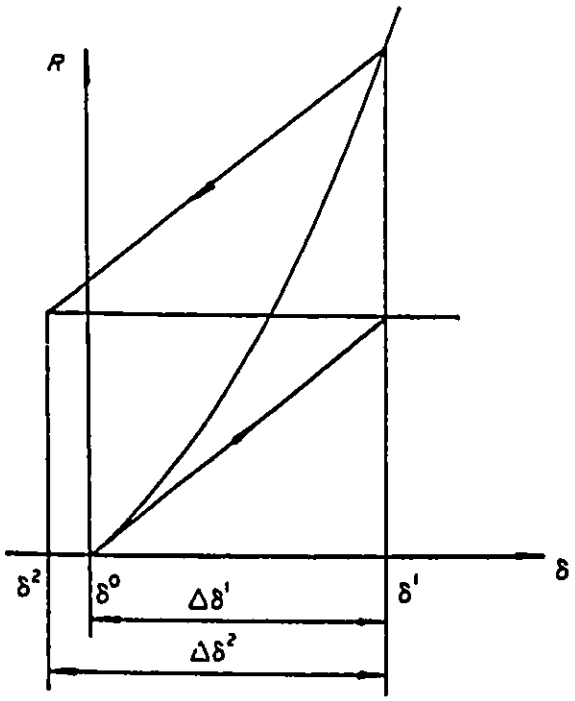

Figure 4.9: Possible Divergence

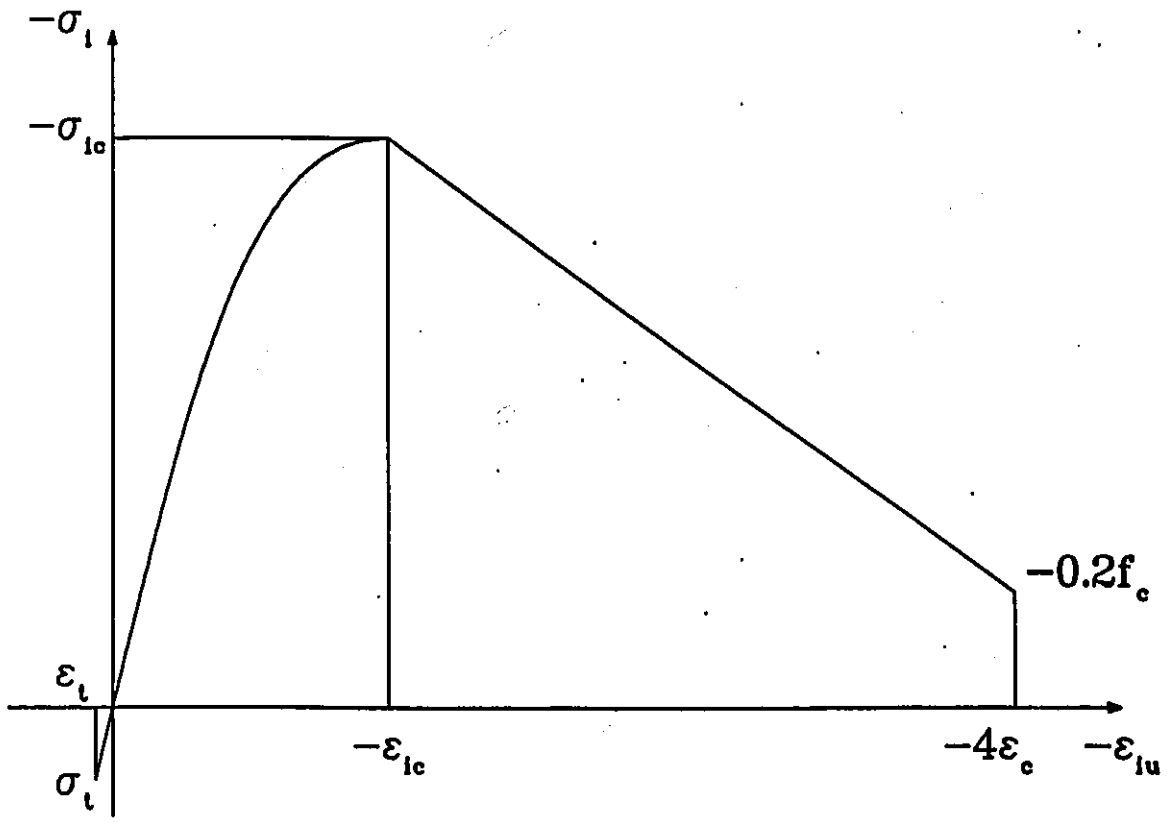

Figure 4.10: Equivalent Uniaxial Stress-Strain Model

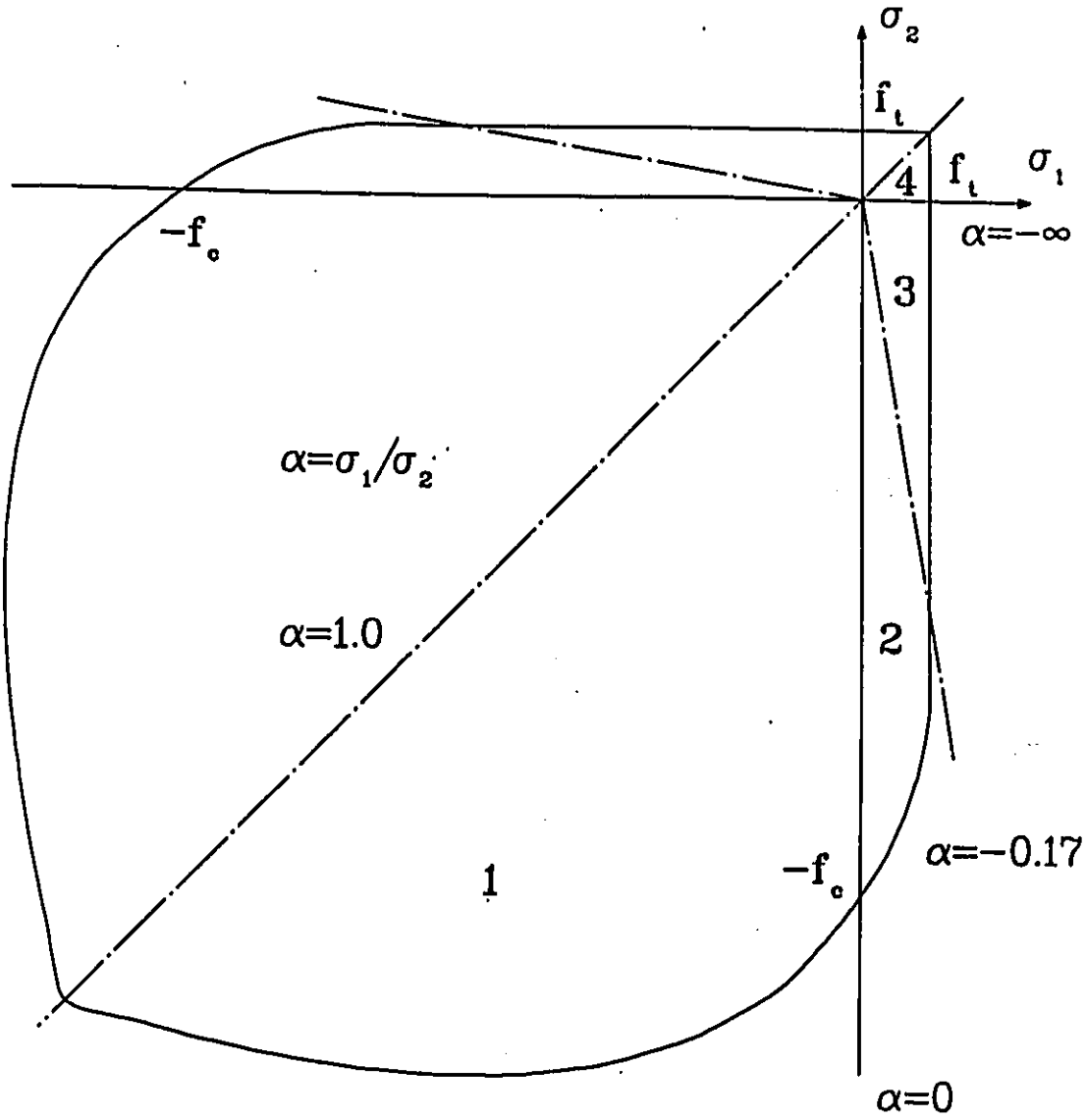

Figure 4.11: Biaxial Strength Envelope

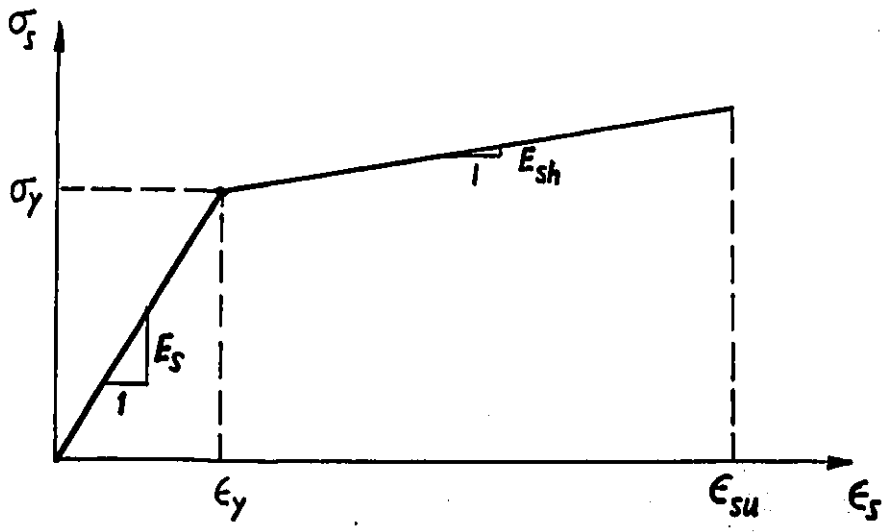

Figure 4.12: Material Model of Steel

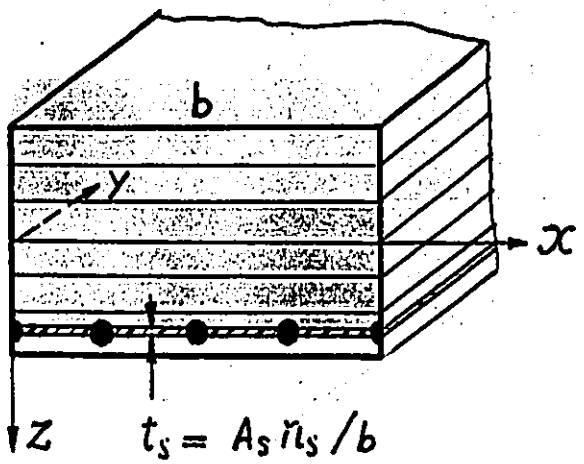

Figure 4.13: Layers of Strip

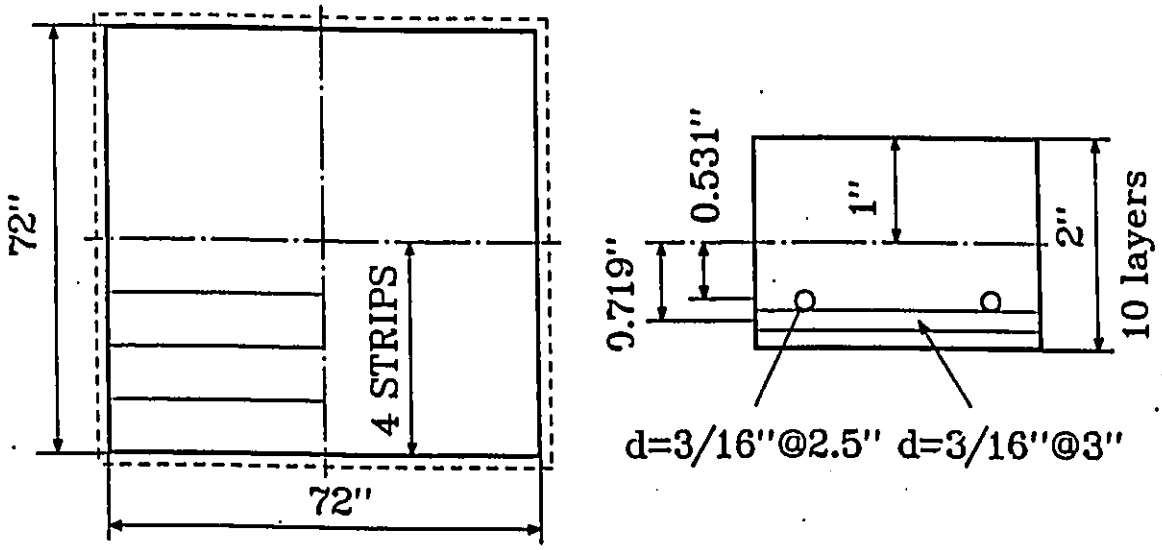

Figure 4.14: Taylor Slab

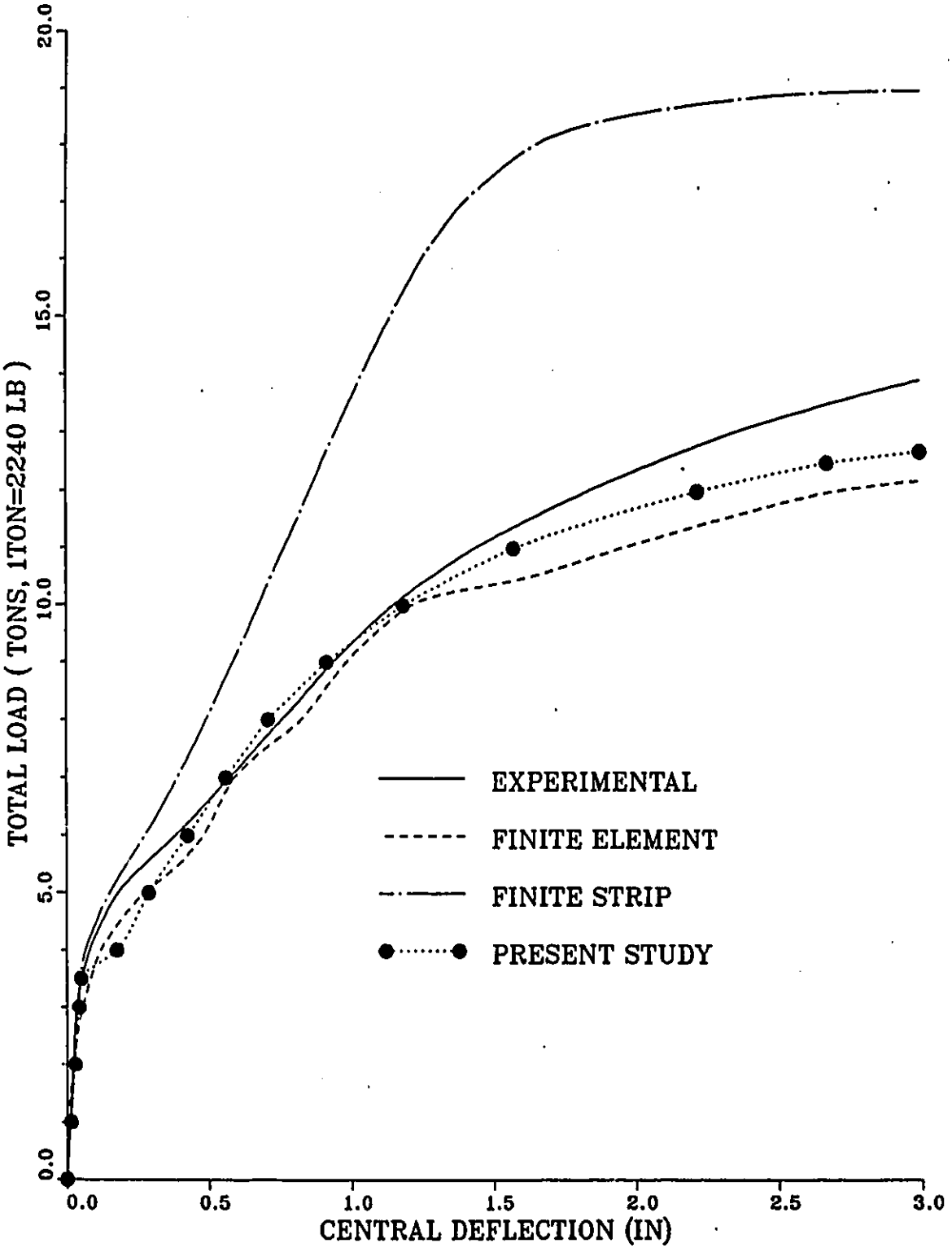

Figure 4.15: Deflection of Taylor Slab

Chapter 5

COMBINED ANALYSIS

If a plate structure has constant cross-section and its end support condition does not change transversely, the finite strip method has proven to be the most efficient numerical structural analysis method. However, if the structure has any irregularities, e.g. a rectangular plate with openings, the finite strip method is no longer applicable on its own and the finite element method or the boundary element method has to be used. In this case, however, if these methods can be combined together, with the finite strips being used for the regular part of the plate and the finite elements or boundary elements modelling the irregular part, then the efficiency of the finite strip method and the universality of the latter methods are both utilized to their full advantage.

In the present study, special transition elements are used to connect the two different regions. One side of such a transition element coincides with the nodal line of adjacent finite strip and has the same degrees of freedom; on the opposite side there are a number of nodes which are connected with the finite

element or boundary element. Inside the transition element the deflection is expressed in terms of the degrees of freedom of the finite strip nodal line and the nodes of the finite element or boundary element by their corresponding shape functions. Using the principle of minimum total potential energy, the stiffness matrix and load vector of the transition element can be obtained.

5.1 FINITE STRIP METHOD FOR REGULAR PART

The regular region of the plate is subdivided into a number of finite strips. Within each strip, the deflection is expressed as:

$$w = \sum_{m=1}^{r} (f_1(\xi)w_{1m} + bg_1(\xi)\theta_{1m} + f_2(\xi)w_{2m} + bg_2(\xi)\theta_{2m})Y_m(y) \qquad (5.1)$$

where l and b are the length and width of the strip respectively. $f_1(\xi)$, $f_2(\xi)$, $g_1(\xi)$ and $g_2(\xi)$ are transverse shape functions which are Hermitian cubic polynomials:

$$f_1(\xi) = 1 - 3\xi^2 + 2\xi^3, \quad f_2(\xi) = 3\xi^2 - 2\xi^3,$$
$$g_1(\xi) = \xi - 2\xi^2 + \xi^3, \quad g_2(\xi) = \xi^3 - \xi^2, \quad (\xi = x/b) \qquad (5.2)$$

$Y_m(y)$ is the m-th series term of beam vibration eigenfunctions, its expression is listed in Subsection 2.1.1 according to the end conditions of the plate strip.

Following the standard procedure in Section 2.1, it is not difficult to obtain the stiffness matrix and load vector of such a strip.

5.2 COMBINED WITH FINITE ELEMENT METHOD

5.2.1 FINITE ELEMENT METHOD FOR IRREGULAR PART

In this analysis, the irregular region of plate is analyzed by a number of conforming rectangular plate elements (Fig.5.1) [74] with four degrees of freedom at each node which are

$$\{\delta\} = (w, \frac{\partial w}{\partial x}, \frac{\partial w}{\partial y}, \frac{\partial^2 w}{\partial x \partial y})^T$$

The shape function of this element is:

$$\begin{aligned} w \;=\; & f_1(\xi)f_1(\eta)w_i + bg_1(\xi)f_1(\eta)\frac{\partial w_i}{\partial x} + af_1(\xi)g_1(\eta)\frac{\partial w_i}{\partial y} + abg_1(\xi)g_1(\eta)\frac{\partial^2 w_i}{\partial x \partial y} \\ & + f_1(\xi)f_2(\eta)w_j + bg_1(\xi)f_2(\eta)\frac{\partial w_j}{\partial x} + af_1(\xi)g_2(\eta)\frac{\partial w_j}{\partial y} + abg_1(\xi)g_2(\eta)\frac{\partial^2 w_j}{\partial x \partial y} \\ & + f_2(\xi)f_1(\eta)w_k + bg_2(\xi)f_1(\eta)\frac{\partial w_k}{\partial x} + af_2(\xi)g_1(\eta)\frac{\partial w_k}{\partial y} + abg_2(\xi)g_1(\eta)\frac{\partial^2 w_k}{\partial x \partial y} \\ & + f_2(\xi)f_2(\eta)w_l + bg_2(\xi)f_2(\eta)\frac{\partial w_l}{\partial x} + af_2(\xi)g_2(\eta)\frac{\partial w_l}{\partial y} + abg_2(\xi)g_2(\eta)\frac{\partial^2 w_l}{\partial x \partial y} \end{aligned} \tag{5.3}$$

where $\xi = x/b$ and $\eta = y'/a$.

This type of element meets the continuity requirement between any adjacent elements not only for the deflection w and the tangential derivative $\frac{\partial w}{\partial s}$ but also for the normal derivative $\frac{\partial w}{\partial n}$. Therefore, this element is a conforming plate bending element, and it achieves considerable improvement in accuracy in comparison with rectangular elements having only 3 degrees of freedom at each node.

5.2.2 TRANSITION ELEMENT

A row of rectangular transition elements is used to connect the finite element region with the finite strip region. One side of each transition element coincides with the nodal line of adjacent strip and has the same degrees of freedom. On the opposite side there are two corner nodes which are attached to the nodes of adjacent finite elements and have the same degrees of freedom as these finite element nodes (Fig.5.2). Inside the transition element, the deflection w is expressed in terms of degrees of freedom of nodal line and two nodes by their corresponding shape functions in the form:

$$\begin{aligned} w &= \sum_{m=1}^{r}(f_1(\xi)w_{1m} + bg_1(\xi)\theta_{1m})Y_m(y) \\ &\quad + f_2(\xi)f_1(\eta)w_k + bg_2(\xi)f_1(\eta)\frac{\partial w_k}{\partial x} + af_2(\xi)g_1(\eta)\frac{\partial w_k}{\partial y} + abg_2(\xi)g_1(\eta)\frac{\partial^2 w_k}{\partial x \partial y} \\ &\quad + f_2(\xi)f_2(\eta)w_l + bg_2(\xi)f_2(\eta)\frac{\partial w_l}{\partial x} + af_2(\xi)g_2(\eta)\frac{\partial w_l}{\partial y} + abg_2(\xi)g_2(\eta)\frac{\partial^2 w_l}{\partial x \partial y} \end{aligned} \tag{5.4}$$

where $\xi = x/b$ and $\eta = y'/a$.

It should be noted that the nodal line 1 and nodes k, l have the same type of shape function in the direction x, which are Hermitian cubic polynomials. This is in order to simulate certain basic deformation patterns more accurately, such as one dimensional bending in the direction y, torsion about the axis y, etc.

The stiffness matrix and the load vector can be obtained in accordance with standard finite strip formulation. Simply assembling the stiffness matrices and load arrays of these transition elements with those of finite strips and

No.of Strips	2	3	4	Theory
No.of Sym.Terms	3	3	5	
Mesh of elements	2 by 4	3 by 6	4 by 8	
w_{max} (m)	0.0113105	0.0111349	0.0110848	0.0110074
M_x at A (MN-m/m)	-4.390	-4.747	-4.896	
M_x at B (MN-m/m)	-4.719	-4.916	-5.001	
M_y at C (MN-m/m)	-5.111	-4.915	-5.071	-5.130
M_x at E (MN-m/m)	2.496	2.380	2.331	
M_y at E (MN-m/m)	2.445	2.376	2.322	2.375

Table 5.1: Deflection and Moments in Clamped Square Plate

finite elements will lead immediately to the formulation for the whole plate structure.

5.2.3 NUMERICAL EXAMPLES

1. Clamped square plate under uniform load

This example is chosen to verify the present method. The square plate is clamped along four edges and is subjected to uniform load. The length of each side is 10.0 m, the thickness is 0.5 m. The material properties are $E = 100000MPa$ and $\nu = 0.3$. The intensity of the load is $q = 1.0MN/m^2$. Half the plate is divided into finite strips, the other half into finite elements. The mesh is shown in Fig.5.3 and the results are listed in Table 5.1. The analytical results are also given in this table for comparison. From this table it can been seen that the method achieves satisfactory accuracy in evaluating maximum deflection and bending moment.

2. Square plate supported by walls and columns

A square plate with a rectangular opening is supported by walls and columns

(Fig.5.4). The length of each side is 9.0 m and the thickness is 0.2 m. The material properties are E=25000 MPa, and $\nu = 0.15$. The plate is subjected to uniform load of intensity $q = 10kN/m^2$.

The part supported by columns is divided into 6 by 18 conforming rectangular plate elements with 4 degrees of freedom at each node; the rest of the plate is divided into 11 strips and one row of transition elements that connect the strips to the finite elements.Five symmetrical series terms are used. For simplicity, the walls are regarded as simple supports, and the columns as point supports.

The resulting deflection along line C-C and the bending moment M_x along the lines B-B and C-C are shown in Fig.5.5. The CPU time spent for the analysis is 4.2 sec. on a Mainframe AMDAHL-5860.

The structure was also analyzed using an 18×18 array of the above-mentioned elements at a cost of 12.1 sec. of CPU time. However, the results show no discernible difference from the previous solution when the results of both methods are drawn on the same figure.

5.3 COMBINED ANALYSIS WITH BOUNDARY ELEMENT METHOD

5.3.1 BOUNDARY ELEMENT ANALYSIS FOR IRREGULAR REGION

In this analysis, the boundary of the irregular region is [illegible] into a number of boundary elements. Each element has between 2 and 11 nodes,and all the

boundary functions along the element are expressed in terms of their nodal values by Lagrange interpolation [75]. A source point is located at a little distance from the boundary on the outside normal line passing through each node. Applying a unit force and a unit normal moment at each source point respectively and implementing the Maxwell-Betti theorem provide the two integration equations:

$$\int_s (WV^f + \Theta M^f)\, ds + \sum_{i=1}^{N_c} W_i C_i^f = \int_A pw^f\, dA + \int_s (W^f V + \Theta^f M)\, ds + \sum_{i=1}^{N_c} W_i^f C_i \tag{5.5}$$

$$\int_s (WV^m + \Theta M^m)\, ds + \sum_{i=1}^{N_c} W_i C_i^m = \int_A pw^m\, dA + \int_s (W^m V + \Theta^m M)\, ds + \sum_{i=1}^{N_c} W_i^m C_i \tag{5.6}$$

where

A and s denote the plate area and the boundary coordinate,

w is deflection in domain,

W and Θ are boundary deflection and normal rotation,

M,V and C are boundary moment, equivalent shear and corner force,

f and m are superscripts identifying the fundamental solutions for the unit force and the unit moment respectively,

N_c is the number of corners.

All four boundary functions W, Θ, M and V are unknowns on the interface between the transition strip and the neighboring boundary element, but among them only two are unknown on the other boundaries after imposing displacement and force boundary conditions.

At the ends of interface, double nodes are used [76] (Fig.5.6). Both nodes A

and B have the same coordinates, but may have different boundary conditions. In order to make the number of unknowns at nodes A and B match the number of the boundary integration equations, the corner forces at these two nodes may be expressed in terms of the normal rotations of their respective element in the form:

$$C_A = D(1-\nu)(\frac{\partial^2 w}{\partial s \partial n})^{(1)} = D(1-\nu)\sum_{j=1}^{N_1}\frac{\partial L_j^{(1)}}{\partial s}\Theta_j \tag{5.7}$$

$$C_B = -D(1-\nu)(\frac{\partial^2 w}{\partial s \partial n})^{(2)} = -D(1-\nu)\sum_{j=1}^{N_2}\frac{\partial L_j^{(2)}}{\partial s}\Theta_j \tag{5.8}$$

where

(1) and (2) are the superscripts identifying the elements ending at node A and starting at node B respectively;

N_1 and N_2 are the numbers of nodes on boundary elements 1 and 2 respectively;

L_j is the Lagrange shape function of node j and is expressed as:

$$L_j(s) = \prod_{\substack{i=1 \\ i \neq j}}^{N} \frac{s - s_i}{s_j - s_i} \tag{5.9}$$

Substituting the expressions for fundamental solutions into the boundary integral equations and implementing the boundary element discretization technique [75,76] produce the following boundary element matrices:

$$[H^1, H_I^1]\begin{Bmatrix} U^1 \\ U_I^1 \end{Bmatrix} = [G^1, G_I^1]\begin{Bmatrix} P^1 \\ P_I^1 \end{Bmatrix} + \{B^1\} \tag{5.10}$$

where

U denotes the values of deflection and normal rotation at all the nodes,

P represents the values of equivalent shear and normal moment at all the nodes,

B is the effect of the loads in domain,

1 is the superscript identifying the boundary element region,

I is the subscript defining the interface between the transition strip and the boundary elements.

For each node on the interface there are 4 unknowns (W,Θ,V and M) versus 2 equations. Therefore, two more equations are required for each of these nodes.

5.3.2 TRANSITION STRIP AND COMBINED SOLUTION

A transition strip is inserted between the finite strip region and the boundary element region and connects the two regions together. One side of the transition strip coincides with the nodal line of the adjacent strip and has the same degrees of freedom as this nodal line. On the opposite side there are a number of nodes which are attached to the nodes of the neighboring boundary elements and have the same displacement parameters (deflection W and normal rotation Θ) as they do (Fig.5.7). Inside the transition strip the deflection w is expressed in terms of the degrees of freedom of the nodal line and the nodes by their corresponding shape functions in the form:

$$w = \sum_{m=1}^{r}(f_1(\xi)w_{1m} + bg_1(\xi)\theta_{1m})Y_m(y) + \sum_{j=1}^{N} L_j(f_2(\xi)w_j + ag_2(\xi)\theta_j) \quad (5.11)$$

where

N is the number of nodes of this strip along the interface,

L_j is the Lagrange shape function of node j.

It should be noted that the nodal line and nodes 1 to N have the same type of shape functions in the direction x, which are Hermitian cubic polynomials, in order to simulate certain basic deformation patterns more accurately as noted earlier.

Using the principle of minimum total potential energy, the stiffness matrix and the load vector of the transition strip are generated.

Assembling the stiffness matrix and load vector of the transition strip with those of the finite strips and applying condensation technique [6] effect a transformation of the finite strips and transition strip into a substructure having only the degrees of freedom of the nodes on the interface. The matrix equation of this substructure is of the form:

$$[K]\{U_I^2\} = \{F_I^2\} + \{B^2\} \tag{5.12}$$

where

F_I^2 is the vector of unknown interaction nodal forces,

B represents the effects of external load,

2 is the superscript identifying the finite strip and transition strip region.

At all nodes on the interface, the displacement on both sides must be the same, and the interaction force must be the same in magnitude and opposite in direction.These requirements give the following relationships

$$\{U_I^2\} = \{U_I^1\} \tag{5.13}$$

$$\{F_I^2\} = -[M]\{P_I^1\} \tag{5.14}$$

where [M] is the transformation matrix from the distributed boundary forces on the interface boundary element to the nodal forces at the nodes of the transition strip, and its elements M_{ij} are given by

$$M_{ij} = \int_c L_i(y) L_j(y)\, dy$$

Substituting Equations (5.13) and (5.14) into (5.12) gives a set of equations:

$$[K]\{U_I^1\} = -[M]\{P_I'\} + \{B^2\} \tag{5.15}$$

Combining matrices (5.10) and (5.15) together will yield a set of equations that are just sufficient in number to solve for all the unknowns in the boundary element region, including the unknowns at the nodes on the interface; these latter can be substituted back into the matrix of the finite strip and transition strip region, and all the unknown nodal parameters in this region can then be readily obtained. Thereafter it is a straightforward procedure to compute the displacement and stress components at any points of interest.

5.3.3 NUMERICAL EXAMPLES

1. Simply supported square plate under uniform load

This example is chosen to verify the present method. A square plate is hinged along four edges and subjected to uniform load. The length of each side is L, Poisson's ratio is $\nu = 0.3$, Flexural rigidity is D, and the intensity of the load is q. Three different meshes are used to analyze the plate (Fig.5.8). The upper part of each mesh is divided into finite strips with equal width 0.1L. Five symmetrical terms are used in the series of longitudinal shape functions.

Mesh	w_{max} $= \alpha qL^4/D$ α	$(M_x)_{max}$ $= \beta qL^2$ β	V_{max} $= \delta qL$ δ	R nqL^2 n
m=3	0.004063	0.04804	0.4205	0.0618
m=5	0.004062	0.04790	0.4205	0.0646
m=7	0.004063	0.04789	0.4205	0.0654
Theory	0.00406	0.0479	0.420	0.065

Table 5.2: Deflection and Stresses in Simply Supported Square Plate

The boundary of the lower part is simulated by 4 boundary elements with equal nodal spacing 0.1L. Both parts are connected by a transition strip with a width of 0.1L. The numerical results are listed in Table 5.2. In this table, w_{max} and $(M_x)_{max}$ are the deflection and bending moment at the plate center respectively, V_{max} is the equivalent shear force at the center of the bottom edge, and R is the corner force at the lower corners. In comparison with plate theory [59], it can be seen that the accuracy of the present method is satisfactory.

2. Simply supported square plate with an opening and a skew corner

A square plate is simply supported along all four sides and subjected to uniform load $q = 10\ KN/m^2$. The length of each side is 10.0 m, and the thickness 0.2 m. The material properties are $E = 25000$ MPa and $\nu = 0.15$. One corner is cut off at 45 degrees, and a square opening is located near another corner, as shown in Fig. 5.9.

The part including the opening and the skew corner is analyzed by 9 boundary elements with 50 nodes whilst the rest of the plate is analyzed by 5 finite strips and one transition strip with 10 series terms.

The resulting bending moments M_x and M_y along line A-B-C are depicted in Fig. 5.10.

The plate was also analyzed by the boundary element method alone, with 9 elements and 58 nodes. The results of this analysis if plotted on Fig. 5.10 would be indistinguishable from those already shown.

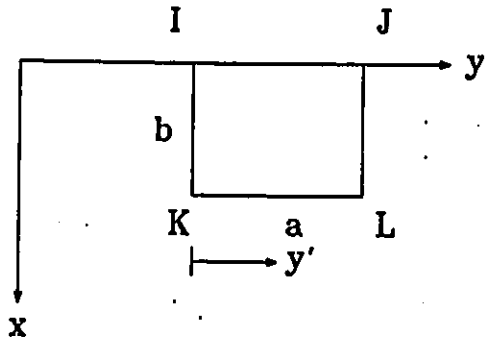

Figure 5.1: Rectangular Finite Element

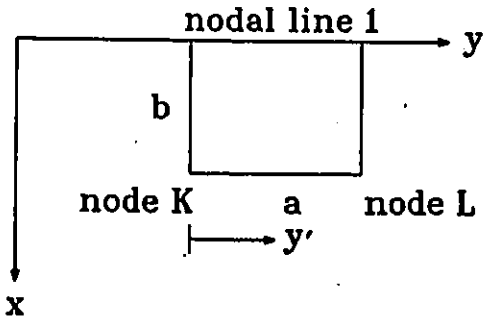

Figure 5.2: Transition Element

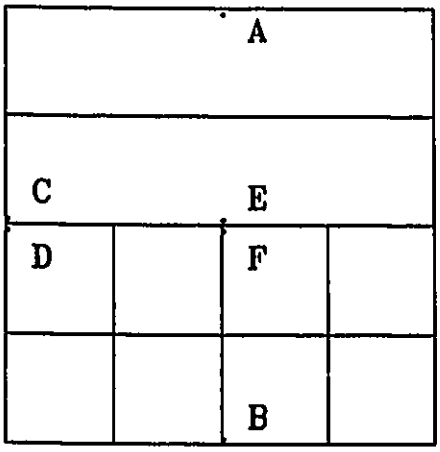

Figure 5.3: Square Plate

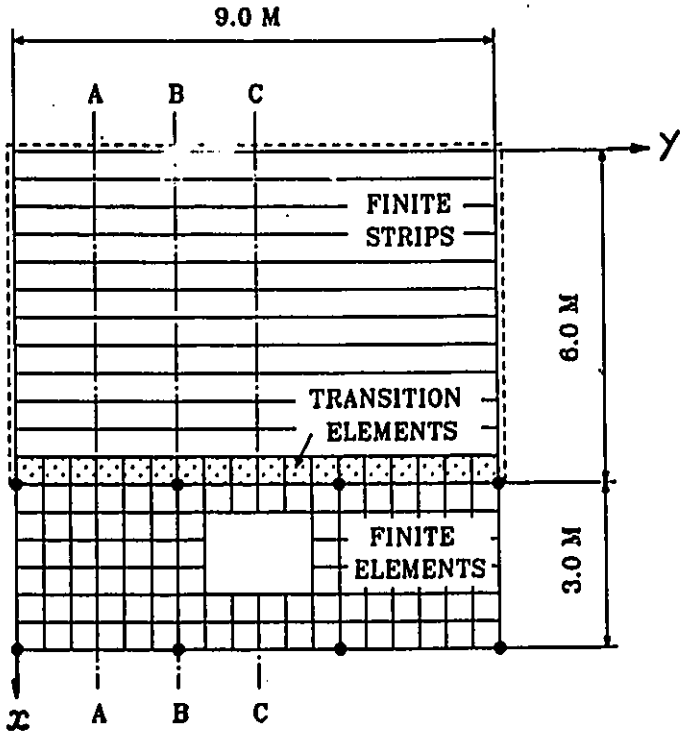

Figure 5.4: Plate Supported by Walls and Columns

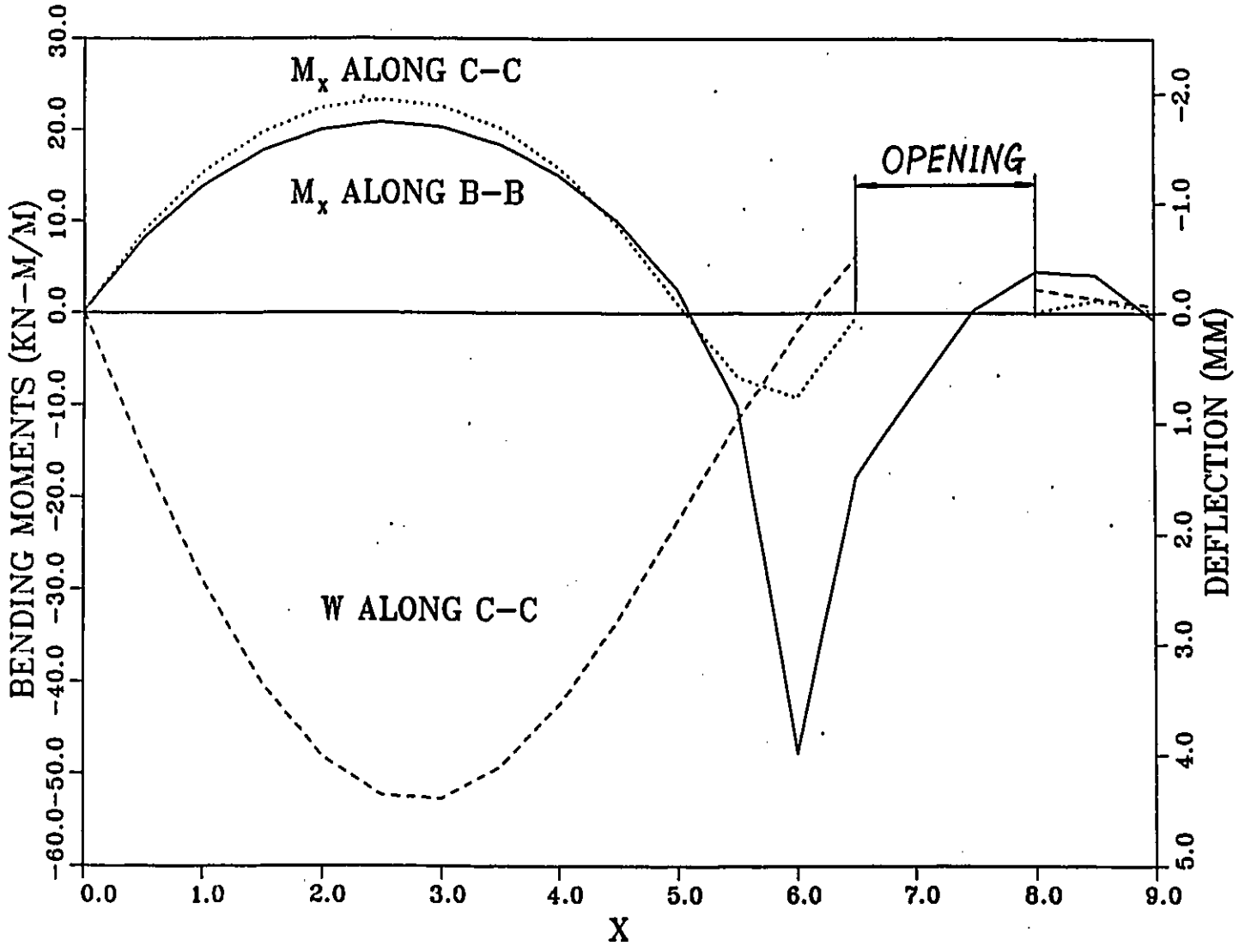

Figure 5.5: Deflection and Bending Moments of Plate in Fig.5.4

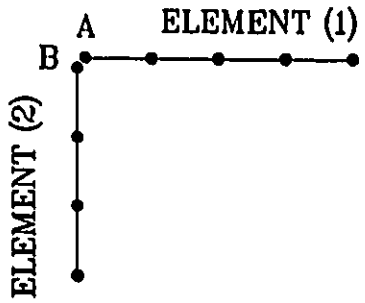

Figure 5.6: Double Nodes

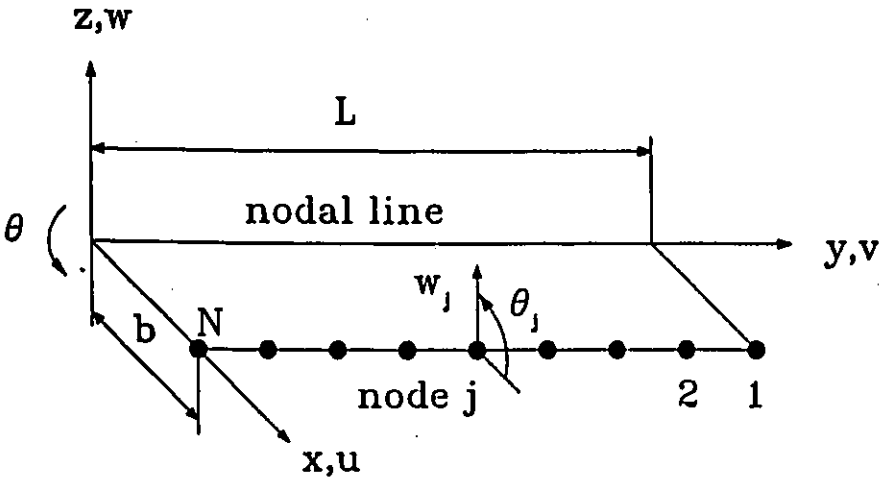

Figure 5.7: Transition Strip

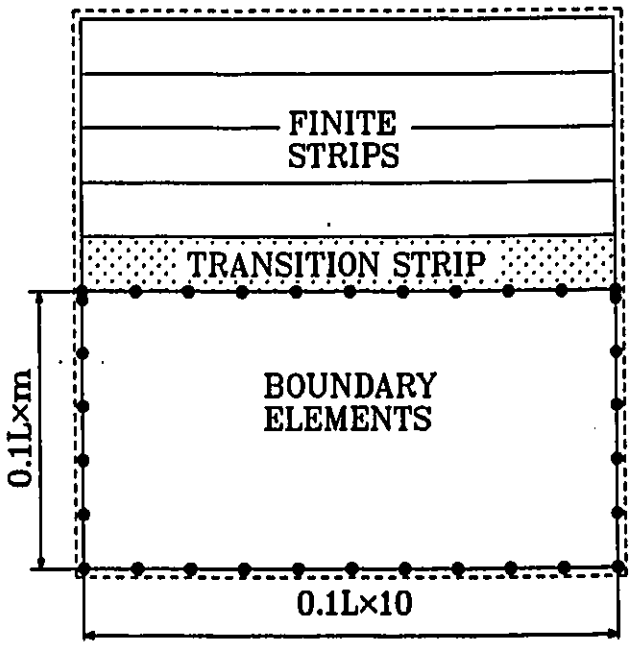

Figure 5.8: Simply Supported Square Plate under Uniform Load

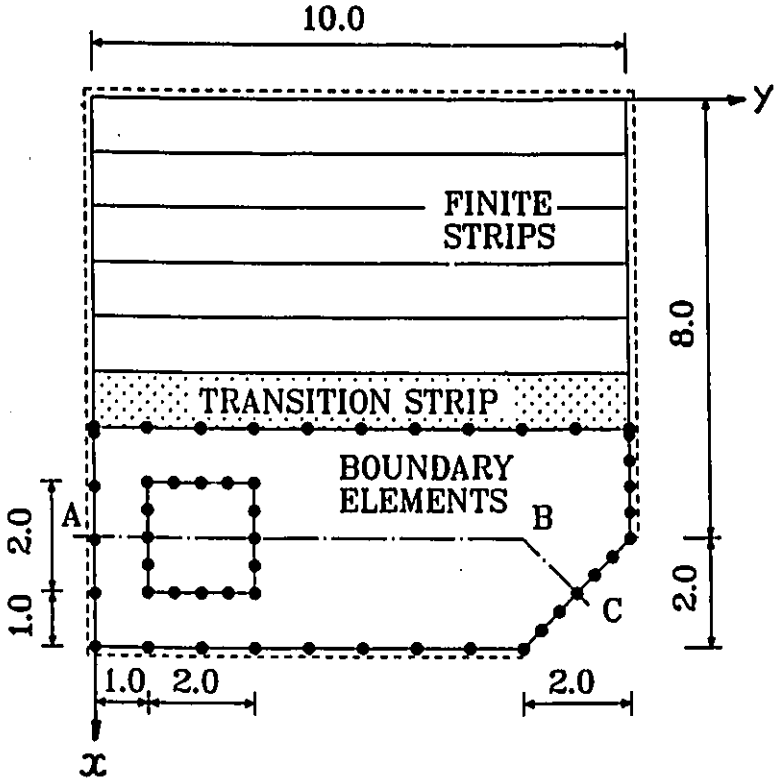

Figure 5.9: Plate with Opening and Skew Corner

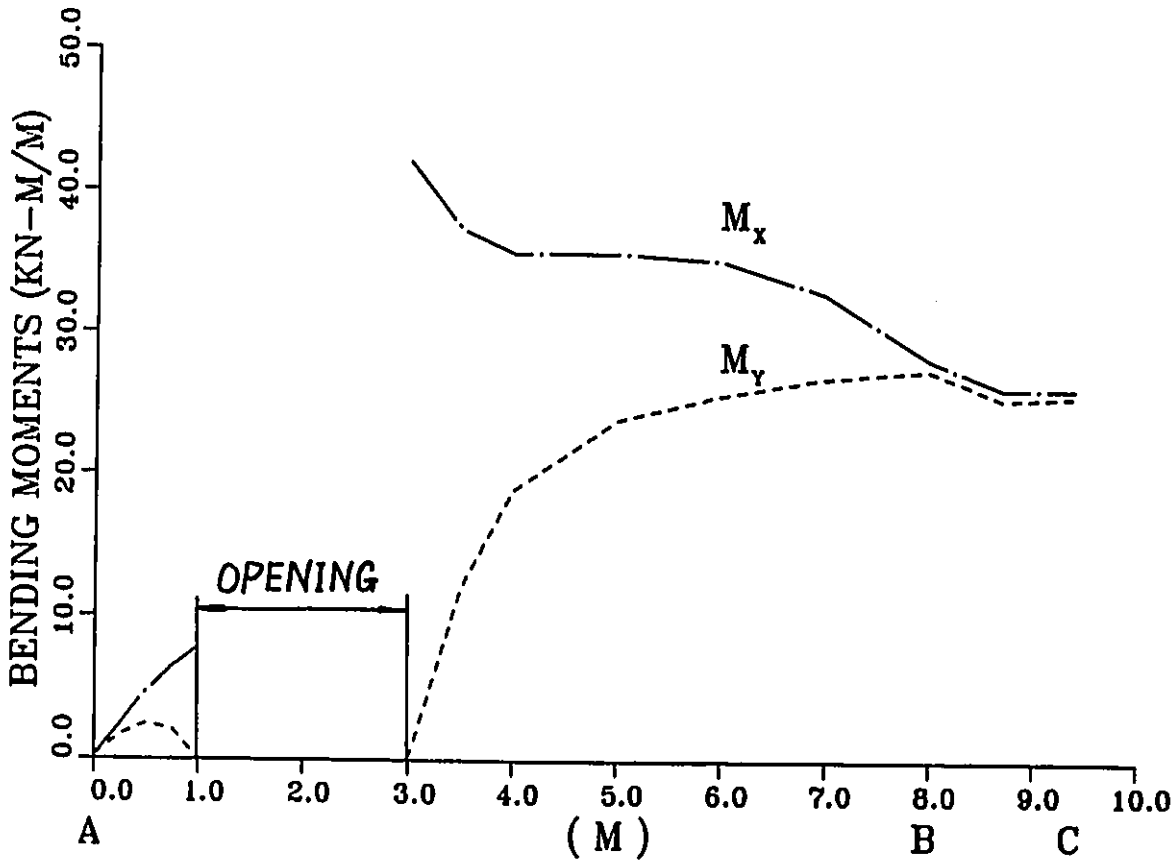

Figure 5.10: Bending Moments along A-B-C

Chapter 6

CONCLUSIONS AND RECOMMENDATIONS

6.1 CONCLUSIONS

In the present study, the objectives proposed earlier have been accomplished. The main achievements are listed as follows:

(1) The semi-analytical finite strip method has been extended to the analysis of continuous haunched slab-on-girder and box-girder bridges. In this analysis, three types of finite strip are developed, which being top flange plate strip, vertical web strip and bottom flange shell strip. For each type of the above strip, appropriate curvilinear coordinate system is chosen, strain-displacement relationships and displacement functions are derived. This method gives high efficiency for distributed loading, improved accuracy for the longitudinal stresses over intermediate supports. The results obtained are in reasonable agreement with those from finite element analysis or experimental analysis.

(2) The spline finite strip method ha been extended to the analysis of con-

tinuous haunched slab-on-girder and box-girder bridges. In this analysis, three types of strip are developed, which being top flange plate strip, vertical web strip and bottom flange shell strip. For all of the above strips, Cartesian coordinate system is chosen and some coordinate transformations are performed, strain-displacement relationships and displacement functions are derived. This method is more flexible than semi-analytical finite strip method in dealing with point loads, continuity and variety of boundary conditions, and shows higher efficiency in most load cases. Satisfactory results are obtained in numerical examples.

(3) The finite strip method has been extended to nonlinear analysis of cable-stayed bridges. By using the finite strip method for continuous structures combined with the flexibility approach, the girder is transformed into a substructure with d.o.f at cable attachment points only, thus, only very few unknowns are involved in nonlinear iterations. In the analysis, cables are calculated according to theory of catenary, therefore, the nonlinearities due to sag and angle change of cables are taken into consideration accurately. Furthermore, initial stiffness iteration is employed for nonlinear solution. Consequently, the present method is more accurate than those based on simpler theory, and more efficient than finite element method.

(4) The efficiency of geometrically nonlinear finite strip analysis of plates is improved. In this analysis, modified Newton-Raphson method is used, i.e. the initial stiffness matrix is formed and inverted only once during all the iterations. Besides, the different series terms remain uncoupled if they are

not coupled in linear analysis. This enhances the efficiency of nonlinear finite strip analysis significantly. In order to avoid possible divergence, the flexural stiffness is amplified by a factor, which depends on the current maximum displacement and has been worked out by computational experiments. Numerical example shows that this method does not need too many iterations even for very large deflection, and its convergency is dependable.

(5) The accuracy of materially nonlinear finite strip analysis of reinforced concrete slabs is improved. The concrete is treated as a incrementally orthotropic linear elastic material. By introducing the concept of equivalent uniaxial strain, the actual biaxial stress state is transformed into two independent uniaxial stress states, in each of which the elastic modulus and principal stress depend on the current equivalent uniaxial strain and can be determined by diagram and strength envelope based on experiments. For reinforcement, bilinear elasto-plastic material model is used, and the tensile stiffening effect is included. In analysis, the finite strip is divided into concrete layers and each layer of reinforcement is replaced by a smeared steel layer. Newton-Raphson method is employed for nonlinear solution in order to reduce the number of iterations required and to ensure converging to correct answer. Numerical example shows the satisfactory accuracy of this analysis.

(6) The finite strip method is combined with finite element method in order to analyze a rectangular plate with some irregularities, such as openings and change in boundary conditions. The plate may be divided into two

parts, namely a regular part, which is analyzed by finite strip method, and a irregular part, which is analyzed by finite element method. A type of transition element is developed in order to connect both parts together. In the present study, conforming rectangular plate elements with 4 d.o.f at each node are chosen, and displacement functions of the transition element are derived. The combined analysis shows a better efficiency and the same accuracy in comparison with conventional finite element analysis.

(7) The finite strip method is combined with boundary element method in order to analyze a rectangular plate with some irregularities. The plate may be divided into two parts, namely a regular part simulated by finite strips and an irregular part analyzed by boundary element method. A type of transition strip is developed in order to connect both parts together. The displacement functions are derived in this thesis. This combined analysis gives satisfactory results in all the numerical examples.

6.2 RECOMMENDATIONS

The following topics might be recommended for future work:

(1) Higher order displacement functions in the transverse direction may be employed for all types of finite strip developed in this thesis in order to improve accuracy and efficiency further, especially for materially nonlinear analysis, in which the accuracy of stresses is very important;

(2) All the methods introduced in the present study may be applied to skew, curved or arbitrary shaped bridges;

(3) The spline finite strip method may be extended to materially nonlinear analysis of arbitrary shaped reinforced concrete slabs;

(4) Some newly developed methods may be applied to analysis of other types of structure, such as roofs, floors of buildings etc..

REFERENCES

1. Y.Guyon, Calcul des ponts larges a poutres multiples solidarisees par les entretoises. Annales des Ponts et Chaussees, 24, pp.683-718, 1946.

2. C.Massonnet, Methode de calcul des pont a poutres multiples tenant compute de leur resistance a la torsion. Publ. IABSE, 10, pp.147-182, 1950.

3. A.R.Cusens and R. P. Pama, Distribution of Concentrated Loads on Orthotropic Bridge Decks. The Structural Engineer, Vol.47,9, pp.277-285,Sept.,1969.

4. M.S.Troitsky and A.K.Azad, Analysis of Orthotropic Steel Bridge Decks by a Stiffness Method. Proc. Inst. Engrs., Part 2, Vol.55, pp.447-462, June,1973.

5. A.C.Scordelis, Analytical Solution for Box Girder Bridges. Development in Bridge Design and Construction, pp.200-216, Crosby Lockwood, 1971.

6. R.D. Cook,D.S. Malkus and M.E. Plesha, Concepts and Applications of Finite Element Analysis, 3rd edt. John Wiley & Sons, New York, 1989.

7. R.Jategaonkar,L.G.Jaeger and M.S.Cheung, Bridge Analysis Using Fi-

nite Elements, The Canadian Society for Civil Engineering, Desktop Monograph Series, 1985.

8. Y.K.Cheung, The Finite Strip Method in the Analysis of Elastic Plates with Two Opposite Simply Supported Ends. Proc. Inst. Civ. Engrs.,Vol.40, pp.1-7, Dec. 1968.

9. G.H.Powell and D.W.Ogden, Analysis of Orthotropic Steel Plate Bridge Decks. Proc. ASCE, Vol. 95, No. ST5,pp. 909-922, May,1969.

10. Y.K.Cheung, Finite Strip Method Analysis of Elastic Slabs. Proc. ASCE Vol. 94, No. EM 6, pp.1365-1378, Dec.,1968.

11. Y.K.Cheung, Analysis of Box Girder Bridges by Finite Strip Method. Proc. Second Int. Symposium on Concrete Bridge Design, Chicago, ACI Publications SP 26, pp. 357-378, April,1969.

12. Y.K.Cheung, The Analysis of Cylindrical Orthotropic Curved Bridge decks. IABSE Publications, Vol. 29-II,pp.41-52,1969.

13. Y.K.Cheung and M.S.Cheung, Analysis of Curved Box Girder Bridge by Finite Strip Method. IABSE Publications. Vol.31/I, pp. 1-19, 1971.

14. M.S.Cheung, Y.K.Cheung and A.Ghali, Analysis of Slab and Girder Bridges by the Finite Strip Method. Building Science, Vol.5, No.2,pp.95-105, Oct.1970.

15. M.S.Cheung, Y.K.Cheung and D.V.Reddy, Frequency Analysis of Certain Single and Continuous Span Bridges, Development in Bridge Design and Construction, pp.188-199, Crosby Lockwood, 1971.

16. T.G.Brown and A.Ghali, Finite Strip Analysis of Skew Slabs, Proc. McGill-EIC Conference in Finite Element Method in Civil Engineering, pp.1141-1151, 1972.

17. T.G.Brown and A.Ghali, Semi-Analytic Solution of Skew Box Girder Bridges, Paper 7838, Proc. Instn. Civ. Engrs. Part 2, Vol. 59, pp. 487-500, Sept., 1975.

18. J.S.Przemieniecki, Finite Element Structural Analysis of Local Instability, AIAAJ., Vol.11,pp.33,1973.

19. W.H.Wittrick and R.J.Plank, Buckling under Combined Loading of Thin, Flat-Walled Structures by a Complex Finite Strip Method. Int.J.Num.Meth.Eng.,Vol.8,pp.323, 1974.

20. Y.C.Loo, Analysis of Continuous Highway Box Bridges with Intermediate Stiffening, Eighth Aust. Road Res. Board Conf. pp.13-20, 1976.

21. C.I.Wu and Y.K.Cheung, Frequency Analysis of Rectangular Plates Continuous in One or Two Directions, Earthquake Engineering and Structural Dynamics, Vol.3,1974.

22. C.Delcourt and Y.K.Cheung, Finite Strip Analysis of Continuous Folded Plates, Proceedings, International Association of Bridge and Structural Engineers, pp.1-16,May, 1978.

23. D.Bucco,J.Mazumdar and G.Sved, Application of the Finite Strip Method Combined with the Deflection Contour Method to Plate Bending Problems,Computers and Structures,Vol.10,pp.827-830,1979.

24. Y. K. Cheung, Finite Strip Method in Structural Analysis, Pergaman Press, 1976.

25. Y.C.Loo and A.R.Cusens, The Finite-Strip Method in Bridge Engineering, A Viewpoint Publication, 1978.

26. J.A.Puckett, Compound Strip Method for the Analysis of Continuous Elastic Plates, Str.Research Report No.48, Civil Eng.Dept.,Colorado State Univ.,Fort Collins,Oct.,1983.

27. J.A.Puckett and R.M.Gutkowski, Compound Strip Method for Analysis of Plate Systems, Journal of Structural Engineering, ASCE, Vol.112, No.1,Jan.,1986.

28. T.R.Graves-Smith and S.Sridharan, A Finite Strip Method for the Post-Buckled Analysis of Plate Structures, Int.J.Mech.Sci. 20, 833-842, 1978.

29. S.Sridharan and T.R.Graves-Smith, Postbuckling Analyses with Finite Strips, J.Eng.Mech.Div.,ASCE, 107, 869-887, 1981.

30. G.J.Hancock, Non-Linear Analysis of Thin Sections in Compression, J.Struct.Div.,
ASCE,107,455-471,1981.

31. P.Langyel and A.R.Cusens, A Finite Strip Method for the Geometrically Nonlinear Analysis of Plate Structures, Int.J.Num.Meth.Eng., 19, 331-340, 1983.

32. J.T.Gierlinski and T.R.Graves-Smith, The Geometric Non-Linear Analysis of Thin-Walled Structures by Finite Strips, Thin-Walled Structures, 2, 27-50, 1984.

33. Z.G.Azizian and D.J.Dawe, Geometrically Non-Linear Analysis of Rectangular Mindlin Plates Using the Finite Strip Method, Computers and Structures 21, 423-436, 1985.

34. A.O.Olawale and R.J.Plank, The Collapse Analysis of Steel Columns in Fire Using a Finite Strip Method, Int.J.Num.Meth.Eng.,Vol.26,No.12,2755-2764,1988.

35. M.S.Cheung,S.F.Ng and Zhong Bingzhang, Finite Strip Analysis of Beams and Plates with Material Nonlinearity, Computers and Structures, Vol.33,

No.1,pp.289-294,1989

36. S.F.Ng,M.S.Cheung and Zhong Bingzhang, A Finite Strip Method for the Analysis of Structures with Material Nonlinearility, Journal of Structural Engineering,ASCE,to be published.

37. C.M.Guo, A.A.Mufti, L.G.Jaeger and M.S.Cheung, Nonlinear Earthquake Response Analysis of Reinforced Concrete Bridges Using the Finite Strip Method, Proceedings of Ninth World Conference on Earthquake Engineering, Tokyo-Kyoto, Japan, August 1988.

38. S.B.S.Abayakoon,M.D.Olson and D.L.Anderson, Large Deflection Elastic-Plastic Analysis of Plate Structures by finite strip Method, Int.J.Num. Meth.Eng.,Vol.28,No.2,pp.331-358,1989.

39. Y.K.Cheung,S.C.Fan and C.Q.Wu, Spline Finite Strip in Structure Analysis, Proceedings, The International Conference on Finite Element Method, Shanghai,pp.704-709,1982.

40. Y.K.Cheung and S.C.Fan, Static Analysis of Right Box Girder Bridges by Spline Finite Strip Method, Proc.Instn.Civ.Engrs,Part 2,75,pp.311-323,June,1983.

41. M.J.Chen,L.G.Tham and Y.K.Cheung, Spline Finite Strip for Parallelogram Plate, Proceedings, International Conference on Accuracy Estimates and Adaptive Refinements in Finite Element Computation (ARFEC),Lisbon,Vol.1,pp.95-104,June,1984.

42. L.G.Tham,W.Y.Li,Y.K.Cheung anf M.J.Chen, Bending of Skew Plates by Spline-Finite-Strip Method, Computers and Structures, Vol.22,No.1, pp.31-38,1988.

43. W.Y.Li,Y.K.Cheung and L.G.Tham, Spline Finite Strip Analysis of General Plates, Journal of Engineering Mechanics,ASCE, Vol.112,No.1, Jan.,1986.

44. Y.K.Cheung,L.G.Tham and W.Y.Li, Application of Spline-Finite-Strip Method in the Analysis of Curved Slab Bridge, Proc.Instn.Civ.Engrs,Part 2,81,pp.111-124, Mar.,1986.

45. P.Cheung, H.Dade and W.Zongmu, Static, Vibration and Stability Analysis of Stiffened Plates Using B Spline Functions, Computers and Structures, Vol.27, No.1, pp.73-78, 1987.

46. T.Mizusawa, Application of Spline Strip Method to Analyse Vibration of Open Cylindrical Shells, Int.J.Num.Meth.Eng.,Vol.26,No.3,663-676,1988.

47. D.S.Zhu and Y.K.Cheung, Postbuckling Analysis of Shells by Spline

Finite Strip Method, Computers and Structures, Vol.31,No.3,pp.357-364,1989.

48. M. S. Cheung and Wenchang Li, Finite Strip Analysis of Continuous Structures, Canadian Journal of Civil Engineering,Vol.15,pp.424-429, 1988.

49. M. S. Cheung and Wenchang Li, Analysis of Haunched, Continuous Bridges by Finite Strip Method, Computers and Structures,Vol.28,No.5, pp.621-626,1988.

50. M.S.Cheung and Wenchang Li, Analysis of Continuous, Haunched Box-Girder Bridges by Finite Strips, Journal of Structural Engineerng, ASCE,Vol.115,No.5,pp.1076-1087,May.1989.

51. M.S.Cheung and Wenchang Li, Analysis of Haunched, Continuous Bridges by Spline Finite Strips, Computers and Structures, Vol.36, No.2, pp.297-300, 1990.

52. M.S.Cheung, Wenchang Li and L.G.Jaeger, Analysis of Continuous Steel Boxes, Journal of Computing in Civil Engineering, ASCE, in review.

53. M.S.Cheung, Wenchang Li and L.G.Jaeger, Nonlinear Analysis of Cable-Stayed Bridge by Finite Strip Method,Computers and Structures,Vol.29, No.4,pp.687-692,1988.

54. M.S.Cheung, Wenchang Li and L.G.Jaeger, Improved Finite Strip Method for Nonlinear Analysis of Long Span Cable-Stayed Bridges, Canadian Journal of Civil Engineering, Vol.17, Feb. 1990.

55. M.S.Cheung and Wenchang Li, A modified Finite Strip Method for Geometrically Nonlinear Analysis of Plates, Computers and Structures, Vol.33, No.4, pp.1031-1035, 1989.

56. M.S.Cheung and Wenchang Li, Finite Strip Method for Materially Nonlinear Analysis of RC Slabs, Computer and Structures, Vol.35, No.5, pp.603-607, 1990.

57. M. S. Cheung and Wenchang Li, Combined Finite Strip / Finite Element Solution for Analysis of Plates, Computers and Structures, in review.

58. M. S. Cheung and Wenchang Li, Combined Finite Strip / Boundary Element Solution for Analysis of Plates, Computers and Structures, in review.

59. S.Timoshenko and S.Woinowsky-Krieger,Theory of Plates and Shells, second edit. McGraw-Hill Book Company,Inc. 1959.

60. M.S.Cheung and M.Y.T.Chan, Live Load Field Test on the Muskwa River Bridge,
Canadian Journal of Civil Engineering, Vol.5,pp186-201,1978.

61. P. M. Prenter, Splines and Variational Methods, John Wiley and Sons, 1975.

62. Task Committee on Cable-Suspended Structures of the Committee on Special Structures of the Committee on Metals of the Structural Division, Tentative Recommendations for Cable-Stayed Bridge Structures, Journal of the Structural Division, ASCE, 103(ST5),929-959, 1977.

63. W.Podolny et al. Construction and Design of Cable-stayed Bridges, Wiley-Interscience, New York, 1976.

64. M.C.Tang, Analysis of Cable-Stayed Girder Bridges, Journal of the Structural Division, ASCE, 97(ST5),1481-1496, 1971.

65. T.Kajita and Y.K.Cheung Finite Element Analysis of Cable-Stayed Bridges, IABSE, Pub. 33-II,101-112, 1973.

66. S.Timoshenko and J.N.Goodier, Theory of Elasticity, Third edt. McGraw-Hill Book Company, Inc. New York, 1970.

67. D. Darwin and D. Pecknold, Inelastic Model for Cyclic Biaxial Loading of Reinforced Concrete, SRS No. 409, University of Illinois at Urbana-Champaign, Illinois, July 1974.

68. A. F. Kabir, Nonlinear Analysis of Reinforced Concrete Panels, Slabs and Shells for Time Dependent Effects, Ph.d. Dissertation, Division of Structural Engineering and Structural Mechanics, University of California, Berkeley, UC-SESM Report No. 76-6, December 1976.

69. D. Darwin and D. Pecknold, Nonlinear Biaxial Stress-Strain Law for Concrete, Journal of the Engineering Mechanics Division, ASCE, Vol. 103, No. EM2. April 1977. pp.229-241.

70. D. R. J. Owen and E. Hinton, Finite Element in Plasticity (Theory and Practice).Pineridge Press Limited,1980.

71. J.V.Greunen, Nonlinear Geometric, Material and Time dependent Analysis of Reinforced and Prestressed Concrete Slabs and Panels, Department of Civil Engineering, University of California, Berkeley, California,

October 1979.

72. R. I. Gilbert and R. F. Warners, Tension Stiffening in Reinforced Concrete Slabs, Journal of the Structural Division, ASCE, Vol. 104 No. ST12, December 1978.

73. R. Taylor et al. Effect of the Arrangement of Reinforcement on the Behavior of Reinforced Concrete Slabs, Magazine of Concrete Research, Vol. 18, No. 55, June 1966, pp.85-94.

74. C.A. Brebbia and J.J. Connor, Fundamentals of Finite Element Techniques. London, Butterworths; 1973.

75. Ahmed Abdel-Akher; Gilbert A. Hartley, Evaluation of Boundary Integrals for Plate Bending. International Journal for Numerical Methods in Engineering, Vol. 28, 75-93; 1989.

76. C.A. Brebbia, J.C.F. Telles and L.C. Wrobel, Boundary Element Techniques, Theory and Applications in Engineering, Springer-Verlag, 1984.